Title
MOLECULAR BEAM STUDIES OF THE F + REACTION

Author
Neumark, D.M.

Publication Date
1984-08-01

Lawrence Berkeley Laboratory
UNIVERSITY OF CALIFORNIA

Materials & Molecular Research Division

Submitted to the Journal of Chemical Physics

MOLECULAR BEAM STUDIES OF THE F + H_2 REACTION

D.M. Neumark, A.M. Wodtke, G.N. Robinson,
C.C. Hayden, and Y.T. Lee

August 1984

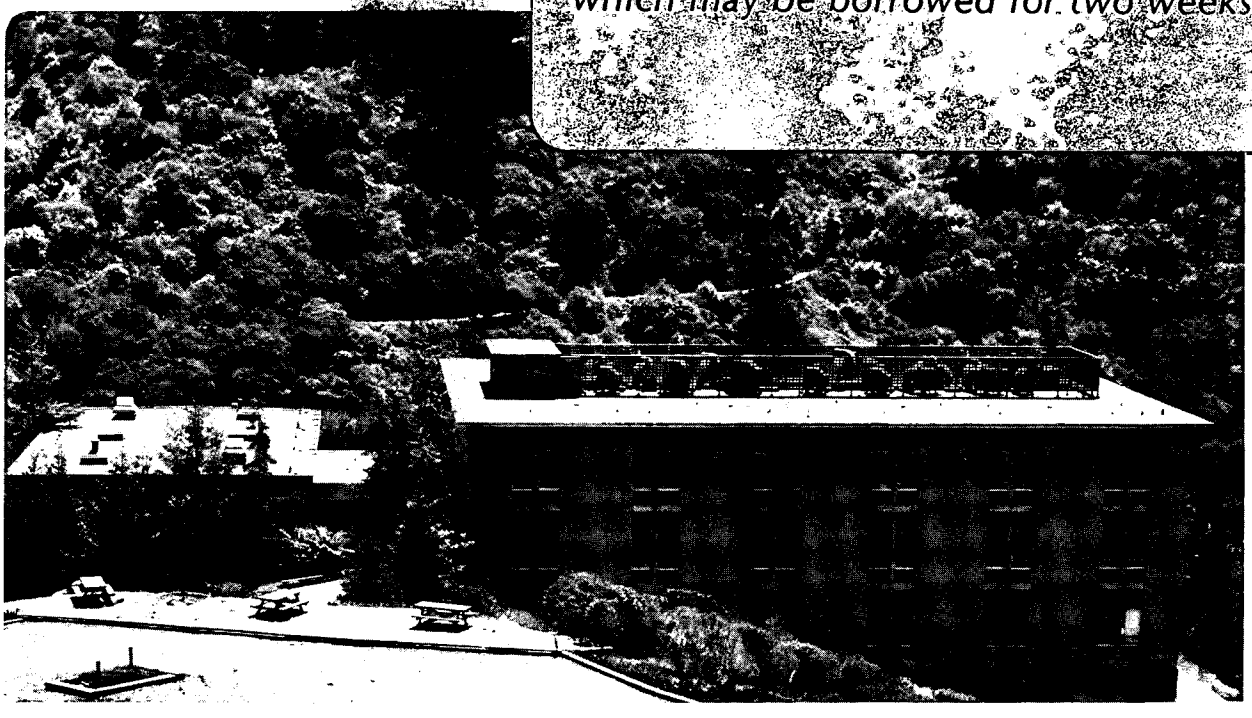

Prepared for the U.S. Department of Energy under Contract DE-AC03-76SF00098

DISCLAIMER

LBL-17810

MOLECULAR BEAM STUDIES OF THE F + H_2 REACTION

D. M. Neumark, A. M. Wodtke, G. N. Robinson,
C. C. Hayden,* and Y. T. Lee

Materials and Molecular Research Division, Lawrence Berkeley Laboratory
and Department of Chemistry, University of California,
Berkeley, California 94720

This work was supported by the Assistant Secretary for Energy Research,
Office of Basic Energy Sciences, Chemical Sciences Division of the
U.S. Department of Energy under Contract No. DE-AC03-76SF00098

MOLECULAR BEAM STUDIES OF THE F + H_2 REACTION

D. M. Neumark,[1] A. M. Wodtke, G. N. Robinson,
C. C. Hayden,[2] and Y. T. Lee

Materials and Molecular Research Division, Lawrence Berkeley Laboratory
and Department of Chemistry, University of California,
Berkeley, California 94720

Abstract

The dynamics of the F + H_2 reaction have been investigated in a high resolution crossed molecular beam study. Differential cross sections and kinetic energy distributions were obtained for each HF vibrational state. The v = 1 and v = 2 states were predominantly backward-scattered, but substantial forward scattering was observed for HF (v = 3) over the range of collision energies accessible in our apparatus, from 0.7 to 3.4 kcal/mole. The results strongly suggest that dynamical resonances play a significant role in the reaction dynamics of F + H_2 and that resonance effects are most prominent in the v = 3 product channel. Quantal reactive scattering calculations on F + H_2 predict that the v = 2 channel should be most strongly affected by resonances. This discrepancy is attributed to inadequacies in the potential energy surface used in the calculations, and several modifications to the surface are proposed based on the experimental results. Other features of the reaction are also discussed, including the integrated partial cross sections, the effect of H_2 rotation, and the reactivity of $F(^2P_{1/2})$.

---

[1]Current address: Joint Institute of Laboratory Astrophysics, University of Colorado, Boulder, CO 80309

[2]*Current address: Dept. of Chemistry, University of Wisconsin, Madison, WI 53706

1. Introduction

The reaction, $F + H_2 \rightarrow HF + H$, has been extensively studied over the past 15 years. Although much of the early interest in this reaction centered on its application to chemical lasers, it has become a prototype in the field of reaction dynamics because of its accessibility to both detailed theoretical and experimental study. It was one of the first reactions in which vibrationally state-resolved product distributions were measured; chemical laser [1] and infrared chemiluminescence studies [2,3] at thermal energies showed that the HF vibrational distribution was highly inverted with most of the population in $v = 2$ and $v = 3$. The effect of varying reactant translation and rotation on the final state distributions was later investigated using the same techniques [4-8]. The $F + D_2$ reaction was the first reaction in which vibrationally state-resolved product angular distributions were obtained in a crossed molecular beams experiment [9]. The results showed that all the products were predominantly backward-scattered, indicating that collinear approach of the reactants is most likely to lead to reaction. Accurate rate constants for $F + H_2$ and $F + D_2$ have recently been determined over a wide temperature range using various experimental methods [10,11].

Theoretical studies on the dynamics of the $F + H_2$ reaction have focused on developing both an accurate potential energy surface and techniques for scattering calculations using model surfaces. An ab initio potential energy surface has been calculated and has provided important information on the general features of the true surface [12], but since its exothermicity and barrier height are incorrect [13],

scattering calculations using it cannot be meaningfully compared with experimental results until the accuracy of the ab initio calculation is further improved. A seemingly more productive approach has been to carry out classical trajectory calculations on model semi-empirical surfaces, usually of the LEPS form [14], and to optimize the surface parameters in order to match the experimental results. The most extensive studies of this type have been performed by Muckerman [15], Polanyi [16], and their coworkers, who investigated the effects of small changes in the surface on the reaction cross section and the product angular distribution. Polanyi's study showed that reactant translational energy had a substantially greater effect on the reaction dynamics than vibrational energy. This is the expected result for an exothermic reaction with a barrier in the entrance channel [17].

The potential energy surface most commonly used in reactive scattering studies of $F+H_2$ is the Muckerman 5 (M5) surface [18]. This is an LEPS surface with the correct exothermicity which, when used in classical trajectory calculations, reproduces the rate constant determined by Mercer et al. [19] and the experimental values for product energy disposal [2] . The surface has a barrier of 1.064 kcal/mole in the entrance channel for collinear approach of the reactants that rises rapidly as the F-H-H bending angle increases. Several problems are found to be associated with this surface, however. Mercer's value for the activation energy was 1.71 kcal/mole, but more reliable recent studies [10,11], show that E_a is closer to 1.0 kcal/mole. In addition, the pre-exponential A factor of the rate constant for M5 derived

from trajectory studies is considerably lower than the A factor determined in the newer experiments [20]. The larger activation energy and smaller A factor suggest that the entrance channel barrier on M5 is too high and rises too quickly with increasing deviation from collinear approach. Besides, as Jakubetz and Connor have mentioned [21], using classical trajectory calculations to test the ability of a surface to reproduce experimental data may be invalid if quantum effects are important.

Quantum mechanical scattering calculations have indeed predicted that quantal effects in the form of dynamical resonances [22] should play a significant role in the reaction dynamics of $F + H_2$. A quantal collinear reactive scattering calculation by Schatz et al. [23] of the reaction probability vs. collision energy on the M5 surface shows that, in addition to broad features due to direct scattering producing HF (v = 2) and HF (v = 3), there is a sharp peak with a width of about 0.01 eV for the production of HF (v = 2) just above the HF (v = 3) threshold. Argand diagrams and time delay analysis show that the sharp peak is due to interference between direct and resonant reactive scattering [24,25]. Calculations at higher energy also display strong resonance effects, with peaks typically occurring near a threshold for an HF vibrational state [23,26]. Connor has performed collinear calculations on several surfaces and obtained dramatically different resonance structure for each case [26]. The exact nature of the resonances therefore depends critically on the details of the potential energy surface in the strong coupling region near the transi-

tion state. This is the most important region of the surface as it determines many of the experimental observables mentioned previously.

Reactive scattering and kinetics experiments often yield a rough picture of the potential energy surface for a reaction, but even a detailed kinetics study in which state-to-state rate constants are determined does not, in general, lead to a quantitative understanding of the transition state and strong coupling region. Attempts to study the transition state via emission and absorption have not yielded much information as these experiments typically involve electronic transitions between two unknown surfaces [27-30]. The experimental observation of resonances should therefore provide a considerably more direct and sensitive probe of the strong coupling region than has previously been available. Since it will yield information on quasi-bound states supported by the potential energy surface, the observation of resonances is, in principle, equivalent to performing vibrational spectroscopy of the transition state [25].

We have performed a high resolution crossed molecular beams study of the $F + H_2$ reaction in an attempt to observe the effects of dynamical resonances. In order to view our results in the proper perspective, it is necessary to understand what features of the potential energy surface cause resonances to appear in collinear and three-dimensional calculations, and how dynamical resonances can actually be observed in a reactive scattering experiment.

2. Properties of Dynamical Resonances

Identifying the elements of the potential energy surface responsible for the resonances in the F + H_2 reaction is not entirely straightforward. The physical origin of these resonances has been attributed to quasi-bound FH_2 states localized in the strong coupling region of the surface near the potential energy barrier that live for a short time before decomposing to products [25,31]. It is not immediately clear why these states should exist at all; the M5 surface, for example, has no wells near the barrier which one might think are necessary to support quasibound states.

The origin of dynamical resonances can be understood more easily in a collinear scattering calculation. If the scattering wavefunction is separated into translational and vibrational motion, vibrationally adiabatic curves can be derived which are effective potentials for the translational motion of reactants or products described by a single quantum number for the vibrational action [32,33]. Even in the absence of wells on the potential energy surface, the adiabatic curves can develop barriers and wells as the potential energy surface perpendicular to the translational coordinate narrows and widens, respectively, and these features become more pronounced for the curves corresponding to higher vibrational quantum numbers. The wells can support quasi-bound states similar to shape or Feshbach resonances and provide an additional pathway between reactants and products.

The problem with this picture is that the adiabatic curves are highly coordinate-dependent. In reactive scattering, it is not clear how to define translation and vibration in a global manner that describes reactants and products. This problem is particularly troublesome in $F + H_2$ which is clearly not a vibrationally adiabatic reaction. An important step towards resolving this difficulty is due to the work of Pollak and coworkers on periodic orbit dividing surfaces (PODS), which are classical stable orbits on a potential energy surface [34]. They proved that a PODS with vibrational action $(n + 1/2)$ corresponds to either an adiabatic well or a barrier for the state $v = n$ [35]. The PODS is an intrinsic property of the potential energy surface and does not depend on any coordinate system. In fact, each PODS defines a locally adiabatic coordinate system in which vibration is parallel to the bound orbit and translation is perpendicular to it. In addition to locating the adiabatic wells and barriers, Pollak and Child have found another set of periodic orbits which, when subjected to a quantization condition, match very well with the resonance energies in the quantal calculations [36]. These resonant periodic orbits oscillate between the reactant and product sides of the strong coupling region just inside the adiabatic barriers. The orbit corresponding to the lowest $F+H_2$ resonance is bounded by the $v = 0$ reactant and $v = 3$ product barriers.

The PODS formulation provides an easily visualized picture of dynamical resonances. However, since the resonant periodic orbits are classically bound, they cannot be accessed by reactants or products in

a classical calculation. The coupling between the bound orbits and the continuum can be estimated by incorporating a semi-classical approximation into the theory [37], but extending this procedure to $F+H_2$ is difficult because the resonances have several decay pathways. In order to understand the results of the quantal reactive scattering calculations better, one needs to construct a global coordinate system in which the adiabatic curves retain some physical significance even for a non-adiabatic process. The best one can do is to devise a system in which the reaction can be described with as few adiabatic curves as possible. Natural collision coordinates [38] do not work well in this regard for $F + H_2$ [33]. Far more success has resulted using hyperspherical coordinates [39,40].

Launay and LeDourneuf have calculated a set of adiabatic curves for the M5 surface in hyperspherical coordinates [40]. The curve that correlates to H_2 ($v = 0$) has a small barrier and a well which supports a quasi-bound state at the same energy as the resonance spike in the collinear scattering calculation of the energy dependence of the HF ($v = 2$) reaction probability. This quasi-bound state can be accessed by a collision of $F + H_2$ ($v = 0$) at the resonance energy, and reaction occurs by its subsequent decay to HF ($v = 2$) product. Although the HF($v = 3$) state is an energetically accessible decay product of this resonance, the height and width of the barrier on the adiabatic curve which correlates to HF ($v = 3$) results in the exclusive formation of $v = 2$.

This view of the resonance is slightly oversimplified. A comparison of the wells and barriers on the adiabatic curves obtained by Launay and LeDourneuf with the true adiabatic wells and barriers found by Pollak [35] shows that while the heights and locations of the barriers more or less agree, the true adiabatic well which correlates to HF (v = 3) is substantially lower. Another set of hyperspherical adiabatic curves has been calculated by Römelt [41] with the origin of the coordinate system chosen somewhat differently from that of Launay and LeDourneuf. Romelt's barriers are similar to those on the adiabatic curves of Launay and LeDourneuf which correlate to H_2 (v = 0) and HF (v = 3), but inside the critical region there are significant differences. One can conclude here that the strong coupling inside the critical region causes the adiabatic wells to lose some of their physical significance. The lowest quasi-bound state is probably best described as having both H_2 (v = 0) and HF (v = 3) character, and, more importantly, as being confined within the critical region by the H_2 (v = 0) barrier on the reactant side and the HF (v = 3) barrier on the product side. It is therefore quite similar to the classical periodic orbit corresponding to the lowest energy resonance [37]. Indeed, recent stabilization calculations on F + H_2 by Thompson and Truhlar [42] confirm this picture, showing that the probability density of the lowest energy resonant wavefunction is trapped in the critical region of the M5 potential energy surface.

In order to relate dynamical resonances to experimental observables, one must consider the results of approximate three-dimensional quantal reactive scattering calculations on M5 [31,43-46]. In these calculations, the total and partial reactive cross sections do not show any sharp structure as the collision energy is varied. There are two effects to be considered when comparing collinear and three-dimensional resonances. The first is that the energy of the quasi-bound state will be higher in the three dimensional case by the additional zero-point energies of the FH_2 bending modes. The second, more important, effect is the contribution of collisions with nonzero orbital angular momentum to the reaction. A quasi-bound state formed by a collision of orbital angular momentum $\underline{L}$ will have rotational energy on the order of $B\underline{L}\ (\underline{L} + 1)$, where B is the rotational constant of the complex. If an $\underline{L} = 0$ resonance occurs at energy E_0, then at approximately $E_0 + B\underline{L}\ (\underline{L} + 1)$ a quasi-bound state can be formed by a collision of orbital angular momentum $\underline{L}$. Consequently, as Redmon and Wyatt [43] show clearly, as the collision energy is increased beyond E_0, collisions with progressively larger values of orbital angular momentum will be brought into resonance. The large number of partial waves involved in reactive scattering allows the resonance to be accessed over a wide energy range. Thus resonances appear as broad, smooth features in the collision energy dependence of the total cross section that are difficult to distinguish from the substantial contribution from direct scattering.

Although reactive resonances cannot be observed in a state-resolved total cross section measurement, they can be seen in a reactive scattering experiment in which state-resolved differential cross sections are determined. Classical [18] and quasi-classical [46-48] trajectory studies on M5 show that the HF product angular distribution is dominated by backward scattering at 180° with respect to the incident F beam up to collision energies of 5 kcal/mole. This is clearly related to the entrance channel properties of the potential energy surface that favor collinear, low impact parameter approach of the reactants. The quantal calculations predict, however, that as the collision energy is raised from 2 to 3 kcal/mole, the v = 2 distribution shifts from backward-peaked to sideways-peaked, whereas the v = 3 distribution remains backward-peaked [43]. This is attributed to dynamical resonance effects. As the collision energy is raised, quasi-bound states are formed by progressively higher impact parameter collisions, and their subsequent decay to v = 2 product leads to a state-selective broadening of the v = 2 angular distribution. The shift in the v = 2 distribution will be even more pronounced if the lifetime of the quasi-bound state is an appreciable function of the rotational period of the complex. The experimental determination of the angular and kinetic energy distributions for each product vibrational state therefore offers the most promise for characterizing resonances in reactive scattering.

Earlier molecular beam work carried out in our laboratory in search of resonances in F + H_2 showed that the HF (v = 2) angular distribution did broaden and exhibit slight sideways-peaking as the collision energy was raised from 2-3 kcal/mole, but the results for v = 3 were

inconclusive since the range of our angular scan was limited because of the high m/e=20 background near the F beam, precluding the observation of sideways or forward-scattered v = 3 product at any energy [49,50]. This was a serious shortcoming because without this information on the v = 3 product, the state-specificity of the v = 2 side-ways-peaking could not be confirmed. The case for a resonance is much stronger if a clearly state-specific effect can be found. Recently, several improvements to the apparatus were made which permit the scattering of the product vibrational states to be much better resolved and allow the determination of a complete differential cross section for the v = 3 product. Some of the F + para-H_2 results obtained with the new configuration have recently been reported [51]. This article discusses the complete results for F + p-H_2 and F + n-H_2 at collision energies ranging from 0.7 to 3.4 kcal/mole and the following article reports on our studies of the F + D_2 and F + HD reactions.

3. Experimental

Figure 1 shows a top cross sectional view of the experimental arrangement. The F and H_2 beams with FWHM angular spreads of 2° and 3°, respectively, intersected at 90° inside a vacuum chamber where the pressure was ~ 7×10^{-7} torr with both beams on. The collision region defined by the intersection of the two beams was about 0.080" on a side. The scattered HF product was detected by a rotating ultra-high vacuum mass spectrometer consisting of an electron-impact

The selector was spun at 500 Hz and the resulting most probable F beam velocity was 8.7×10^4 cm/sec. The wheel assembly was mounted on two bearings and connected to a three phase synchronous motor [57] by a flexible coupling shaft [58]. Barden SR4SSTA5 bearings coated with Bray 3L-38 grease [58] were used for the wheel assembly and inside the motor. The motor was powered by a three-phase supply of our own design. The frequency of the spinning wheels was monitored by a slotted optical switch containing an LED and a phototransistor [60]. The wheel assembly and motor were clamped to an aluminum base which was bolted to the bottom of the differential chamber. It was necessary to dynamically balance each wheel separately as well as the entire assembled selector to achieve smooth operation at 500 Hz.

Early attempts to study the $F + H_2$ reaction with this source configuration were frustrated because of the high rate of effusion of HF that formed in the differential region and entered the main chamber via the 2nd defining slit. Only about 1 of the effusive beam passed through the velocity selector and the remaining F atoms were free to collide with the chamber walls and eventually form HF. We constructed a liquid nitrogen-cooled cold shield inside the differential region consisting of several large 1/8" copper plates in order to maximize HF cryopumping. One plate was located between the velocity selector and the 2nd defining slit and admitted the beam through a 9/32" hole. The cold shield and the use of Fomblin pump oil virtually eliminated effusive HF background at angles greater than 10° away from the F beam.

The supersonic H_2 beam was produced by expanding pure H_2 through a 70 μ orifice into a source chamber. The orifice was 0.4" from the tip of a nickel skimmer with an entrance hole of 0.018" diameter [61]. The beam, which was essentially defined by the nozzle and skimmer geometry, then entered the main chamber; in order to minimize the distance between the source orifice and the collision region no differential pumping region was used for the H_2 source. An 0.080" collimating slit in the main chamber between the skimmer and the interaction region prevented background H_2 in the source chamber from effusing through the skimmer and directly intersecting the F beam outside the collision region.

The source was fabricated by brazing a platinum electron microscope aperture with a 70 μ orifice [62] to a copper tube. The tube had several turns of coaxial heater [63] brazed to it as well as a liquid nitrogen contact. The source temperature could be varied continuously from 90°K to 600°K. This gave a collision energy range from 0.7 to 3.5 kcal/mole. The source temperature was monitored by a thermocouple clamped to the tube just behind the orifice. The thermocouple was connected to a temperature control unit of our own design which regulated the voltage across the heating coil. The H_2 source chamber was pumped by a Varian VHS-400 diffusion pump with a nominal pumping speed of 8000 liter/sec which was backed by a 330 CFM roots blower/mechanical pump combination. The operating pressure in the source was 6×10^{-4} torr. Typical H_2 stagnation pressures were 80 psi at room temperature, 120 psi at 720°K, and 45 psi at 85°K. Matheson Ultra-High Purity H_2 (99.999% pure) was used for the n-H_2 experiments. The

para-H_2 was made in the Low Temperature Laboratory of the Berkeley Chemistry Department and stored in aluminum tanks at 200 psi. Previous photoelectron spectroscopy work showed that para-H_2 stored in this manner lasted 1-2 weeks without significant conversion [64].

In the original configuration of the detector, each of the three differential regions was pumped by a 200 l/sec ion pump. In order to reduce the rare gas background for this experiment, the ion pumps previously in use on the apparatus were chemically cleaned and baked out into a turbomolecular pump prior to mounting them onto the apparatus. The rare gas pumping capability of the detector was further improved by adding a 110 l/sec turbomolecular pump to the outermost region and a 330 l/sec turbomolecular pumped backed by a 110 l/sec turbo-pump to the 2nd region. The two 110 l/sec pumps exhausted into the main chamber. The turbomolecular pumps could be isolated from the detector with all-metal valves [65] so that routine maintenance could be performed on them without venting the detector. The resulting reduction in the mass 20 background was substantial. With the detector isolated from the main chamber, the mass 20 background count rate under normal detector operating conditions was 150 Hz. The count rate observed before the turbomolecular pumps were installed was never below 800 Hz.

Angular scans of the HF product were taken by modulating the H_2 beam with a 150 Hz tuning fork chopper [66] and recording the modulated HF signal as a function of angle. The chopper was located in the main chamber between the skimmer and the collimating slit and could be moved out of the path of the H_2 beam for time-of-flight measurements. Typical counting times were 266-532 seconds at each angle which yielded

error bars of less than 3% except at the lowest collision energies. The angular resolution of the detector was 1.25°, and points were taken every 2° except near the F beam where they were taken at 1° intervals.

Time-of-flight measurements were performed on both beams to characterize their velocity distributions, and on the HF reactive scattering product. The TOF wheel and motor assembly was bolted to the rotating detector. For the analysis of the beam velocity distributions, TOF measurements were done using a 7" diameter stainless steel wheel with 4 equally spaced 0.010 mil slots. The wheel was spun at 300 Hz. A multichannel scaler connected to an LSI 11 microcomputer controlled the data acquisition. Typical channel widths were 1 μsec for the H_2 beam and 2 μsec for the F beam. The H_2 beam time-of-flight measurements were deconvoluted to account for the length of the ionizer and other broadening effects [67]. The resulting velocity distributions had typical FWHM spreads of 3 percent. TOF measurements on the F beam confirmed that its peak velocity was identical to that expected from the the velocity selector design parameters. The F beam velocity showed no detectable variation over the course of the experiment even though the velocity selector was removed and replaced several times. This was a welcome change from the earlier studies with supersonic F beams where the size of the source orifice would change over time and alter the beam characteristics. As the F beam velocity has a large effect on the LAB kinematics of this reaction, the constant velocity was yet another advantage gained by using a velocity-selected

beam. The spread in center-of-mass collision energies due to the beam velocity distributions was about 0.1 kcal/mole.

The HF product velocity distribution was determined using the cross-correlation TOF method [68] because of the low signal intensity. A 7" Be-Cu wheel photoetched with a 255 element pseudorandom sequence was used. The wheel was spun at 490 Hz which corresponded to 8 μsec/channel resolution in the TOF spectra. Typical TOF counting times were 1-2 hours. Spectra were taken every 2° where the signal was more intense and at larger intervals at angles far from the F beam where the lower signal necessitated longer counting times.

4. Results

4.1 Product Angular Distributions

Measurements of the product angular distributions were taken at several collision energies for F + p-H_2 and F + n-H_2. The H_2 source conditions for each energy are displayed in table 1. The H_2 stagnation pressure was adjusted so that the pressure in the main chamber was the same at all energies with the H_2 beam on. In order to obtain the same beam velocities for n-H_2 and p-H_2, it was necessary to run the n-H_2 at a slightly higher temperature. This was expected since more rotational relaxation can occur in a supersonic expansion of p-H_2 than for n-H_2 in the temperature range we studied because H_2 can undergo only even ΔJ rotational transitions. For example, at 304°K, 79% of the n-H_2 is in J = 0 or J = 1 and cannot relax any further. On the other hand, 51% of the p-H_2 is in J = 0, and the remaining 49% of the molecules, all of which are in even J states and most of which are in J = 2,

can in principle relax to J = 0 and increase the beam velocity in the process. Photoelectron spectroscopy on supersonic molecular beams of p-H_2 and n-H_2 shows that substantial relaxation does occur [69]; more than 80% of the p-H_2 ends up in J = 0 under our operating conditions. Although the F + p-H_2 and F + n-H_2 angular distributions at the same collision energies were quite different for $E \leq 1.84$ kcal/mole, no difference was observed at the higher energies where it was necessary to heat the nozzle above room temperature. This may have been due either to a large amount of rotationally excited p-H_2 remaining after the expansion, or to wall-catalyzed para → ortho conversion at the higher temperatures. In any case, no data for high temperature F + p-H_2 reactions are reported here.

The HF product angular distribution for F + p-H_2 at 1.84 kcal/mole is shown in fig. 2. The LAB angle, Θ, is measured from the F beam. The laboratory angular distribution shows considerable structure which can be related to the important features of the product velocity and angular distributions in the center-of-mass frame of reference with the aid of the Newton diagram below the distribution.

The Newton diagram shows the relationship between the LAB and CM velocity vectors. $\underline{v}_F$ and $\underline{v}_{H_2}$ are the LAB reactant velocities, and the CM reactant velocities are $\underline{u}_F$ and $\underline{u}_{H_2}$ ($\underline{u}_{H_2}$ is not drawn to scale). The origin in the center-of-mass coordinate system is the tip of the vector representing the velocity of the center-of-mass in the LAB frame. The angle between this vector and v_F is labelled Θ_{cm}. The CM scattering angle will be denoted by θ, where $\theta = 0^\circ$ is defined as the direction of the incident F beam in the CM coordinate system.

HF product scattered near $\theta = 0^\circ$ is referred to as forward-scattered, while HF scattered near $\theta = 180^\circ$ is described as backward-scattered. The 'Newton circles' show the maximum CM speed for HF product formed in the indicated vibrational state and therefore delineate the LAB angular range over which each state will be observed.

The peaks in the angular distribution, indicated by the dotted lines, occur at LAB angles where the LAB velocity vector is nearly tangent to a Newton circle. The broad peaks at $\Theta = 28^\circ$ and $\Theta = 45^\circ$ appear to be from backward-scattered $v = 3$ and $v = 2$ product, respectively. The sharp peak at $\Theta = 8^\circ$ appears to be from forward-scattered $v = 3$. This prominent feature could not be clearly observed in our previous studies of $F + H_2$. In the work using a supersonic beam of F in N_2, $\underset{\sim}{v}_F$ was considerably faster than in this experiment. Θ_{cm} was therefore much smaller, and any forward scattered $v = 3$ product would have been so close to the F beam that it would have been obscured by HF impurity in and near the beam. In the studies where F was seeded in Kr carrier gas, elastically scattered ^{80}Kr which was ionized to Kr^{4+} interfered with the observation of reactively scattered HF near the F beam. In the current configuration, any forward scattered $v = 2$ would have been on the other side of the F beam but still within the angular range of the rotatable detector. No evidence of forward-scattered $v = 2$ was observed at any collision energy.

The LAB angular distributions for $F + n\text{-}H_2$ of five collision energies ranging from 0.68 to 3.42 kcal/mole and $F + p\text{-}H_2$ at four collision energies ranging from 0.68 to 1.84 kcal/mole are shown in figs. 3 and 4.

The scans were taken on different days, and some variation in experimental conditions unavoidably occurred. This was mostly due to the variation of the F_2 dissociation ratio resulting from running the F oven at slightly different temperatures. However, we spent one day measuring representative angles at each collision energy so that the complete angular distributions could be correctly scaled for constant F and H_2 flux. The scaling factors obtained by this procedure are listed in table I. The only angular distributions that required substantial adjustment were the two lowest F + p-H_2 runs and F + n-H_2 at 0.68 kcal/mole.

The structure described above in the F + p-H_2 data is evident in nearly all the angular distributions. The sharp forward v = 3 peak and broad backward v = 3 peak occur in every angular distibution, and the backward v = 2 peak is distinct except in the 0.68 kcal/mole measurements. Several trends are noteworthy. For both F + p-H_2 and F + n-H_2, the magnitude of the forward peak increases as the collision energy is raised, except for F + p-H_2 at 1.0 kcal/mole where the scaling is more uncertain. For F + n-H_2 collision energies $\geq$ 1.0 kcal/mole, the backward v = 3 peak decreases relative to the forward peak as the collision energy is raised. The same trend is seen in the F + p-H_2 scans at 1.30 and 1.84 kcal/mole. However, this trend reverses as the collision energy is lowered from 1.30 kcal/mole; the two lowest energy F + p-H_2 angular distributions show that the backward peak falls off faster than the forward peak as the energy decreases. For F + n-H_2, the low collision energy fall-off of the backward peak occurs only at 0.68 kcal/mole.

A comparison of the F + p-H_2 angular distributions with F + n-H_2 at the same collision energy shows the ratio of the forward-to-backward v = 3 peak heights to be considerably larger for F + p-H_2. The high quality of the data at 1.84 kcal/mole allows the determination of the F+H_2 (J = 1) LAB angular distribution using the formula

$$N_{J=1}(\theta) = 4/3 \left(N_{n-H_2}(\theta) - \frac{1}{4} N_{p-H_2}(\theta) \right).$$

This formula is exact if the rotational distributions of even J states are the same in n-H_2 and p-H_2, and all the odd J rotational population of the n-H_2 is in J = 1. The results of Pollard et al. [69] show these to be very reasonable assumptions. Figure 5 shows the angular distributions for p-H_2 (labelled J = 0) and H_2 (J = 1). The forward peak is lower in the J = 1 distribution, whereas the backward v = 2 and v = 3 peaks are higher. In addition, the v = 3 signal for J = 1 spans a slightly wider LAB angular range. The v = 3 Newton circle for F + H_2 (J = 1) is slightly larger than that for F + H_2 (J = 0) because of the additional H_2 rotational energy. The figure therefore shows that some of the rotational energy ends up as product recoil energy. Higher J states do contribute slightly to the product angular distributions shown in fig. 5 but the major differences are due to J = 1 and J = 0.

4.2 Time-of-Flight Measurements of Velocity Distributions

In order to determine the product velocity distributions, time-of-flight spectra were taken at E = 1.84 kcal/mole for F + p-H_2, and at 1.84, 2.74 and 3.42 kcal/mole for F + n-H_2. About 20-25 spectra at

different angles were taken at each energy. Representative spectra are shown in figs. 6 to 8.

The TOF spectra show distinct peaks which correspond to various product vibrational states. The peaks are well-separated because of the narrow beam velocity distributions and the fact that product rotational excitation is small relative to the spacing between the vibrational energy levels of the HF product [26]. Each spectrum allows one to quantify the contribution of the individual product vibrational states to the total signal at that LAB angle.

The spectrum at $\Theta = 18^\circ$ for F + p-H_2 at 1.84 kcal/mole (fig. 6) shows the degree of resolution obtained in these measurements. This angle is close to Θ_{cm} at this energy. The fastest peak is from v = 2 product, and the two slower peaks are from v = 3. Most of the v = 3 product flux occurs just inside the v = 3 Newton circle, so at $\Theta = 18^\circ$ the v = 3 product is sampled in two distinct regions of LAB velocity space resulting in two v = 3 peaks appearing in the TOF spectrum. In this spectrum, the two v = 3 peaks represent scattering at nearly the same angle in the center-of-mass. Although scattering in the center-of-mass has cylindrical symmetry about the reactant relative velocity vector, the slower peak is smaller because it is spread out over more time-of-flight channels. This is reflected in the conversion from CM velocity flux to LAB number density at arrival time t, the latter being proportional to t^{-3} [50]. The slow peak expected for the v=2 state is affected even more strongly by this factor and is often not clearly seen in the TOF spectra. The two v = 3 peaks merge at LAB angles that are nearly tangent to the v = 3 circle. The spectra

at $\Theta = 8^\circ$ and $\Theta = 30^\circ$ for p-H_2 are examples of this. The spectrum at $\Theta = 8^\circ$ confirms that the peak in the angular distribution is from v = 3 product. The spectra at larger LAB angles show a contribution from the v = 1 product that is, at least in some cases, distinct from the v = 2 peak. Although the resolution in the TOF spectra at higher energies is somewhat worse, resolved peaks are still evident in all the spectra even at 3.42 kcal/mole (fig. 8).

TOF spectra at angles $\Theta \leq 10^\circ$ were contaminated to some extent by slow, effusive HF originating from the differential pumping chamber of the F beam source. The contribution from the effusive component was determined by blocking the F beam and taking a spectrum at $\Theta = 4^\circ$ where the effusive signal was quite intense. This spectrum was scaled to fit the slow tail in the reactive TOF spectra and subtracted. Figure 9 shows the raw data at $\Theta = 8^\circ$ for F + p-H_2, the scaled effusive TOF, and the result of the subtraction. The contribution from the effusive component was considerably smaller at 10° and was insignificant at 12°.

5. Analysis

Center-of-mass angular and translational energy distributions of the products were obtained for the four energies studied by product time-of-flight measurements. The distributions were determined by forward convolution. A trial CM angular and energy distribution for each vibrational state was input to a computer program. The program performed the necessary CM → LAB transformations [70] and averaged over the beam velocity distributions and detector resolution in order

to generate a LAB angular distribution and TOF spectra. The CM parameters were varied until the computer-generated results matched the data. The best fits to the four LAB angular distributions are shown in figs. 2 and 10–12, and the fits to the sample TOF spectra can be seen in figs. 6–8.

The coupled CM angular and energy distributions are of the form:

$$P_i(E,\theta) = N_i A_i T_i(\theta)\ (E/E_m^i)^{\alpha_i(\theta)}\ (1 - E/E_m^i)^{\beta_i(\theta)} \qquad (1)$$

where

$$\beta_i(\theta) = \alpha_i(\theta)(E_p^i(\theta)/(1-E_p^i(\theta))). \qquad (2)$$

Here i is the product vibrational state, E is the product recoil energy, and $E_m^i = \Delta E + E_{coll} - E_i$ is the maximum recoil energy for product in the ith vibrational state. ΔE is the exothermicity, E_{coll} is the collision energy, and E_i is the vibrational energy of HF(v = i) relative to HF(v = 0). The energetics for the F + H_2 reaction are shown in fig. 13 [12]. For F + p-H_2, the exothermicity used in the data fitting was 32.17 kcal/mole. For F + n-H_2, most of the H_2 was in J = 1 and this rotational excitation was added to the exothermicity to give ΔE = 32.51 kcal/mole.

The adjustable parameters are A_i, an overall intensity factor, $T_i(\theta)$, the intensity at CM angle θ, $E_p^i(\theta)$, the peak in the angle-dependent recoil distribution at θ (expressed as a fraction of E_m^i), and $\alpha_i(\theta)$ which determines the width of the energy distribution. N_i is a normalization factor given by

$$N_i = \left[E_m^i\ B\ (\alpha_i(\theta) + 1,\ \beta_i(\theta) + 1) \right]^{-1} \qquad (3)$$

where

$$B(a,b) = \frac{\Gamma(a)\ \Gamma(b)}{\Gamma(a+b)} \quad .$$

This insures that

$$\int_0^{E_m^i} P_i(E,\theta)\, dE = A_i T_i(\theta) \equiv I_i(\theta) \tag{4}$$

which is the total intensity for state i at θ. The angle-dependent parameters were input in point form every 5° and their values at intermediate angles were obtained by linear interpolation.

The spread in the F beam velocity was by far the most important averaging factor in the forward convolution and it required careful characterization. The transmission function B(v) for a perfectly collimated beam with no angular divergence has been given elsewhere [71]. This should, in principle, be convoluted with the velocity distribution of the F atoms emerging from the oven over the range of transmission in order to obtain a realistic estimate of the F beam velocity distribution. We found this unnecessary, however, as v_F = 8.7×10^4 cm/sec is close to the maximum of the Maxwell-Boltzmann distribution at 920°K where the intensity variation is insignificant over the transmission window of the velocity selector. A larger effect arises from the angular divergence of the F beam. As shown in fig. 1, the beam passes through the side of the velocity selector, where the wheel slots are parallel to the scattering plane, rather than through the top of the selector. The angular divergence in the scattering

plane does not affect the transmission function of the velocity selector, although it does affect the Newton diagram for the reaction and is accounted for in the analysis program. However, for an out-of-plane trajectory through the velocity selector, the transmission function will be somewhat different. Frankl [72] has derived an expression for $B(v,\alpha)$, the dependence of the transmission function on the angular deviation α from an in-plane trajectory. The out-of-plane divergence of the F beam was 2° and the angular offset between the first and last wheel was 17.3°. $B(v,\alpha)$ must be multiplied by the angular transmission function of the two defining slits for the F beam which is approximately triangular and is given by

$$T(\alpha) = 1 - \frac{|\alpha|}{|\alpha_{max}|} \tag{5}$$

where $\alpha_{max} = 1^\circ$ in this case. The angle-averaged transmission function of the selector is then

$$B(v) = \int_{-\alpha_{max}}^{\alpha_{max}} T(\alpha)\, B(v,\alpha)\, d\alpha. \tag{6}$$

This increases the FWHM of the velocity selector from 11% to 12.6% and has a small but noticeable effect on the calculated TOF distributions. One interesting point regarding this correction is that it is underestimated in the F beam TOF measurements. These are taken with a 0.005" hole in front of the detector to limit the gas flow when the detector is looking directly into the beam. This greatly restricts the angular range of the trajectories entering the detector. Consequently, the width of the measured TOF spectrum of the beam is

very close to that expected from the velocity selector with a perfectly parallel beam.

The time-of-flight spectra for all four energies show a common feature at LAB angles which sample v = 3 scattered near 180° in the center-of-mass coordinate. The spectrum for F + p-H_2 at $\Theta = 30°$ is a good example. The faster peak is from v = 2. The slower peak corresponding to v = 3 has a fast shoulder which exceeds the exothermicity for the v = 3 product. In order to fit this, it was necessary to postulate another 'state' corresponding to HF(v = 3) formed from reactants with about 1 kcal/mole internal excitation. This state is labelled v = 3' in the figures. The possible sources for this extra energy are contributions to the reaction from spin-orbit excited $F(^2P_{1/2})$ or rotationally excited H_2. The $F(^2P_{1/2})$ state lies 1.16 kcal/mole above the $(^2P_{3/2})$ ground state and constitutes 21 percent of the F beam assuming thermal equilibrium at 920°K. $H_2(J = 2)$ is 1.03 kcal/mole above J = 0 and makes up 20 percent of the p-H_2 beam. The energy difference between these two alternatives is too small to be resolved in our TOF analysis. For n-H_2, the situation is somewhat different. The exothermicity used in our analysis includes the rotational energy of $H_2(J = 1)$, and the J = 2 state is only 0.68 kcal/mole higher. However, for n-H_2 the J = 3 population is comparable to the J = 2 population and reaction from this state may also be occurring. Indeed, the problematic peaks in the F+n-H_2 spectra could be better fit assuming 1.16 kcal/mole excitation for the v = 3' state than with 0.68 kcal/mole, and the higher value was used in the final fit. The selected value for the energy of

the v = 3' state therefore does not resolve the issue of the source of the excitation. The partial cross section results for each vibrational state presented below, on the other hand, support the hypothesis that v = 3' is from rotationally excited H_2.

Due to their large number, the best fit CM parameters are graphically displayed in figs. 14-17 rather than explicitly listed. The top graph in each of these figures is the most interesting, as it shows the vibrationally state-resolved CM differential cross sections given by eq.(4), as well as the summed differential cross section $\sum_i I_i(\theta)$. Center-of-mass velocity flux contour maps as a function of scattering angle are shown in figs. 18-21. These are contours of the function, $\sum_i uP_i(E(u),\theta)$, where P_i is defined in (1) and u is the HF product CM speed, plotted on a polar (u,θ) coordinate system. Below each map is a 3-D perspective which especially aids in visualizing the v = 3 forward peak. The contour maps, in general, confirm the qualitative trends inferred from the LAB angular distributions. The intensity of the v = 3 peak increases with collision energy and is higher for F + p-H_2 than for F + n-H_2 at the same energy. No backward peak for v = 3 is observed at any energy; the broad peak in the LAB angular distributions corresponding to the back-scattered for v = 3 results from sampling more v = 3 product at LAB angles nearly tangent to the v = 3 circle than at LAB angles closer to the F beam. It is clear, however, that the fraction of v = 3 scattered at $\theta \geq 90^\circ$ decreases with increasing energy. The maps show the v = 2 and v = 1 product is scattered predominantly in the backward hemisphere. The v = 2 product is backward-peaked at 1.84 kcal/mole and shows slight sideways peaking

at the higher energies. The sideways-peaking at higher energies was also seen in our our earlier investigations. The v = 1 product distributions, especially at 1.84 kcal/mole, are less reliable than those for the other states due to the low intensity of that state in the LAB frame. The v = 3' product is scattered entirely into the backward hemisphere. However, any forward-scattered v = 3' at CM angles $\leq 30^\circ$ would be closer than $\Theta = 8^\circ$ to the F beam. We could not obtain reliable TOF data at LAB angles smaller than 8° because of the high effusive HF background near the F beam. The possibility of a narrow forward v = 3' peak therefore cannot be ruled out. The contribution from this state is less reliably assessed at the higher energies where the v = 2 and v = 3 peaks are less well-resolved. In general the data was fit using as little v = 3' as possible, so all the fits, especially those at higher energy, probably underestimate the v = 3' contribution.

The kinetic energy distributions for each vibrational state as a function of scattering angle can be converted into HF rotational population distributions. The recoil energy, E, and the product rotational energy, E_R, for vibrational state i are related by

$$E=\Delta E+E_{coll}-E_i-E_R \qquad (7)$$
$$=E_m^i-E_R.$$

For a fixed CM angle, the recoil energy distribution is given by

$$P(E)=P(E_m^i-E_R), \qquad (8)$$

and

$$P_c(J)=P(E)dE/dJ \qquad (9)$$
$$=2B_i(J+1/2)P(E_m^i-B_iJ(J+1))$$

is the distribution function for the continuous variable J. Here B_i is the rotational constant for vibrational state i. The discrete populations can be derived by what amounts to a quasi-classical approximation:

$$P(J) = \int_{J}^{J+1} P_c(J')\, dJ' \tag{10}$$

Some sample population distributions are shown in fig. 22.

Figures 23-26 show plots of the fraction of available energy appearing as product rotation, $\langle F_J \rangle_i$, and the mean rotational quantum number, $\langle J \rangle_i$, as a function of CM scattering angle for each product vibrational state. These are obtained from the continuous recoil energy distributions by:

$$\langle F_J \rangle_i = 1 - \int_{0}^{E_m^i} \left(\frac{E}{E_m^i}\right) P_i(E,\theta)\, dE \tag{11}$$

$$\langle J \rangle_i = \int_{0}^{E_m^i} J_i(E)\, P_i(E,\theta)\, dE \tag{12}$$

Here $J_i(E)$ is implicitly defined by

$$E_m^i - E = B_i\, J(J+1). \tag{12b}$$

Note that $\langle F_J \rangle_i$ is a vibrationally state-specific quantity that indicates how much energy not already tied up in vibration occurs as product rotation. It is not the same as the commonly used symbol, $\langle f_R \rangle$, which is the fraction of the total available energy appearing as product rotation.

The validity of this procedure is limited by several factors that arise from our inability to resolve individual rotational states. There is a certain amount of ambiguity in transforming a continuous to a discrete distribution, and the shape of the discrete distribution is determined by the functional form assumed for the continuous distribution. Another problem is that the exothermicity used to derive the amount of product rotational energy depends on the reactant rotational state. The values used were for the dominant rotational state, just as in the fitting procedure for the CM scattering. Thus, for example, the contribution to reaction from the 20-25% of the n-H_2 beam in J = 0 is not treated explicitly. Nonetheless, the v = 2 rotational distributions at 1.84 kcal/mole are similar to the most recent chemiluminescence results at an average collision energy of 1.5 kcal/mole [8]. This indicates that, even if the individual state populations are not directly determined, our high resolution experimental results provide a reasonable estimate of the product rotational distributions as well. The relative heights and positions of the two v = 3 peaks observed in many of the TOF spectra are quite sensitive to the details of the assumed kinetic energy distribution and this state is therefore better characterized than the v = 2 state.

Several trends are apparent in the distributions. For each energy, the rotational distribution of the v = 3 state gradually shifts towards lower J at smaller CM angles, and more abruptly near 0°. A comparison of the three F + n-H_2 energies shows that, in general, <J> increases slightly for the v = 2 and v = 3 products as

the collision energy is raised. The only exception to this is in the neighborhood of 0° for v = 3 products where <J> decreases at higher collision energies. The F + n-H_2 distribution shows more rotational excitation than F + p-H_2 at the same collision energy. This agrees with earlier chemiluminescence work [7].

The plots of $\langle F_J \rangle$ for each F+n-H_2 collision energy show quite different behavior for the v = 2 and v = 3 states. Whereas $\langle F_J \rangle$ for v = 2 steadily increases with collision energy, for the v = 3 state at most angles it is less at 2.74 kcal/mole than at 1.84 kcal/mole; the v = 3 results at 3.42 kcal/mole are similar to those at 2.74 kcal/mole. This indicates that reactant translational energy is channeled more efficiently into rotational excitation of v = 2 product than v = 3 product.

We have also computed relative partial cross sections for each product state from the CM parameters. These are given by

$$\sigma_i = 2\pi \int_0^{\pi} I_i(\theta) \sin\theta d\theta \tag{13}$$

$$= \sum_{j=1}^{36} \int_{\theta_i}^{\theta_{i+1}} I_{ij}(\theta) \sin\theta d\theta \tag{14}$$

where

$$I_{ij}(\theta) = A_i \left(T_{ij} + T_{i(j+1)} \frac{\theta - \theta_j}{\theta_{j+1} - \theta_j} \right). \tag{15}$$

A factor of 2π is omitted for convenience as it has no bearing on the relative cross sections. T_{ij} is the angular intensity for state i which, as previously mentioned, is specified at 5° intervals. T_{i1} is at 0° and T_{i37} is at 180°. The result is given by

$$\sigma_i = T_{i1} + T_{i37} + \sum_{j=1}^{36} \frac{T_{i(j+1)} - T_{ij}}{\theta_{j+1} - \theta_j} (\sin\theta_{j+1} - \sin\theta_j). \qquad (16)$$

The relative total cross section is simply $\sigma = \sum_i \sigma_i$. The $v = 2$ and $v = 3$ partial cross sections should be accurate to within a few percent. They are quite insensitive to changes in the CM parameters that are large enough to adversely affect the calculated fits to the LAB data.

Comparing cross sections at different collision energies requires some care. The cross sections obtained by (16) must be multiplied by a correction factor which accounts for both the intensity of the LAB angular distribution and the reactant number densities at each collision energy. The derivation of this factor is not particularly enlightening and may be found elsewhere [54].

The corrected partial and total cross sections are shown in fig. 27. The normalized partial cross sections given by $\sigma_i' = \sigma_i/\sigma$ are shown in fig. 28. The total cross section for $F + p\text{-}H_2$ is indicated by the solid circle in fig. 27, and the partial cross sections are listed in table 2. The branching ratios for each state relative to $v = 2$ are given by σ_i/σ_2 and are listed in table 3. The trends shown here will be discussed in the next section.

One result worthy of immediate discussion, however, is the much larger $v = 3'$ partial cross section at 1.84 kcal/mole from $F + p\text{-}H_2$ than from $F + n\text{-}H_2$ (see table 3). The rotational population of the $n\text{-}H_2$ beam with $J \geq 2$ is about 5 percent, whereas the $p\text{-}H_2$ beam

is about 20% J = 2. Thus the larger amount of v = 3' from F + p-H_2 suggests that it is in fact due to the reaction of ground state F atoms with rotationally excited H_2. The results presented in the following paper on isotope effects substantiate this claim.

6. Discussion

6.1 Angular distributions and dynamical resonances

The angular distributions obtained in this study have shown a striking feature not seen in previous experimental work or in any scattering calculation. This feature, the v = 3 forward peak, was observed at every collision energy we studied, even below 1 kcal/mole where the back-scattered product began to disappear. The distributions also showed highly state-specific behavior. There was no sign of forward-peaked v = 2 product, although this state was side-ways-peaked at the highest collision energies.

The first important question to address is whether our unusual angular distributions can be described within the framework of classical mechanics. We can compare our results to angular distributions obtained in classical and quasi-classical trajectory calculations to see if there is any precedent for a forward v = 3 peak. The distributions obtained from classical calculations are not divided into product internal states. Thus one expects a state-specific effect to be less noticeable than in our experiment. The summed differential cross sections in figs. 14-17 can be directly compared to the angular distributions generated from classical trajectory calculations [15,16,18,73-75]. The experimental results still

show prominent forward peaks, although more scattering occurs in the backward hemisphere because the v = 2 state is predominantly backward-scattered. No classical calculation on any model surface for $F + H_2$ has resulted in an angular distribution of this form for collision energies below 12 kcal/mole. An early calculation by Muckerman showed some forward-scattered product at 2.50 kcal/mole [14], but this distribution decreased monotonically from 180° and showed no sign of a peak at 0°. A calculation on the same surface at 1.00 kcal/mole showed no scattering for $\theta < 30°$.

The differences between our results and trajectory studies are further emphasized by a comparison with quasi-classical calculations. In this method, the reactants are in an initially well-defined state n with vibrational action $(n + 1/2)h$, and a reactive trajectory is assigned to product vibrational state n' if its final action is in the range $[n'h, (n' + 1)h]$. This allows the determination of vibrationally state-resolved differential cross sections which can be more meaningfully compared with the experimental results. The calculations on M5 near 5 kcal/mole collision energy show all the HF vibrational states are dominated by backward-scattering, although a small amount of forward-scattered product occurs for each state [46,48]. The calculated distribution for v = 3 shows a large peak at 180° and a much smaller peak at 0°. This differs sharply from our v = 3 distributions at considerably lower energies which are dominated by forward-scattering and show no peak at 180°.

One can argue that it might be possible to construct a reasonable potential energy surface that can reproduce our results through quasi-classical calculations. After all, until now there has not been much incentive to devise a surface that results in substantial forward-scattered product. However, it seems unlikely that such high state-specificity could be achieved in a classical calculation. It would seem especially difficult to obtain more forward scattering in v = 3 than in the other vibrational states. The high impact parameter collisions necessary for forward scattering result in an effective centrifugal potential in the critical region of the potential energy surface. The v = 3 product is already 0.5 kcal/mole endothermic, and the centrifugal term plus the v = 3 adiabatic barrier should inhibit v = 3 formation from high impact parameter collisions. No such constraints apply to the lower HF vibrational states, as their production is sufficiently exothermic to overcome the possible effects of small exit barriers.

Ron et al. [48] have point out that exit barrier effects for $F + H_2$ tend to be de-emphasized in a forward quasi-classical calculation due to the inclusion of all trajectories resulting in a final vibrational action between 3h and 4h as v = 3 products. The v = 3 exit barrier is responsible for the delayed onset seen in the one-dimensional quantal calculation on the M5 surface in which no v = 3 product is seen until 0.05 eV above its energetic threshold. There is no sign of this effect in a forward quasi-classical calculation on M5 [22]. Exit barriers are much better accounted for in reverse quasi-classical calculations which start with a well defined

product vibrational state. Reverse q-c calculations of the reaction probability to form $H_2(v = 0)$ from $HF(v = 3)$ [23,76] indeed show a delayed onset very close to the predicted value of 2.4 kcal/mole for the $v = 3$ adiabatic barrier height [33]. A reverse calculation of the $H_2(v = 0)$ angular distribution from $HF(v = 3)$ shows much less forward scattering than the $HF(v = 3)$ distribution resulting from a forward calculation at the same total energy [48]. Thus, a more rigorous quasi-classical treatment in which all trajectories with final vibrational action outside a narrow range centered at 3.5h are discarded should result in a $v = 3$ distribution that is even more back-scattered than in the standard quasi-classical calculations.

It appears that the experimental results cannot be easily rationalized by classical considerations. However, the $v = 3$ forward peak is the type of highly state-specific effect that might be expected to result from dynamical resonances. Unfortunately, all the three-dimensional quantal calculations have been performed on M5 and predict that resonance effects will appear in the $v = 2$ state rather than in $v = 3$ [21,43-46]. This was explained in the Introduction as resulting from the magnitude of the $v = 3$ product adiabatic barrier on M5 which prevents decay of the quasi-bound state to $HF(v = 3)$. If our results are due to dynamical resonances, then the quasibound state preferentially decays to form $HF(v = 3)$ and the M5 potential energy surface must be modified to mitigate the effect of this barrier.

The v = 3 forward scattering is observed over a wide energy range. The three-dimensional quantal calculations show that this is the expected behavior for a dynamical resonance. The range of orbital angular momenta over which a resonance is accessible shifts to progressively higher values of $\underline{L}$ as the collision energy is raised. To first order, when a collision occurs with orbital angular momentum $\underline{L}$, the effective centrifugal term displaces the potential energy surface in the vicinity of the transition state and its confining barriers upwards by a constant energy given by $B\underline{L}(\underline{L} + 1)$, where B is an appropriate rotational constant. Pollak has determined the rotational constant for collinear FHH at the M5 v = 3 exit barrier to be 3 cm^{-1}. Suppose the true v = 3 adiabatic barrier height is 1.0 kcal/mole above the reactant zero point energy. For a collision with $\underline{L}$ = 15h, the barrier height will be increase by 2.4 kcal/mole for a total height of 3.4 kcal/mole relative to H_2 (v = 0). This is the highest collision energy we studied. An effect of similar magnitude is expected in the vicinity of the entrance channel barrier. At this energy $\underline{L}$ = 15h corresponds to an impact parameter of about 1Å. Thus the centrifugal effects for reasonable values of $\underline{L}$ are sufficiently large to allow trapping of the quasi-bound state over the energy range we studied.

Although the resonance-enhanced contribution at high $\underline{L}$ should result in a broader product angular distribution than would occur without a resonance, it does not seem likely that an intense forward peak would result simply from collisions at impact parameters near 1 Å. In a classical trajectory study by Blais and Truhlar on

$F + D_2$ [75], angular distributions were obtained at fixed values of the impact parameter. At 6 kcal/mole collision energy, the distributions were backward-peaked at b = 0.5Å and sideways-peaked near 90° at b = 1.45Å, but no product was observed at $\theta < 45°$ even at the higher impact parameter. However, the forward scattering can be significantly enhanced if the resonance lifetime is a non-negligible fraction of the rotational period of the complex. Assuming a rotational constant of 3 cm^{-1}, the rotational period will be 5.5×10^{-13} sec for a collision with $\underline{L}$ = 10h. If the lifetime of the complex is 25% of the rotational period, and this is used as the time delay, τ, due to the resonance, then the energy width of the resonance given by $4h/\tau$ is 0.02 eV or 0.4 kcal/mole. This is somewhat broader than the resonances seen in the collinear calculations, as would be expected since additional bending vibrational degrees of freedom may cause the wells to be shallower and the quasi-bound state lifetime to be shorter. This energy width is comparable to that obtained by Schatz and Kuppermann in a three-dimensional close-coupling calculation for an $\underline{L} = 0$ resonance in $H + H_2$ [77].

The scattering near $\theta = 0°$ is further enhanced by effects associated with angular momentum conservation. Our kinetic energy analysis reveals that most of the v = 3 product is formed in $J \leq 2$ at 1.84 kcal/mole and $J \leq 3$ at the higher energies. This means that for a high orbital angular momentum collision that forms v = 3 product, $\underline{L}$ is largely conserved and appears as $\underline{L}'$, the product orbital angular momentum. The entire reactive encounter therefore occurs in a single plane perpendicular to $\underline{L}$. For truly long-lived complexes that survive

for several rotational periods, the condition $\underline{L} = \underline{L}'$ results in a symmetric angular distribution peaking strongly at 0° and 180° [78]. This occurs because all orientations of $\underline{L}$ perpendicular to the reactant relative velocity vector are equally likely. Thus, while the scattering in each plane perpendicular to $\underline{L}$ for a long-lived complex is isotropic, the sum over all scattering planes results in an angular distribution that approaches $(\sin\theta)^{-1}$ in the limit of large $\underline{L}$. The presence of only a single peak at 0° without a backward peak at 180° in our results indicates that the resonance survives a fraction of a rotation at most. This upper bound is consistent with the calculation in the preceding paragraph. Even if the scattering in a single plane is anisotropic, the $(\sin\theta)^{-1}$ form factor due to the symmetry of the angular momentum vector with repect to the relative velocity should still apply to the large $\underline{L}$ collisions that access the resonance. If the complex survives for a fraction of a rotation before dissociating, the resulting HF product should be preferentially scattered in the range $0° \leq \theta \leq 90°$ which will lead to a peak at 0° in the differential cross section. For collisions that do not strictly conserve $\underline{L}$, the form factor is different and does not provide nearly as much amplification near 0° and 180° [78]. The HF products formed with $J \geq 2$ are, for the most part, the result of collisions in which $\underline{L}$ is not strictly conserved, and the angular distributions for these states might not be expected to be as intense near $\theta = 0°$ as for HF states with $J < 2$. This may explain the abrupt narrowing of the $v = 3$ rotational distributions observed near 0°.

The trend in the three F + n-H_2 contour maps showing enhanced forward scattering of the v = 3 product as the collision energy is raised is reasonable in light of the above considerations. At higher translational energies the resonance is accessed by higher orbital angular momentum collisions which result not only in a stronger correlation between $\underline{L}$ and $\underline{L}'$, but also in a quasi-bound state with a shorter rotational period. If the lifetime of the quasi-bound state remains the same, the complex formed at higher $\underline{L}$ can rotate more before dissociating and increase the amount of HF product scattered into the forward hemisphere. This effect might be countered to some extent by the shorter lifetime of the resonance formed at high $\underline{L}$ as the repulsive centrifugal potential begins to wash out the adiabatic well supporting the quasi-bound state. At sufficiently high energy, the trend towards increased forward scattering should reverse as the contribution from resonances becomes less important. We do not seem to have reached this point in our experiment.

6.2 Implications for the potential energy surface.

The discussion so far has shown that the major features of the HF(v = 3) angular distributions can be explained in terms of dynamical resonances. However, significant differences remain between our results and the quantal calculations on M5 which are most likely due to deficiencies in the M5 surface, some of which were pointed out in the Introduction. The detailed nature of our experimental results allows us to propose further specific changes in the critical region of the surface. One modification suggested above is that the v = 3 adiabatic

exit barrier should be reduced so that the low energy resonance can decay to HF(v = 3). Additional support for this, independent of the existence of resonances, comes from our low energy experiments. The v = 3 exit barrier is responsible for the delayed onset of v = 3 product seen in the collinear and three-dimensional quantal calculations on M5 in which virtually no v = 3 product is predicted below 1.2 kcal/mole collision energy. We, however, observe v = 3 product at collision energies as low as 0.7 kcal/mole. It is true that the small size of the v = 3 Newton circle at low collision energies increases our sensitivity for detecting that state in a LAB angular measurement relative to the v = 2 state [70], but this cannot fully account for the discrepancy between our results and the theoretically predicted dominance of the v = 2 product at low energies. One should note that quantal collinear calculations on slightly different potential energy surfaces show markedly different behavior. Connor's calculation on the Muckerman 1 surface [15], for example, shows no sign of a delayed onset for v = 3, and it shows a sharp spike in the v = 3 reaction probability just above the threshold for v = 3 product [26]. The M1 surface is, however, deficient in that its exothermicity is too low by 3 kcal/mole [18].

The presence of forward scattering at collision energies as low as 0.7 kcal/mole indicates that dynamical resonances are evident at much lower collision energies than in calculations on M5. The calculations predict that the changes in the angular distribution due to the resonance should appear only at collision energies higher than 2 kcal/mole [31,44]. This happens because the lowest energy $\underline{L}$ = 0

resonance on M5 occurs at approximately 1.7 kcal/mole above the reactant zero point energy [80]. Suppose, however, that the correct surface has a deeper or wider adiabatic well than M5 so that the $\underline{L} = 0$ resonance is below our lowest collision energy. In this case even at the lowest energy only nonzero $\underline{L}$ collisions could access the resonance resulting in sideways and forward scattering such as we observed. In fact, it is possible for the energy of the collinear quasi-bound state to be below the reactant zero point energy. Under these circumstances, the resonance will not appear in a collinear calculation, but it will show up in a three-dimensional calculation.

The $v = 2$ angular distributions also merit some discussion. The sideways-peaked $v = 2$ product at 2.74 and 3.42 kcal/mole is similar to what was seen in the previous crossed molecular beams studies of $F + H_2$ [49,50]. The earlier assignment of the sideways-peaking to resonance effects seems somewhat doubtful in light of the current results. It might seem that the quasi-bound state responsible for the $v = 3$ forward peak should be coupled to some extent with the angular distribution of HF($v = 2$). However, Connor's collinear calculation on M1 shows that the resonance just above the $v = 3$ threshold decays almost entirely to $v = 3$ product; similar structure occurs in the $v = 2$ reaction probability curve but it is less intense by at least a factor of 30. In any case, the considerably different energy dependences of the $v = 2$ sideway-peaking and the $v = 3$ forward-peaking make it seem unlikely that the same quasi-bound state decays competitively to both product states. The $v = 2$ broadening and sideways-peaking may be a classical effect not seen on M5 because the bending force constant

near the potential energy barrier in the entrance channel is too high. Although the ab initio PES(12) does not yield accurate values for the potential energy barrier and the exothermicity, it is expected to give more reliable estimate of the bending force constant, and does indeed give a lower bending force constant than M5. Truhlar et al. [79] have recently developed a potential energy surface with a lower entrance channel barrier and an improved bending potential.

6.3 Integrated cross sections

Our F + n-H_2 results show that the total reaction cross section increases with collision energy, although it appears to rise less steeply above 2.74 kcal/mole. This agrees qualitatively with classical and quantal calculations on M5. Each method used to calculate the total cross section gives somewhat different results [44]. The smaller slope of the total cross section vs. energy above 2.74 kcal/mole is most evident in the J_z-conserving quantal calculation [31,43].

The collision energy dependence of the partial and normalized cross sections in figs. 27 and 28 and the branching ratios in table 3 can be summarized as follows. The partial cross section for each product vibrational state increases as the collision energy is raised, but the (v = 3)/(v = 2) branching ratio decreases whereas the (v = 1)/(v = 2) ratio increases. The normalized cross section results show the v = 1 product rising at the expense of v = 3 while the fraction of v = 2 product remains relatively constant. The experimental results for the energy dependence of the (v = 3)/(v = 2) ratio not surprisingly do not agree with quantal calculations on M5 [43,44]. These predict a steadily

increasing (v = 3)/(v = 2) ratio up to collision energies of 0.5 eV. This discrepancy is due largely to the high v = 3 exit barrier on M5, since the v = 3 channel should open up rapidly in the energy range near the barrier. In theoretical studies, this exit barrier also prevents the quasi-bound state from decaying to v = 3 at low collision energies.

Our results for the partial cross sections and branching ratios can also be compared to the previous results obtained with chemical laser (CL) and IR chemiluminescence (IC) techniques. It should be noted that we can independently vary the reactant translational and rotational energy, whereas in the other studies in which the reactant temperature is varied, translation and rotation are simultaneously affected. Nonetheless, our results are in qualitative agreement with the CL studies and, to a lesser extent, with the IC work.

There appears to be considerable variation in the value of the (v = 3)/(v = 2) branching ratio for F + n-H_2 at 300°K among the IC and CL studies ranging from 0.48 [4] to 0.63 [81]. Our result of 0.68 at 1.84 kcal/mole is close to the high value. Although the temperature corresponding to a mean collision energy of 1.84 kcal/mole is about 600°K, our value is in the correct range. It might indeed be expected to be at the high end of the spectrum of values if the variation of this branching ratio in the IC and CL work is due to partial vibrational relaxation, since in our molecular beam experiment the products cannot vibrationally relax through secondary collisions.

Our results concerning the translational energy dependence of the (v = 3)/(v = 2) and (v = 1)/(v = 2) branching ratios agree with the CL work of Coombe [4]. In an IC study by Perry [6] and a more recent one by Barnes [8], the (v = 1)/(v = 2) ratio increased with temperature or collision energy but the (v = 3)/(v = 2) ratio remained constant.

6.4 Effect of reactant rotation

The contour maps for F + n-H_2 and F + p-H_2 at 1.84 kcal/mole in figs. 18 and 19 and the LAB angular distributions in fig. 5 show that there is considerably less forward peaking of the HF(v = 3) product from H_2(J = 1) than from H_2(J = 0). Resonance effects appear to be less pronounced when starting from H_2(J = 1). This may be an indication of the collinear nature of the resonance state and of how reactant rotation is coupled to the degrees of freedom of the reaction intermediate.

It is possible for H_2 rotation to result in bending excitation of the FH_2 complex. This process would be facilitated by a small energy mismatch between the 120cm^{-1} of rotation in H_2(J = 1) and $\omega^{\ddagger}$, the bending frequency of the transition state. For M5, $\omega^{\ddagger}$ = 452cm^{-1}, but on Truhlar's new surface, $\omega^{\ddagger}$ = 76cm^{-1} [79]. Bending motion in the FH_2 complex might be expected to lead to an overall reduction of resonance effects; the lifetime of a quasi-bound state formed with bending excitation would be shortened by any coupling between bending and the reaction coordinate. Our results are therefore consistent with at least some coupling between H_2 rotation and bending motion in the reaction intermediate.

Although resonance effects are less pronounced with $H_2(J = 1)$, the direct reaction appears to be enhanced with $H_2(J = 1)$ at 1.84 kcal/mole. The partial cross sections for $v = 3$ and $v = 2$ are slightly higher for F + n-H_2 than for F + p-H_2 as is the relative total cross section. Classical trajectory calculations on several potential energy surfaces have also predicted that $H_2(J = 1)$ is more reactive than $H_2(J = 0)$ in this energy range [16,18,73]. If the $v = 3$ and $v = 3'$ partial cross sections are summed, then the $(v = 3)/(v = 2)$ branching ratio is slightly higher for F + p-H_2 than for F + n-H_2 at the same collision energy. This agrees with previous experimental work in which the two reactions were studied at the same temperature using the IC and CL techniques [5,7].

6.5 Reactivity of $F(^2P_{1/2})$

The reaction of $F(^2P_{1/2})$ with H_2 does not correlate to ground state products [82], but semi-classical calculations have predicted a small contribution to reaction via a non-adiabatic transition in the entrance channel [83,84]. Close-coupling calculations of inelastic $F(^2P_{1/2})+H_2$ scattering have shown that the near resonant process

$$F(^2P_{1/2}) + H_2(J = 0) \rightarrow F(^2P_{3/2}) + H_2(J = 2)$$

is about an order of magnitude more efficient than any other electronic quenching process [85,86]. This might lead one to propose that if quenching is followed by reaction on the ground state surface with the newly formed $H_2(J = 2)$, then the reactivity of $F(^2P_{1/2})$ should be

higher with p-H_2 than with n-H_2 because of the larger J = 0 population in p-H_2. However, it is not likely that this process can lead to more product than the reaction between $F(^2P_{3/2})$ and $H_2(J = 2)$ already in the beam. Since our data can be fit even if the reactivity of $H_2(J = 2)$ with $F(^2P_{3/2})$ is one half that of $H_2(J = 0)$ and without assuming any contribution to the reaction from $F(^2P_{1/2})$, the contribution from $F(^2P_{1/2})$ must be very small. The F + n-H_2 results clearly indicate as well that $F(^2P_{1/2})$ + $H_2(J = 1)$ does not produce an appreciable amount of product. The angular distributions for the reaction of F + HD (J=0), which will be discussed in the following paper, also do not show any trace of product from $F(^2P_{1/2})$. If $F(^2P_{1/2})$ were to contribute to the formation of products, the additional 1.16 kcal/mole of available energy would be partially channeled into translation and would easily be detected in this high resolution experiment.

7. Conclusion

The vibrationally state-resolved differential cross sections for F + H_2 presented here represent the most detailed experimental study in reaction dynamics to date. The results, at the very least, provide a database which will greatly aid in the development of a potential energy surface of chemical accuracy for this reaction. More significantly, explaining the results in terms of dynamical resonances provides a direct link between the details of the strong coupling region of the potential energy surface and the asymptotic scattering states

observed in our experiment. Within the resonance framework, the results point to specific modifications to be made to the critical region of the M5 surface. The results of our studies on the F + HD and F + D_2 reactions reported in the following paper will further substantiate the importance of dynamical resonances in this system.

8. References

[1] J.H. Parker and G.C. Pimentel, J. Chem. Phys. 51 (1) (1969) 91.

[2] J.C. Polanyi and D.C. Tardy, J. Chem. Phys. 51 (12) (1969) 5717; K.G. Anlauf, P.E. Charters, D.S. Horne, R.G. Macdonald, D.H. Maylotte, J.C. Polanyi, W.J. Skrlac, D.C. Tardy, and K.B. Woodall, J. Chem. Phys. 53 (10) (1970) 4091.

[3] J.C. Polanyi and K.B. Woodall, J. Chem. Phys. 57 (4) (1972) 1574.

[4] R.D. Coombe and G.C. Pimentel, J. Chem. Phys. 59 (1) (1973) 251.

[5] R.D. Coombe and G.C. Pimentel, J. Chem. Phys. 59 (3) (1973) 1537.

[6] D.S. Perry and J.C. Polanyi, Chem. Phys. 12 (1976) 419.

[7] D.J. Douglas and J.C. Polanyi, Chem. Phys. 16 (1976) 1.

[8] J. Barnes, Ph. D. Thesis, University of Toronto, 1983.

[9] T.P. Schafer, P.E. Siska, J.M. Parson, F.P. Tully, Y.C. Wong, and Y.T. Lee, J. Chem. Phys. 53 (1970) 3385.

[10] E. Wurzberg and P.L. Houston, J. Chem. Phys. 72 (9) (1980) 4811.

[11] R.F. Heidner III, J.F. Bott, C.E. Gardner, and J.E. Melzer, J. Chem. Phys. 72, (9) (1980) 4815.

[12] C.F. Bender, P.K. Pearson, S.V. O'Neill, and H.F. Schaefer III, J. Chem. Phys. 56 (9) (1972) 4626; Science, 176 (1972) 1412.

[13] G. DiLonardo and A.E. Douglas, Can. J. Phys. 51 (1973) 434.

[14] S. Sato, J. Chem. Phys. 23 (3) 592 (1955); 23 (12) (1955) 2465.

[15] J.T. Muckerman, J. Chem. Phys. 54 (3), 1155 (1971); 56 (6) (1972) 2947.

[16] J.C. Polanyi and J.L. Schreiber, Discuss. Faraday Soc. 62 (1977) 267.

[17] J.C. Polanyi and W.H. Wong, J. Chem. Phys. 51 (1969) 1439.

[18] J.T. Muckerman, in Theoretical Chemistry - Advances and Perspectives, edited by H. Eyring and D. Henderson (Academic Press, New York, 1981), Vol. 6A, 1-77.

[19] P.D. Mercer and H.O. Pritchard, J. Phys. Chem. 63 (1959) 1468.

[20] J.T. Muckerman and M.B. Faist, J. Phys. Chem. 83 (1) (1979) 79.

[21] W. Jakubetz and J.N.L. Connor, Discuss. Faraday Soc., 62 (1977) 327.

[22] D.G. Truhlar and A. Kuppermann, J. Chem. Phys. 52 384 (1970); 56 (5) (1972) 2232; S-F. Wu and R.D. Levine, Mol. Phys. 22 (1971) 991.

[23] G.C. Schatz, J.M. Bowman, and A. Kuppermann, J. Chem. Phys. 63 (2) (1975) 674.

[24] A. Kupperman and J.A. Kaye, J. Phys. Chem. 85 (1981) 1969.

[25] A. Kuppermann, in Potential Energy Surfaces and Dynamics Calculations, edited by D.G. Truhlar (Plenum Publishing Corporation, New York, 1981); V. Babamov and A. Kuppermann, J. Chem. Phys. 77 (4) (1982) 1891.

[26] J.N.L. Connor, W. Jakubetz, and J. Manz, Mol. Phys. 35 (5) (1978) 1301; 39 (4) (1980) 799.

[27] P.R. Brooks, R.F. Curl and T.C. Maguire, Ber. Bunsenges. Phys. Chem. 96 (1982) 401.

[28] P. Arrowsmith, F.E. Bartoszek, S.H.P. Bly, T. Carrington, Jr., P.E. Charters, and J.C. Polanyi, J. Chem. Phys. 73 (11) (1980) 5895.

[29] H.-J. Foth, J.C. Polanyi, and H.H. Telle, J. Phys. Chem. 86 (26) (1982) 5027.

[30] One notable exception, although it applies to photodissociation and not reactive scattering: D.G. Imre, J.L. Kinsey, R.W. Field, and D.H. Katayama, J. Phys. Chem. 86 (1982) 2564.

[31] R.E. Wyatt, J.F. McNutt, and M.J. Redmon, Ber. Bunsenges. Phys. Chem. 86 (1982) 437.

[32] S-F. Wu, R.B. Johnson, and R.D. Levine, Mol. Phys. 25 (1973) 609.

[33] S.L. Latham, J.F. McNutt, R.E. Wyatt, and M.J. Redmon, J. Chem. Phys. 69 (8) (1978) 3746.

[34] E.Pollak, M.S. Child, and P. Pechukas, J. Chem. Phys. 72 (3) (1980) 1669.

[35] E. Pollak, J. Chem. Phys. 74 (10) (1981) 5586.

[36] E. Pollak and M.S. Child, Chem. Phys. 60 (1981) 23.

[37] E. Pollak, J. Chem. Phys. 76 (12) (1982) 5843.

[38] R.A. Marcus, J. Chem. Phys. 45 (12) (1966) 4493; 45 (12) (1966) 4500.

[39] A. Kuppermann, J.A. Kaye, and J.P. Dwyer, Chem. Phys. Lett. 74 (2) (1980) 357.

[40] J.M. Launay and M. LeDourneuf, J. Phys. B 15 (1982) L455.

[41] J. Romelt, Chem. Phys. 79 (1983) 197.

[42] T.C. Thompson and D. G. Truhlar, J. Phys. Chem. 88 (1984) 210.

[43] M.J. Redmon and R.E. Wyatt, Chem. Phys. Lett. 63 (2) (1979) 209.

[44] M. Baer, J. Jellinek, and D.J. Kouri, J. Chem. Phys. 78 (6) (1983) 2962.

[45] R.W. Emmons and S.H. Suck, Phys. Rev. A 27 (4) (1983) 1803.

[46] R.B. Walker, N.C. Blais, and D.G. Truhlar, J. Chem. Phys 80 (11) (1984) 246.

[47] N.C. Blais and D.G. Truhlar, J. Chem. Phys. 76 (9) (1982) 4490.

[48] S. Ron, M. Baer, and E. Pollak, J. Chem. Phys. 78 (7) (1983) 4414.

[49] R.K. Sparks, C.C. Hayden, K. Shobatake, D.M. Neumark, an Y.T. Lee, in Horizons in Quantum Chemistry, edited by K. Fukui and B. Pullman (D. Reidel Publishing, Co., 1980) 91-105.

[50] C.C. Hayden, Ph.D. Thesis, University of California, Berkeley, 1982.

[51] D. M. Neumark, A. M. Wodtke, G. N. Robinson, C. C. Hayden, and Y.T. Lee, Phys. Rev. Lett. (in press).

[52] Y.T. Lee, J.D. McDonald, P.R. LeBreton, and D.R. Herschbach, Rev. Sci. Instrum. 40 (11) (1969) 1402.

[53] R.K. Sparks, Ph. D. Thesis, University of California, Berkeley, 1980.

[54] D.M. Newmark, Ph. D. Thesis, University of California, Berkeley, 1984.

[55] Oil filtrations system, Edwards High Vacuum, Inc., El Segundo, CA.

[56] R. van Steyn and N.F. Verster, J. Phys. E 5 (1972) 691.

[57] Hysteresis synchronous motor, TRW Globe Motor Div., Dayton, Ohio.

[58] Servometer Corp., Cedar Grove, N. J.

[59] The Barden Corp., Danbury, CT.

[60] OPB970 slotted optical switch, TRW Optron, Carrollton, TX.

[61] Beam Dynamics, Minneapolis, MN.

[62] Ted Pella, Inc., Tustin, CA.

[63] Semco, Inc., No. Hollywood, CA.

[64] J.E. Pollard, Ph. D. Thesis, University of California, Berkeley, 1983.

[65] Series 265, Granville-Phillips Company, Boulder, CO.

[66] Bulova Electronics Division, Woodside, N.Y.

[67] M. Vernon, Lawrence Berkeley Laboratory Report LBL-12422, 1981.

[68] K. Skold, Nucl. Instrum. Methods, 63 (1968) 114; G. Comsa, R. David, and B.J. Schumacher, Rev. Sci. Instrum. 52 (6) (1981) 789.

[69] J.E. Pollard, D.J. Trevor, Y.T. Lee, and D. A. Shirley, J.Chem. Phys. 77 (10) (1982) 4818.

[70] T.T. Warnock and R.B. Bernstein, J. Chem. Phys. 49 (4) (1968) 1878.

[71] H.U. Hostettler and R.B. Bernstein, Rev. Sci. Instrum. 31 (8) (1960) 872.

[72] D.R. Frankl, Rev. Sci. Instrum. 45 (11) (1974) 1375.

[73] R.L. Jaffe and J.B. Anderson, J. Chem. Phys. 54 (5) (1971) 2224.

[74] R.L. Wilkins, J. Chem. Phys. 57 (2) (1972) 912.

[75] N.C. Blais and D.G. Truhlar, J. Chem. Phys. 58 (3) (1973) 1090.

[76] S.C. Leasure and J.M. Bowman, Chem. Phys. Lett. 39 (3) (1976) 462.

[77] G.C. Schatz and A. Kuppermann, Phys. Rev. Lett. 35 (19) (1975) 1266.

[78] W.B. Miller, S.A. Safron, and D.R. Herschbach, Discuss. Faraday Soc. 44 (1967) 108.

[79] D.G. Truhlar, B.C. Garrett, and N.C. Blais, J. Chem. Phys. 80(1), (1984) 232.

[80] E. Pollak and R.E. Wyatt, J. Chem. Phys. 77 (5) (1982) 2689.

[81] M.J. Berry, J. Chem. Phys. 59 (12) (1973) 6229.

[82] J.T. Muckerman and M.D. Newton, J. Chem. Phys. 56 (6) (1972) 3191.

[83] J.C. Tully, J. Chem. Phys. 60 (8) (1974) 3042.

[84] A.Komornicki, K. Morokuma, and T.F. George, J. Chem. Phys. 67 (11) (1977) 5012.

[85] F. Rebentrost and W.A. Lester, Jr., J. Chem. Phys. 67 (7) (1971) 3367.

[86] R.E. Wyatt and R. B. Walker, J. Chem. Phys. 70 (3) (1979) 1501.

Table 1

Source conditions for the angular scans

Reaction	H_2 source temp(°K)	H_2 source pressure (psig)	beam velocity ($x10^4$cm/s)	collision energy (kcal/mole)	scale factor
F+p-H_2(P)	113	40	15.45	0.68	1.60
F+n-H_2(N)	119	40	15.45	0.68	0.58
P	167	50	19.67	1.00	1.71
N	180	50	19.67	1.00	0.88
P	212	65	22.92	1.30	0.98
P	307	80	27.83	1.84	0.93
N	320	80	27.83	1.84	1.00
N	473	95	34.51	2.74	1.03
N	578	110	38.80	3.42	1.08

Table 2

Relative cross sections for F+p-H_2, 1.84 kcal/mole

(units are same as fig. 27)

v=1	36.5
v=2	185.1
v=3	125.2
v=3'	8.9

Table 3

$F+H_2$ branching ratios

	F+p-H_2 1.84 kcal/mole	F+n-H_2 1.84 kcal/mole	F+n-H_2 2.74 kcal/mole	F+n-H_2 3.42 kcal/mole
v=1/v=2	0.20	0.21	0.23	0.33
v=3/v=2	0.68	0.67	0.53	0.48
v=3'/v=2	0.048	0.015	0.016	0.016

Figure captions

Fig. 1 Top cross-sectional view of the beam sources and collision region. 1) H_2 source(70 μ orifice) 2) coaxial heater cable 3) liquid nitrogen contact 4) 18 mil skimmer 5) supersonic H_2 beam 6) F oven 7) F beam 8) velocity selector 9) differential chamber cold shield 10) radiation shield 11) mounting block for velocity selector 12) 150 Hz tuning fork chopper 13) UHV rotatable mass spectrometric detector

Fig. 2 LAB angular distribution for F+p-H_2, 1.84 kcal/mole, and Newton diagram. Both the data and calculated LAB distributions are shown(● data, —— total calculated, — --- — v = 1, —— —— —— v = 2, ------ v = 3, —— - —— v = 3').

Fig. 3 F+n-H_2 LAB angular distributions at various collision energies.

Fig. 4 F+p-H_2 LAB angular distributions at various collision energies. The distributions labelled (N) are for F+n-H_2.

Fig. 5 LAB angular distributions for F+H_2(J = 0) and J = 1. The innermost and next smallest Newton circles are for HF(v = 3) product from H_2(J = 0) and J = 1, respectively.

Fig. 6 Time-of-flight spectra for F+p-H_2, 1.84 kcal/mole. (Δ data, ——— total calculated, —— --- —— v = 1, —— —— —— v = 2, ------ v = 3, —— - —— v = 3'). The solid line is not shown when it obscures a vibrational state.

Fig. 7 Time-of-flight spectra for F+n-H_2, 1.84 kcal/mole.

Fig. 8 Time-of flight spectra for F+n-H_2, 3.42 kcal/mole.

Fig. 9 TOF spectra for F+H_2, 1.84 kcal/mole, at $\Theta = 8^\circ$, showing effusive contribution observed close to the F beam. Top graph: solid line is raw data, dotted line is scaled TOF spectrum taken at $\Theta = 4^\circ$(see text). Bottom graph shows result of subtracting the effusive background.

Fig.10 LAB angular distribution for F+n-H_2, 1.84 kcal/mole, showing computer-generated fit to the LAB data(● data, ——— total calculated, —— --- —— v=1, —— —— —— v=2, ------ v=3, —— - —— v=3').

Fig. 11 LAB angular distribution for F+n-H_2, 2.74 kcal/mole, showing computer-generated fit to the LAB data.

Fig. 12 LAB angular distribution for F+n-H_2, 3.42 kcal/mole, showing computer-generated fit to the LAB data.

Fig. 13 Energetics of the $F+H_2$ reaction. All values are in kcal/mole.

Fig. 14 Best fit CM parameters for $F+p-H_2$, 1.84 kcal/mole. (——— total(top graph only), —— --- —— v=1, —— —— —— v=2, ------ v=3, —— - —— v=3').

Fig. 15 Best-fit CM parameters for $F+n-H_2$, 1.84 kcal/mole.

Fig. 16 Best-fit CM parameters for $F+n-H_2$, 2.74 kcal/mole.

Fig. 17 Best-fit CM parameters for $F+n-H_2$, 3.42 kcal/mole.

Fig. 18 Center-of-mass velocity flux contour map for $F+p-H_2$, 1.84 kcal/mole, with three-dimensional perspective.

Fig. 19 Center-of-mass velocity flux contour map for $F+n-H_2$, 1.84 kcal/mole, with three-dimensional perspective.

Fig. 20 Center-of-mass velocity flux contour map for $F+n-H_2$, 2.74 kcal/mole, with three-dimensional perspective.

Fig. 21 Center-of-mass velocity flux contour map for $F+n-H_2$, 3.42 kcal/mole, with three-dimensional perspective.

Fig. 22 Sample rotational distributions for HF product at various CM scattering angles.

Fig. 23 Plots of $\langle F_J \rangle$ and $\langle J \rangle$ (see text) for the product vibrational states as a function of CM scattering angle, for $F+p-H_2$, 1.84 kcal/mole
(—— --- —— v=1, —— —— —— v=2, ------ v=3).

Fig. 24 $\langle F_J \rangle$ and $\langle J \rangle$ for $F+n-H_2$, 1.84 kcal/mole. The curves stop its angles where the intensity is zero.

Fig. 25 $\langle F_J \rangle$ and $\langle J \rangle$ for $F+n-H_2$, 2.74 kcal/mole.

Fig. 26 $\langle F_J \rangle$ and $\langle J \rangle$ for $F+n-H_2$, 3.42 kcal/mole.

Fig. 27 Relative cross sections for $F+n-H_2$ as function of collision energy(——— total, —— --- —— v=1, —— —— —— v=2, ------ v=3, —— - —— v=3'). The solid circle is the relative total cross section for $F+p-H_2$, 1.84 kcal/mole.

Fig. 28 Normalized cross sections for $F+n-H_2$ as function of collision energy.

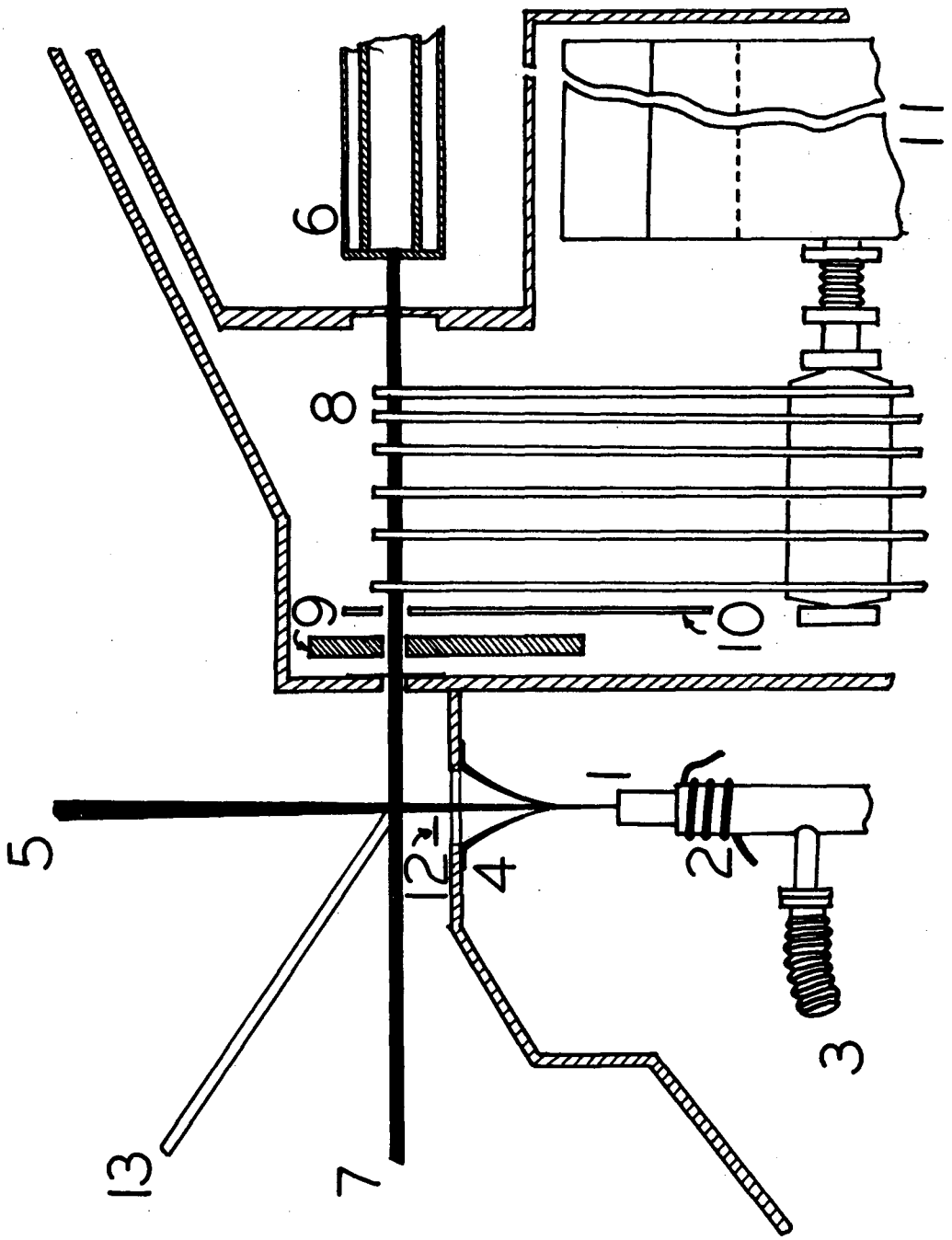

XBL 835-9895

Fig. 1

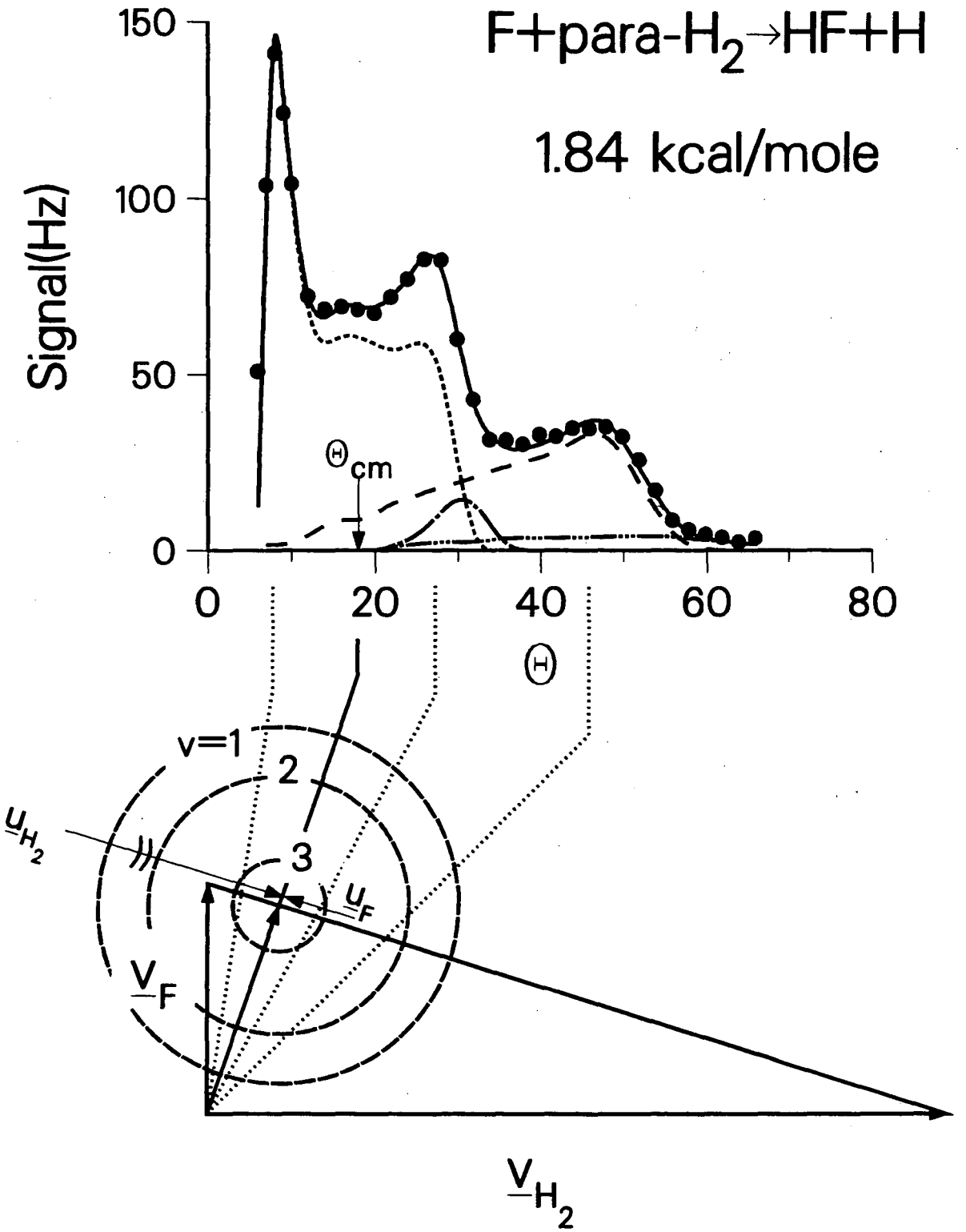

XBL 841-54

Fig. 2

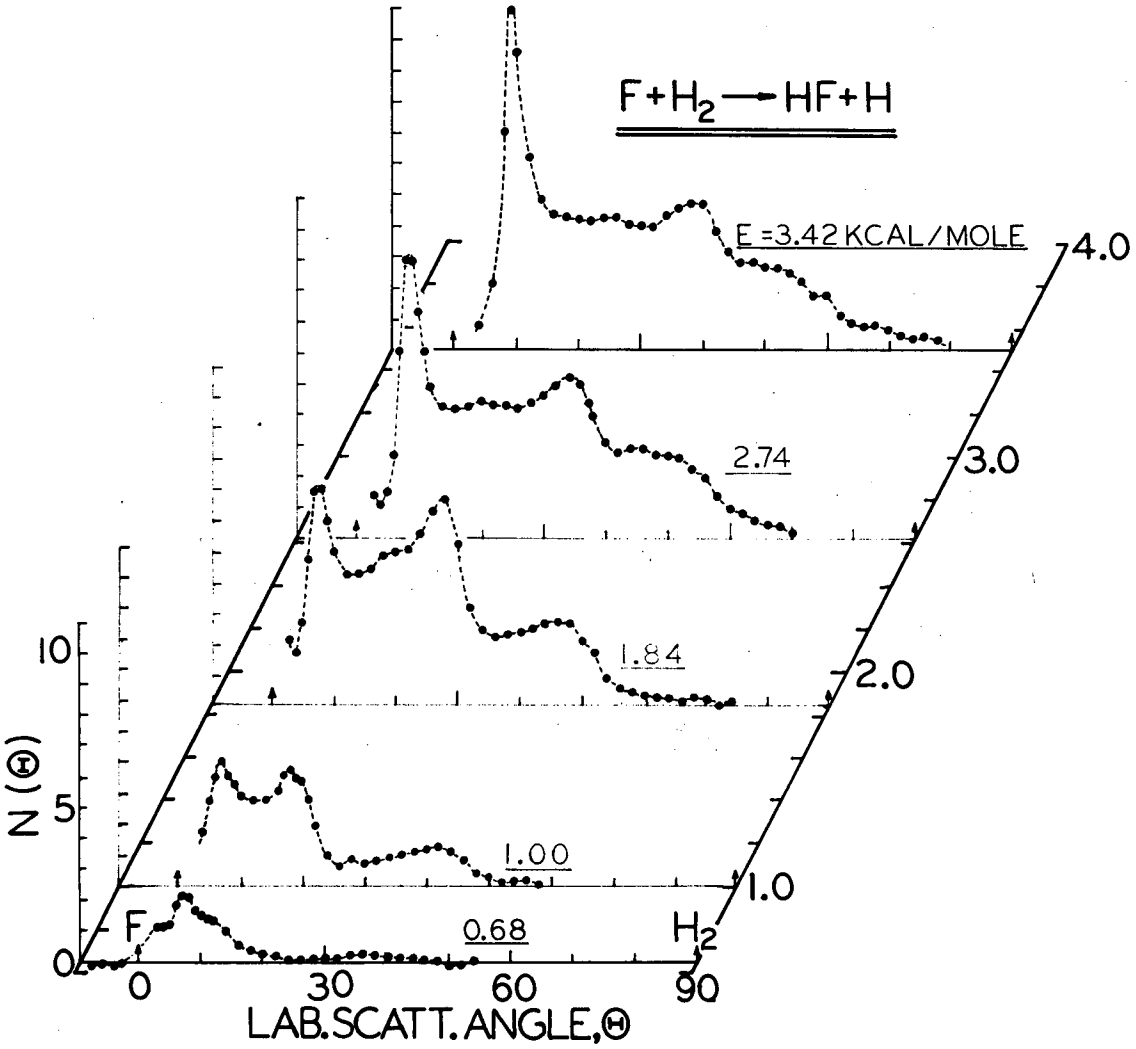

CBB 835-4115A

Fig. 3

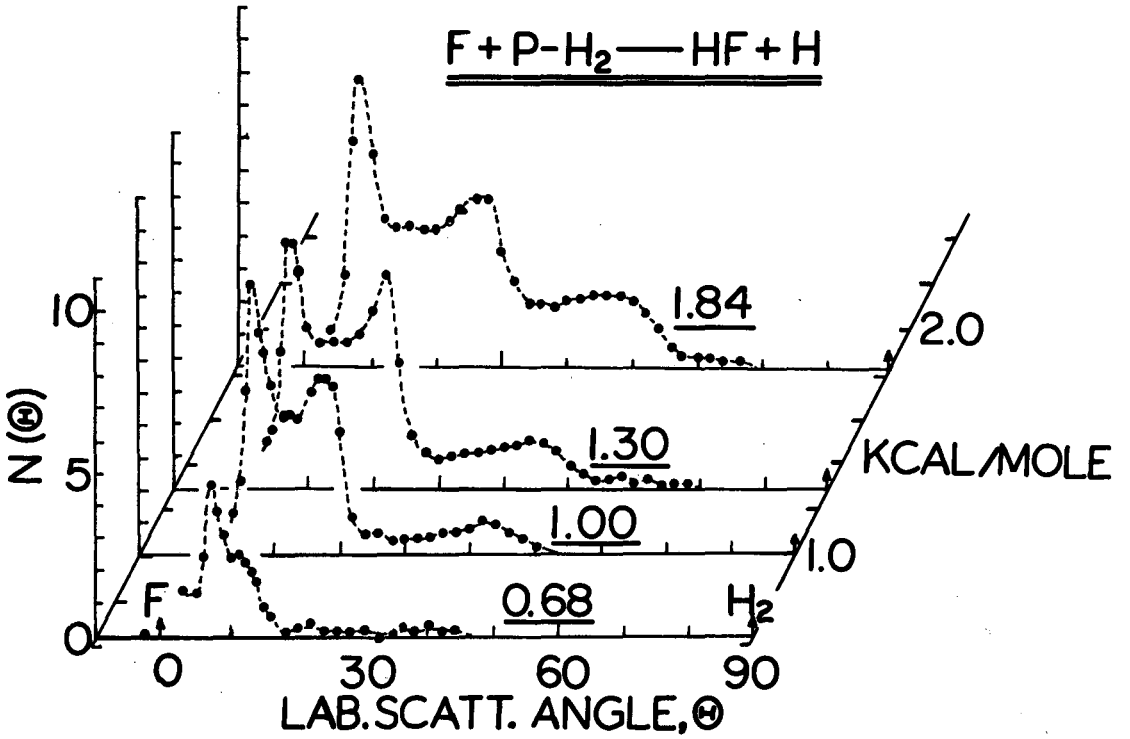
F + P-H2 — HF + H
10
5
0
N(Θ)
1.84
1.30
1.00
0.68
2.0
1.0
KCAL/MOLE
F
H2
0
30
60
90
LAB. SCATT. ANGLE, Θ
XBL 848-3405

Fig. 4

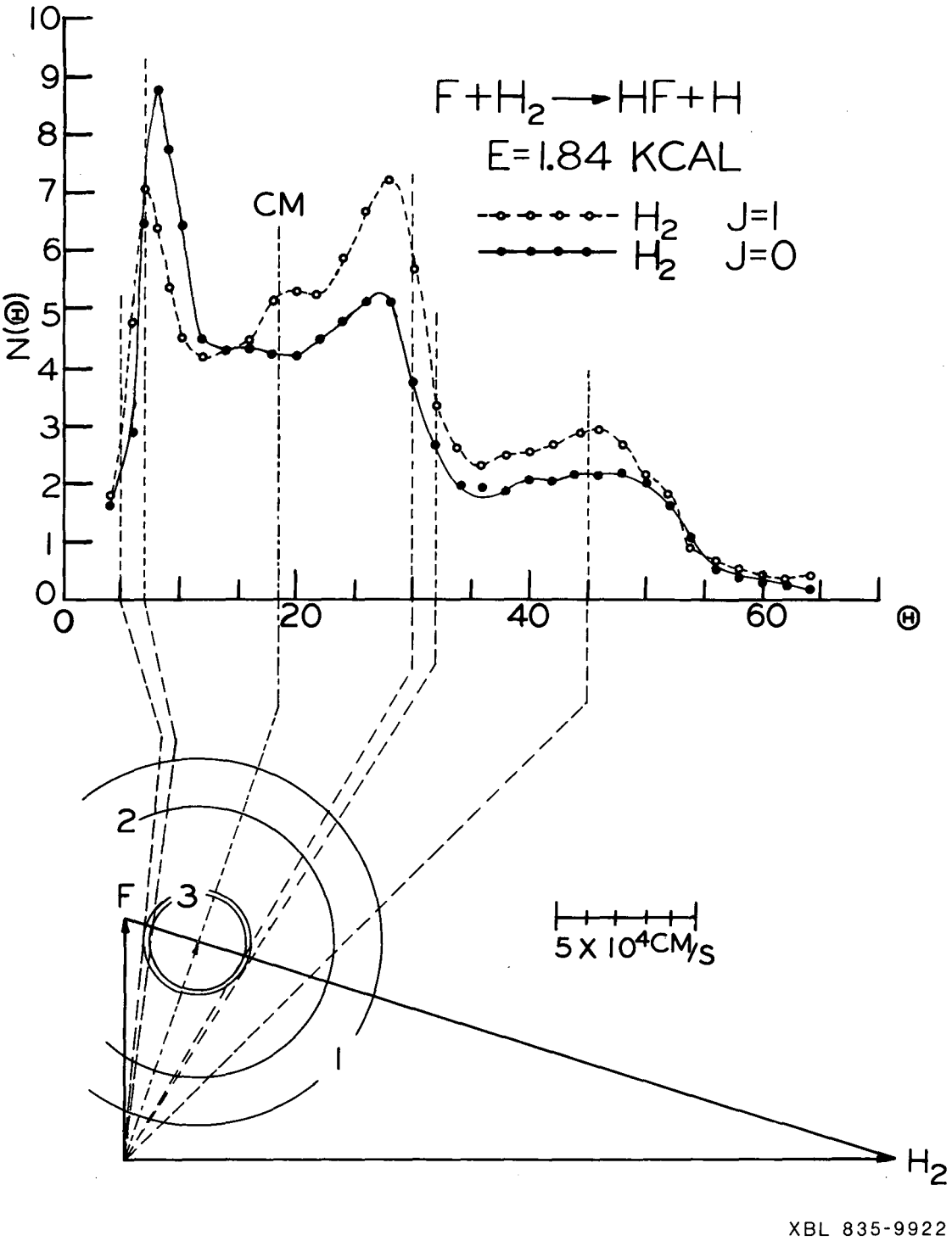
F+H2 → HF+H
E=1.84 KCAL
CM
H2 J=1
H2 J=0
N(Θ)
Θ
0
20
40
60
2
F
3
1
5 X 10^4 CM/S
H2
XBL 835-9922

Fig. 5

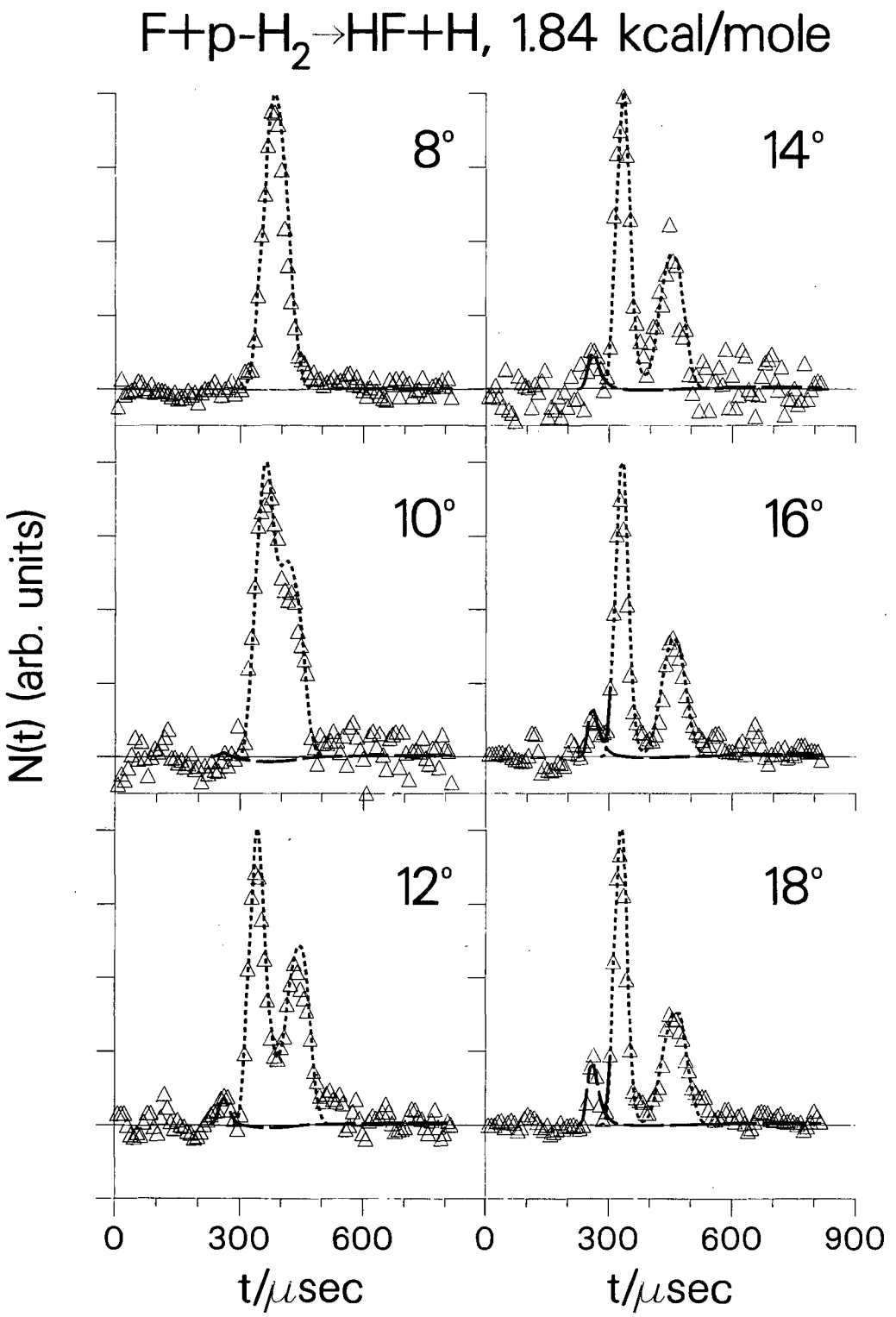

XBL 841-36

Fig. 6a

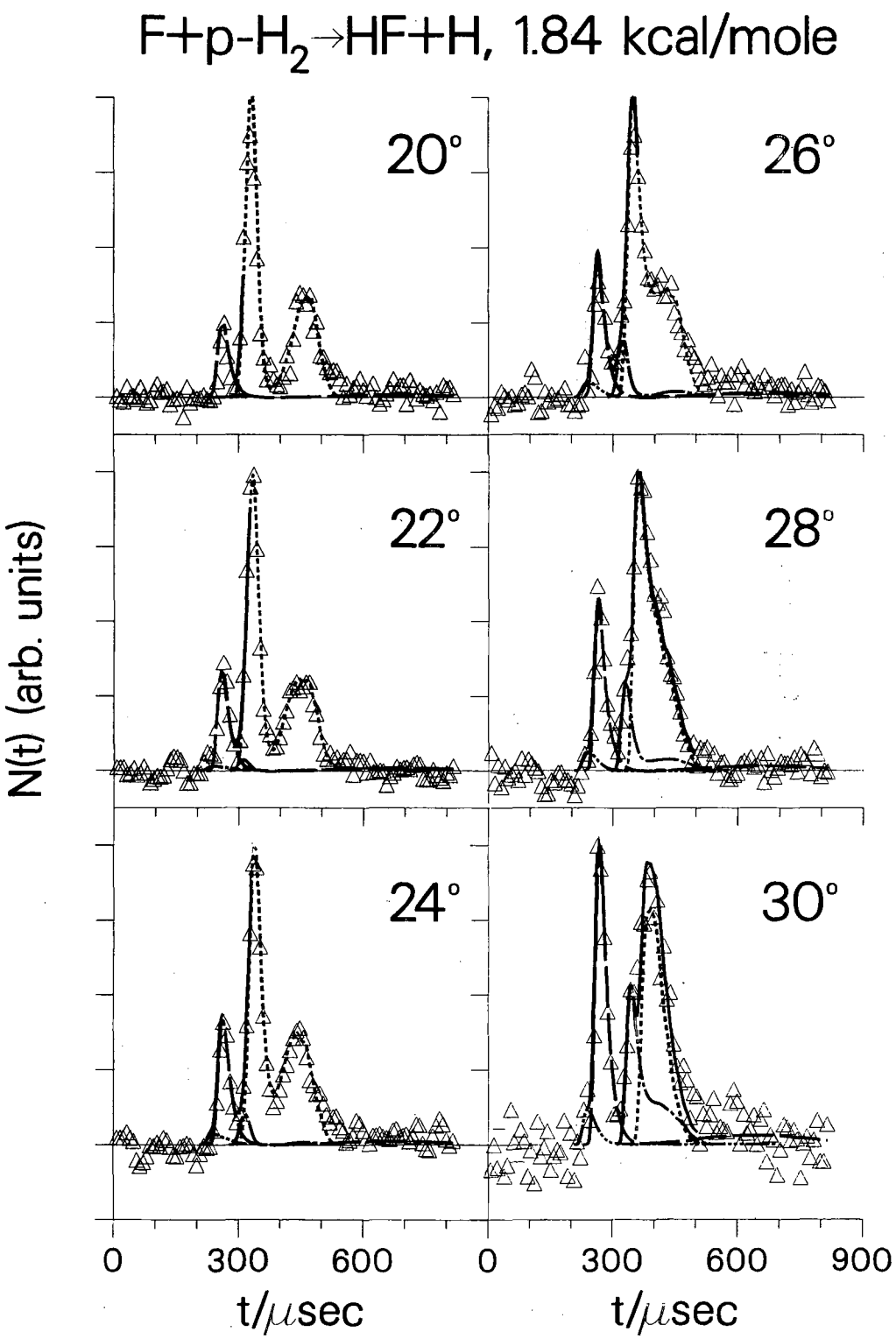

XBL 841-38

Fig. 6b

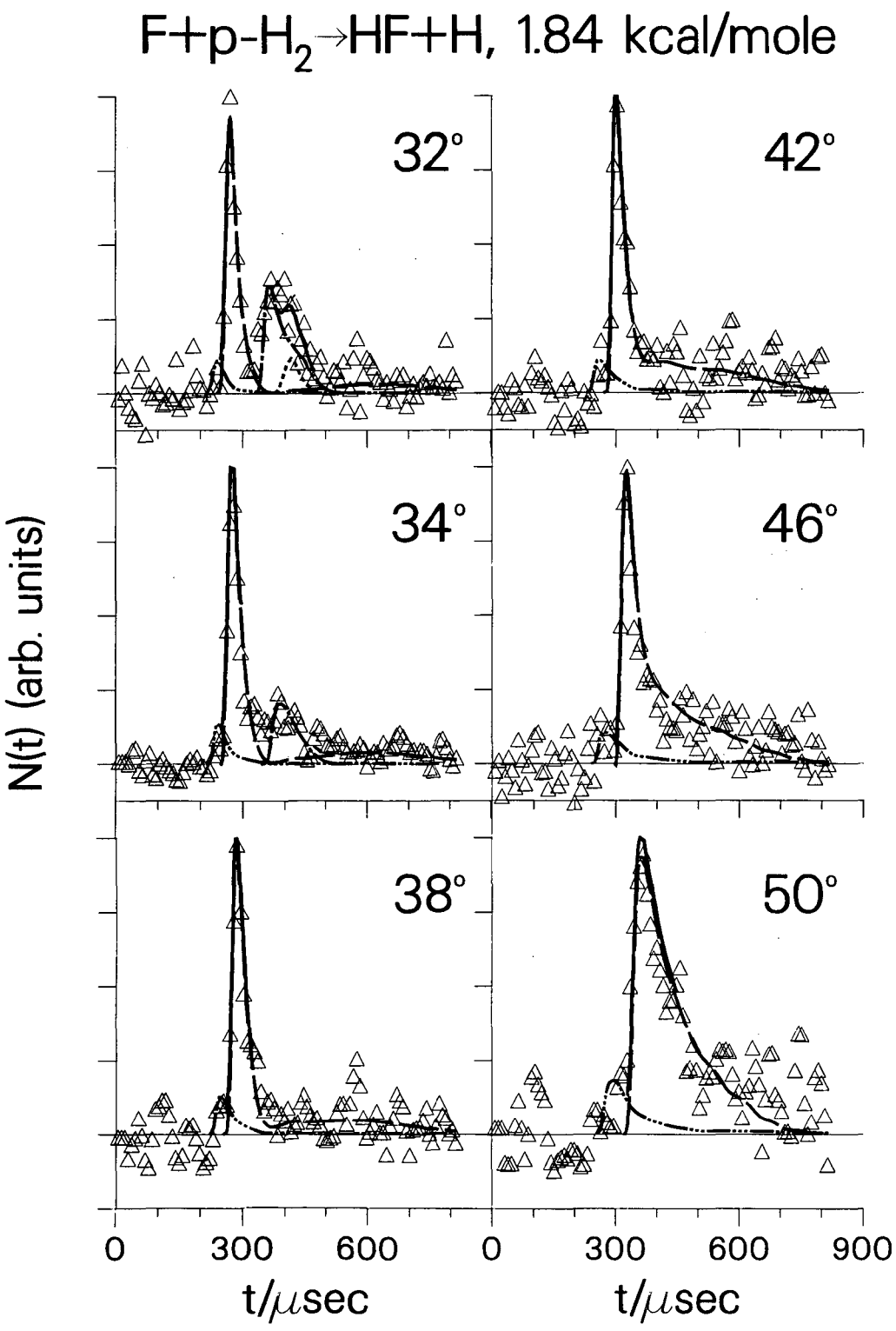

XBL 841-39

Fig. 6c

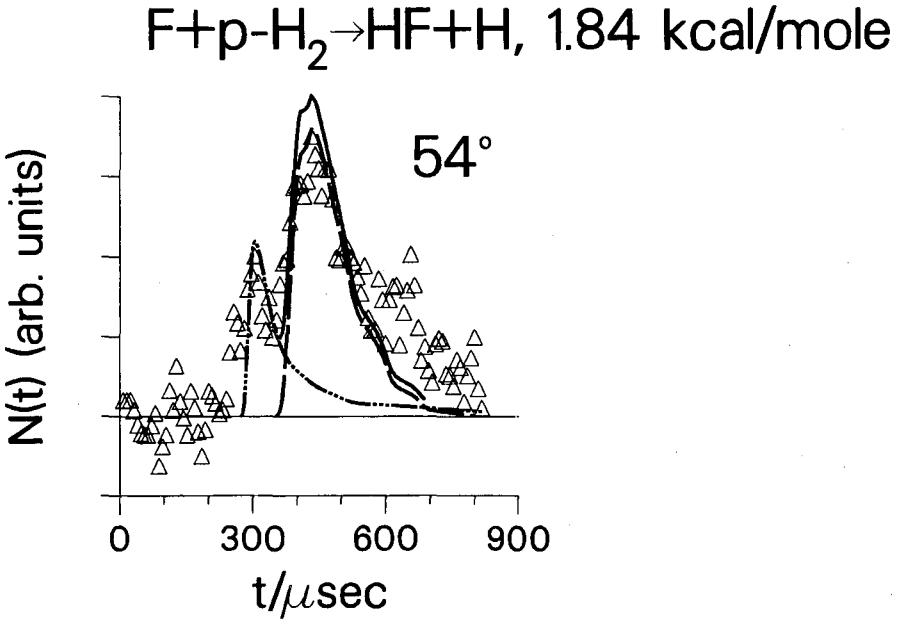

XBL 841-249

Fig. 6d

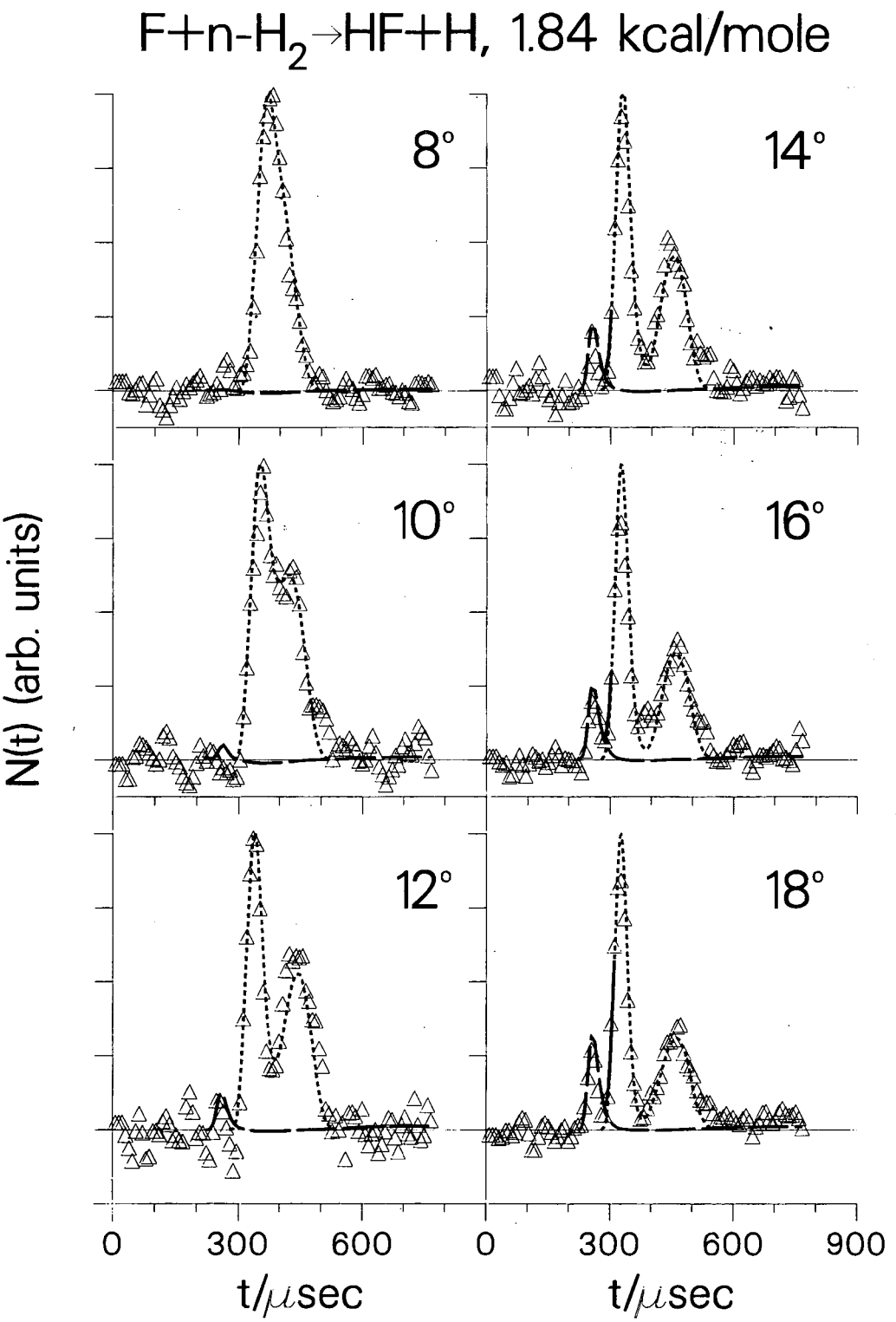

XBL 841-40

Fig. 7a

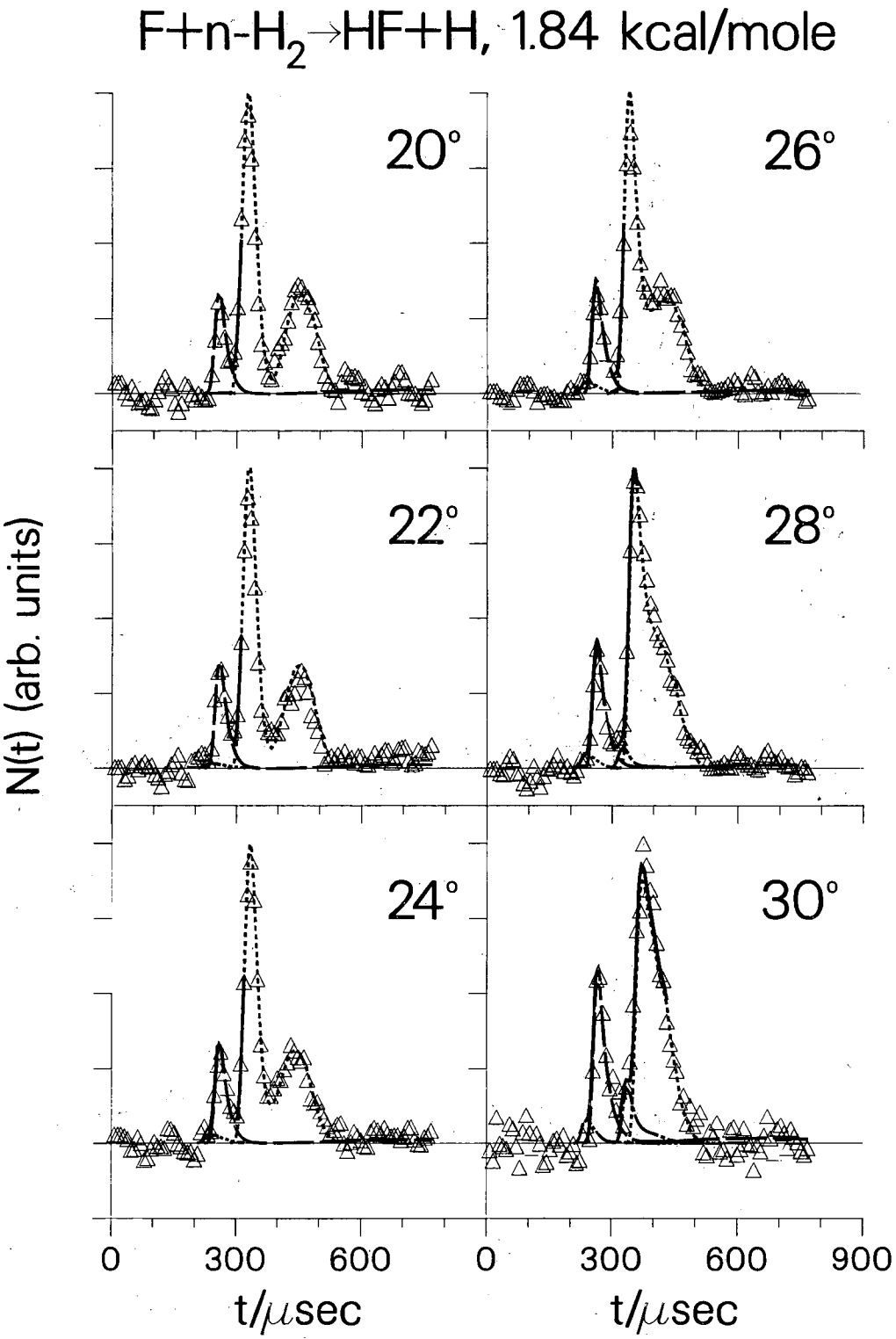

XBL 841-41

Fig. 7b

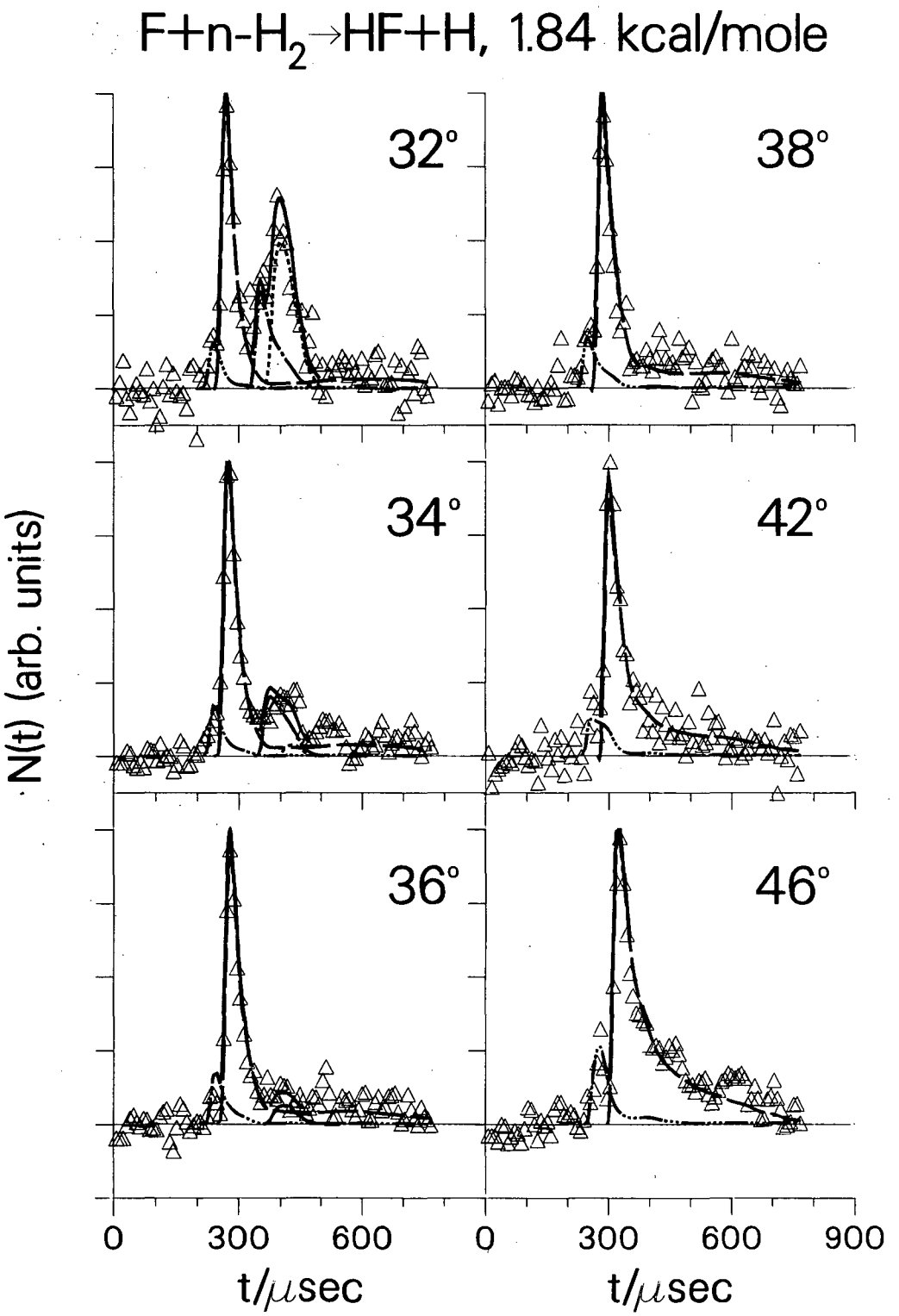

XBL 841-42

Fig. 7c

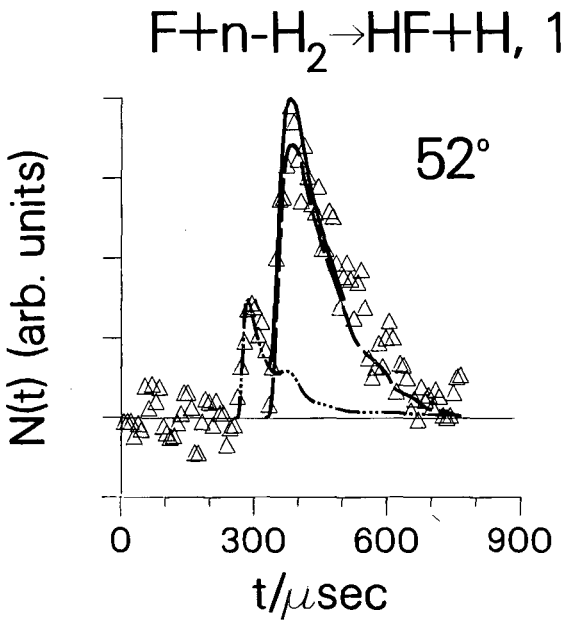

XBL 841-43

Fig. 7d

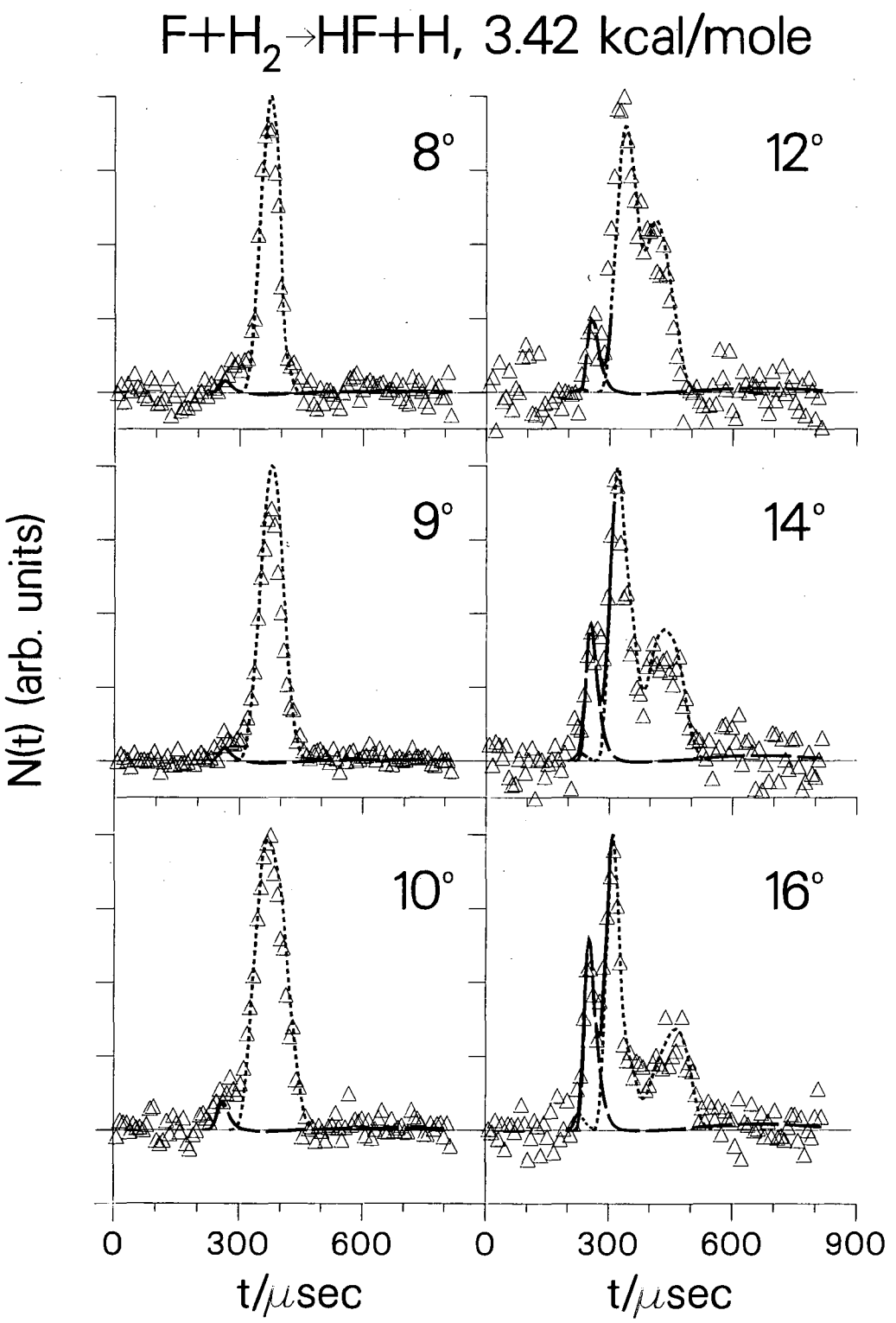

XBL 841-49

Fig. 8a

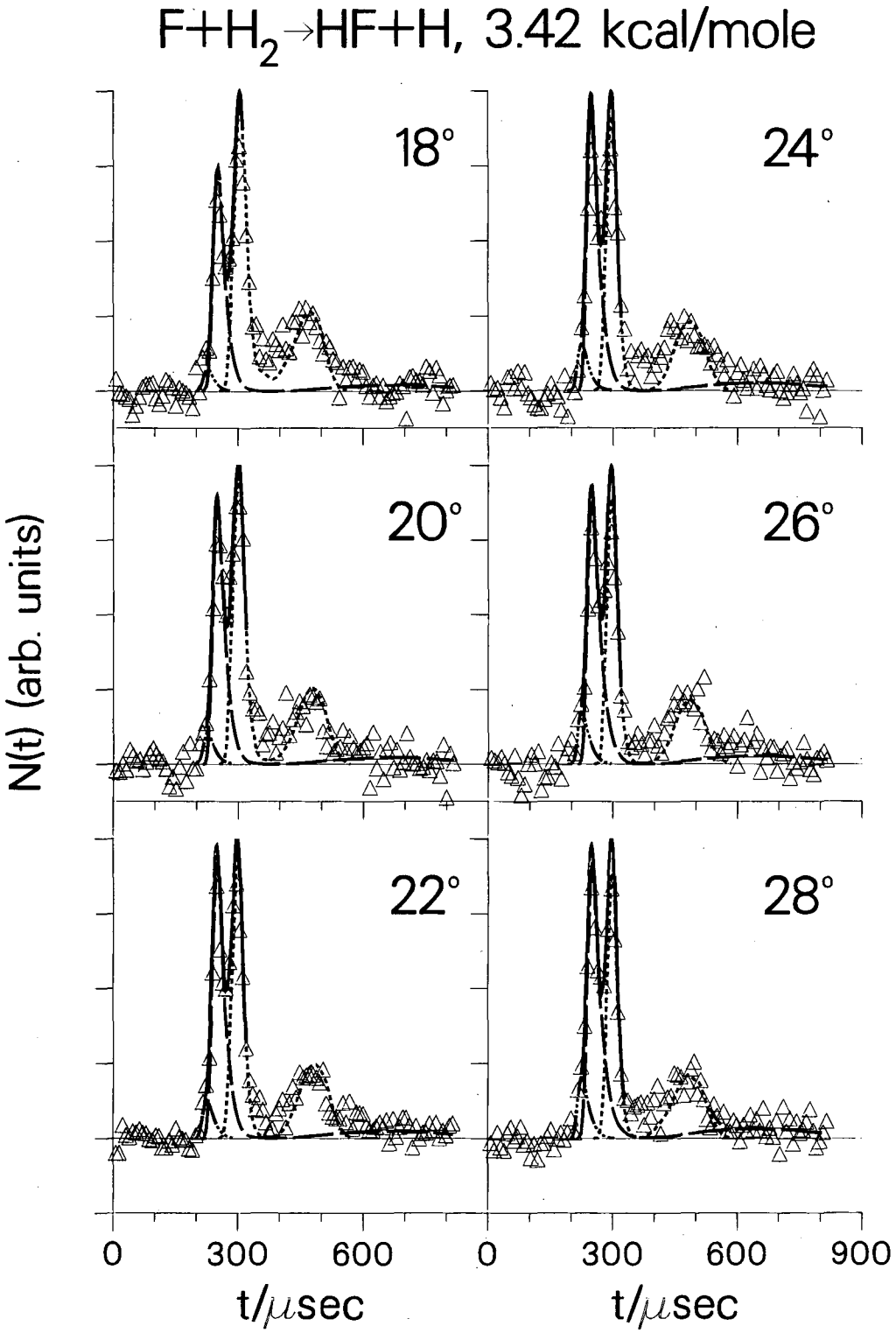

XBL 841-50

Fig. 8b

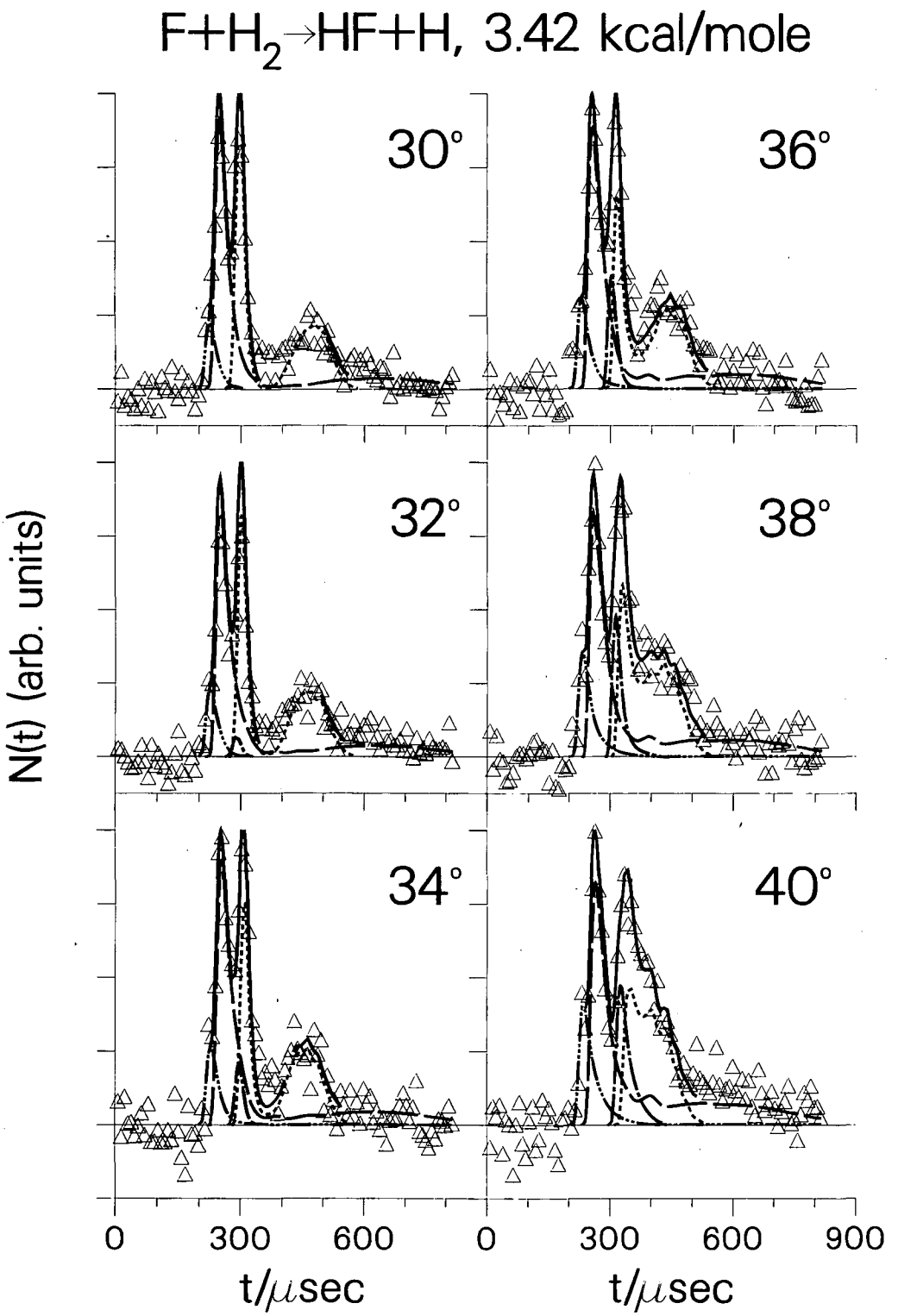

XBL 841-51

Fig. 8c

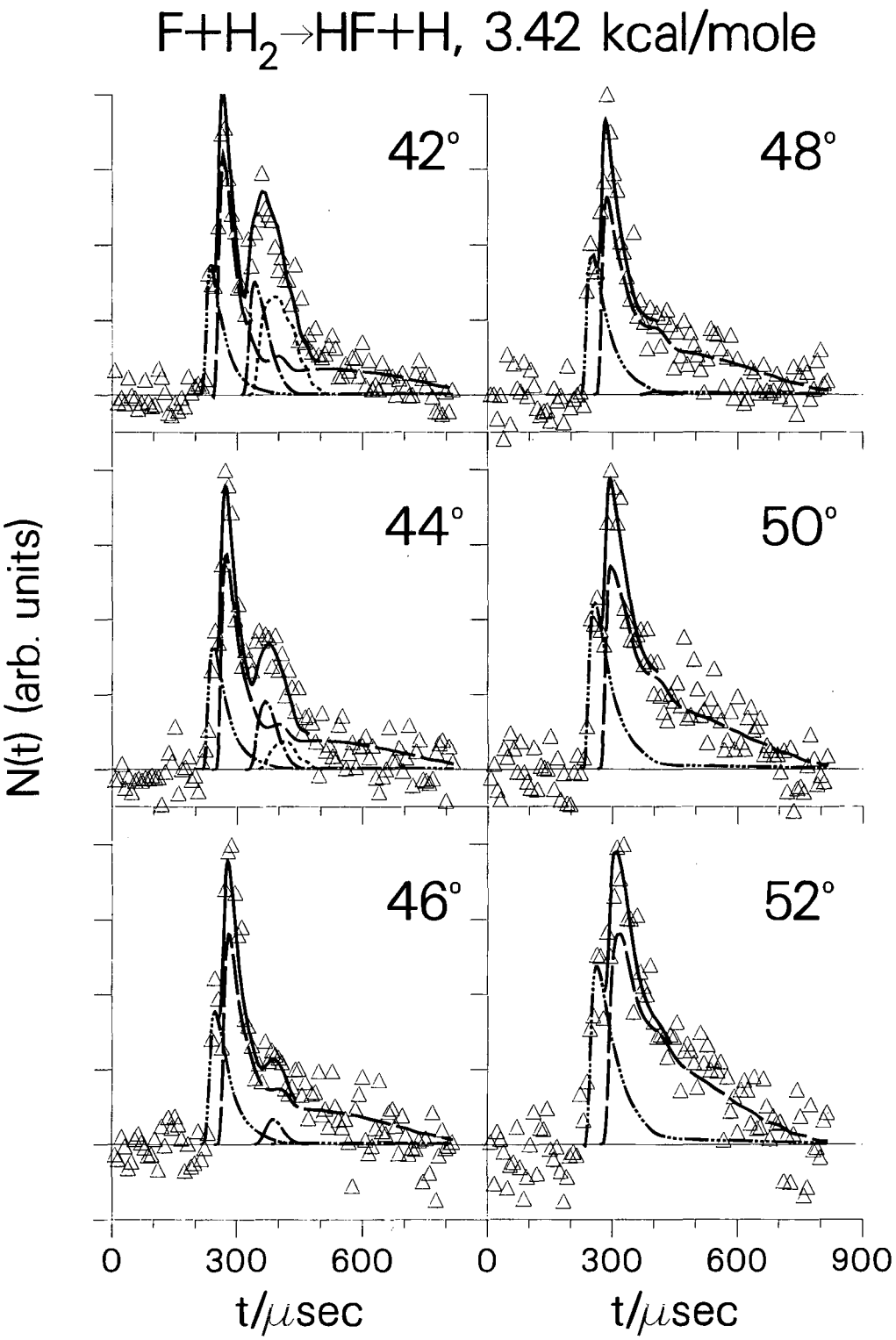

XBL 841-52

Fig. 8d

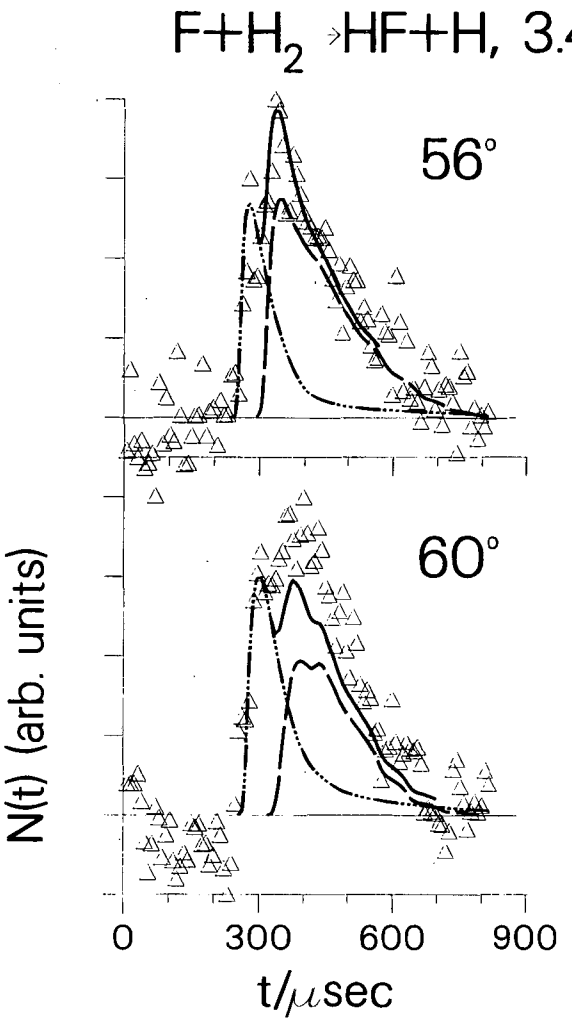

XBL 841-53

Fig. 8e

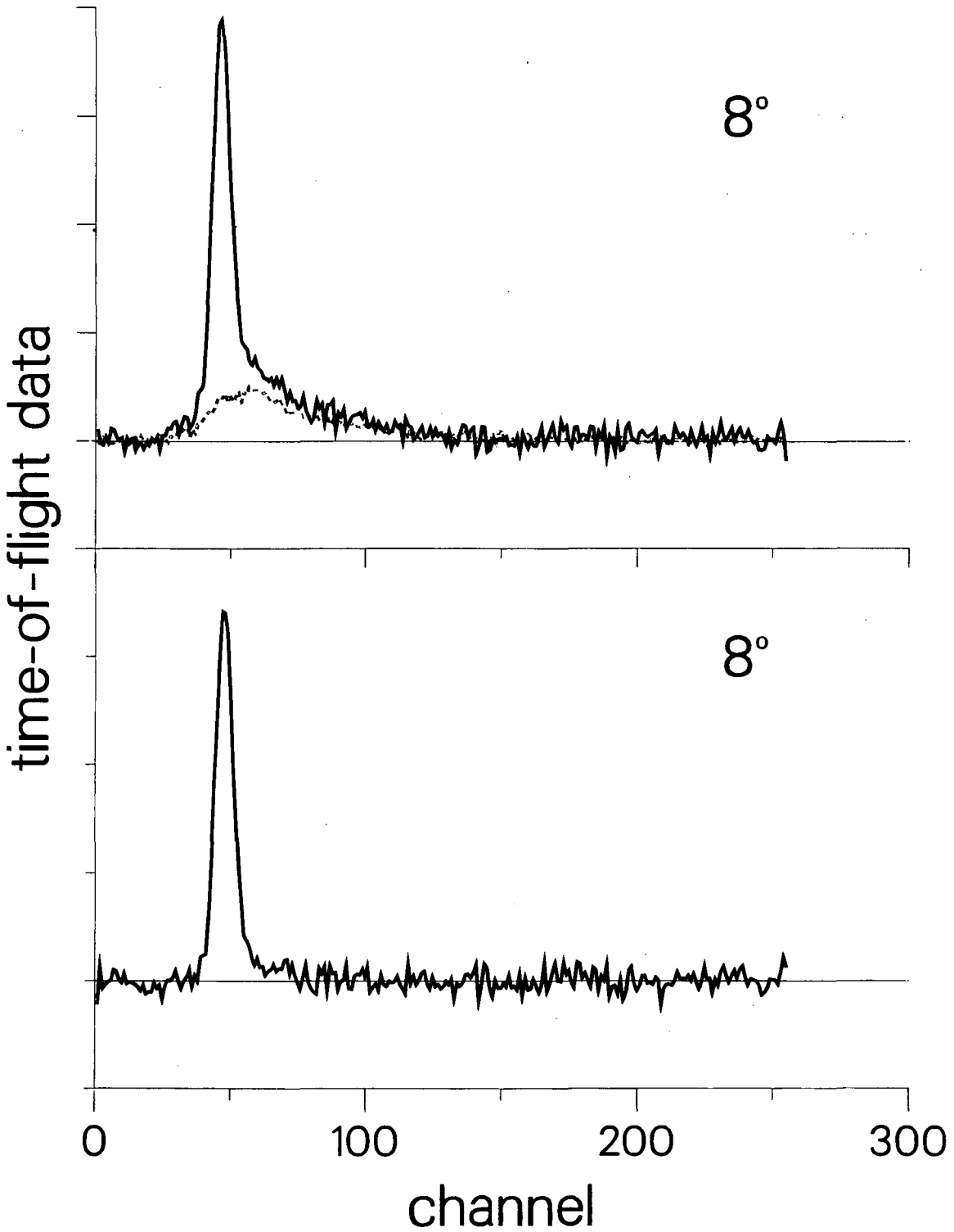

XBL 841-96

Fig. 9

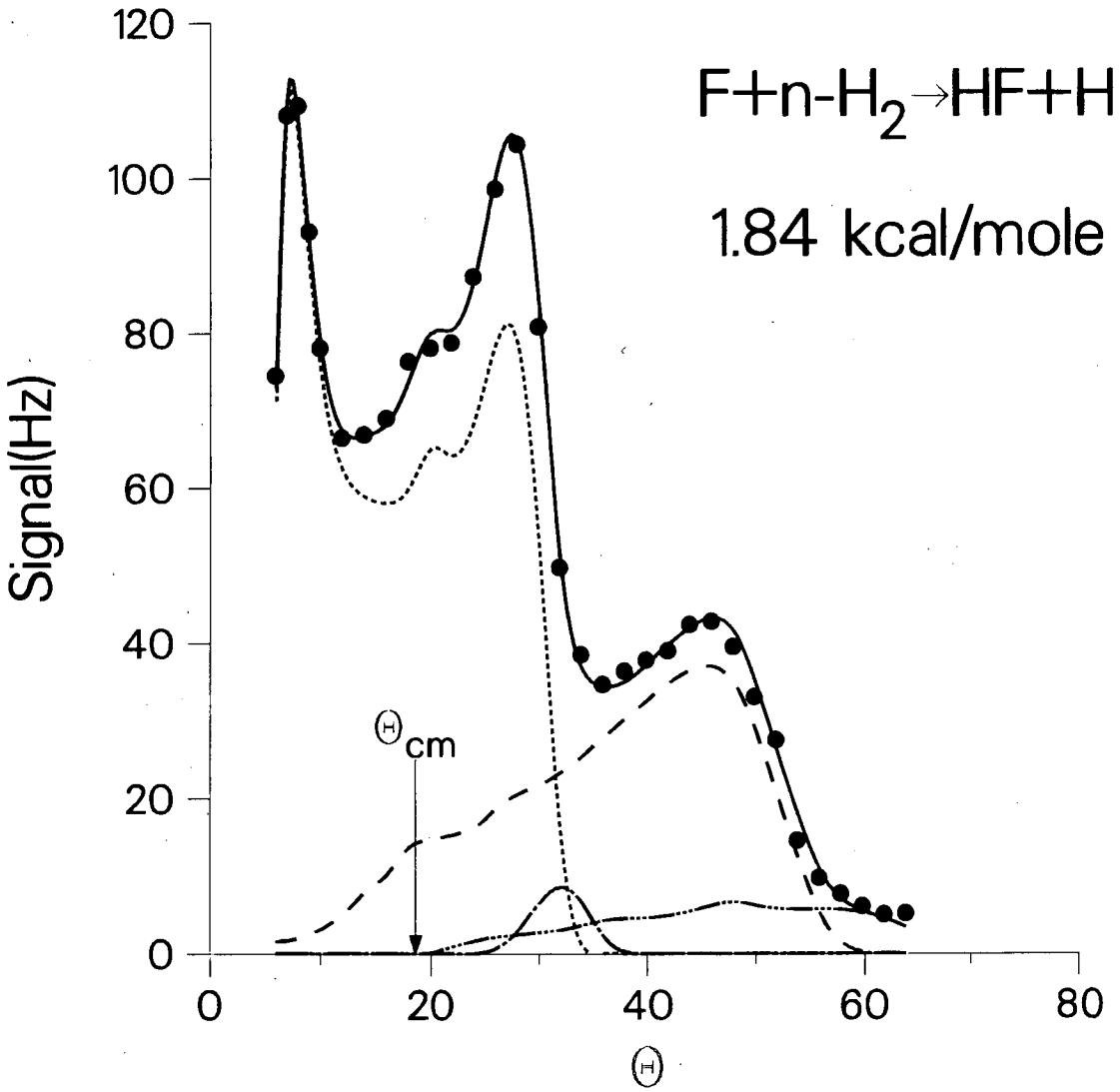

XBL 841-73

Fig. 10

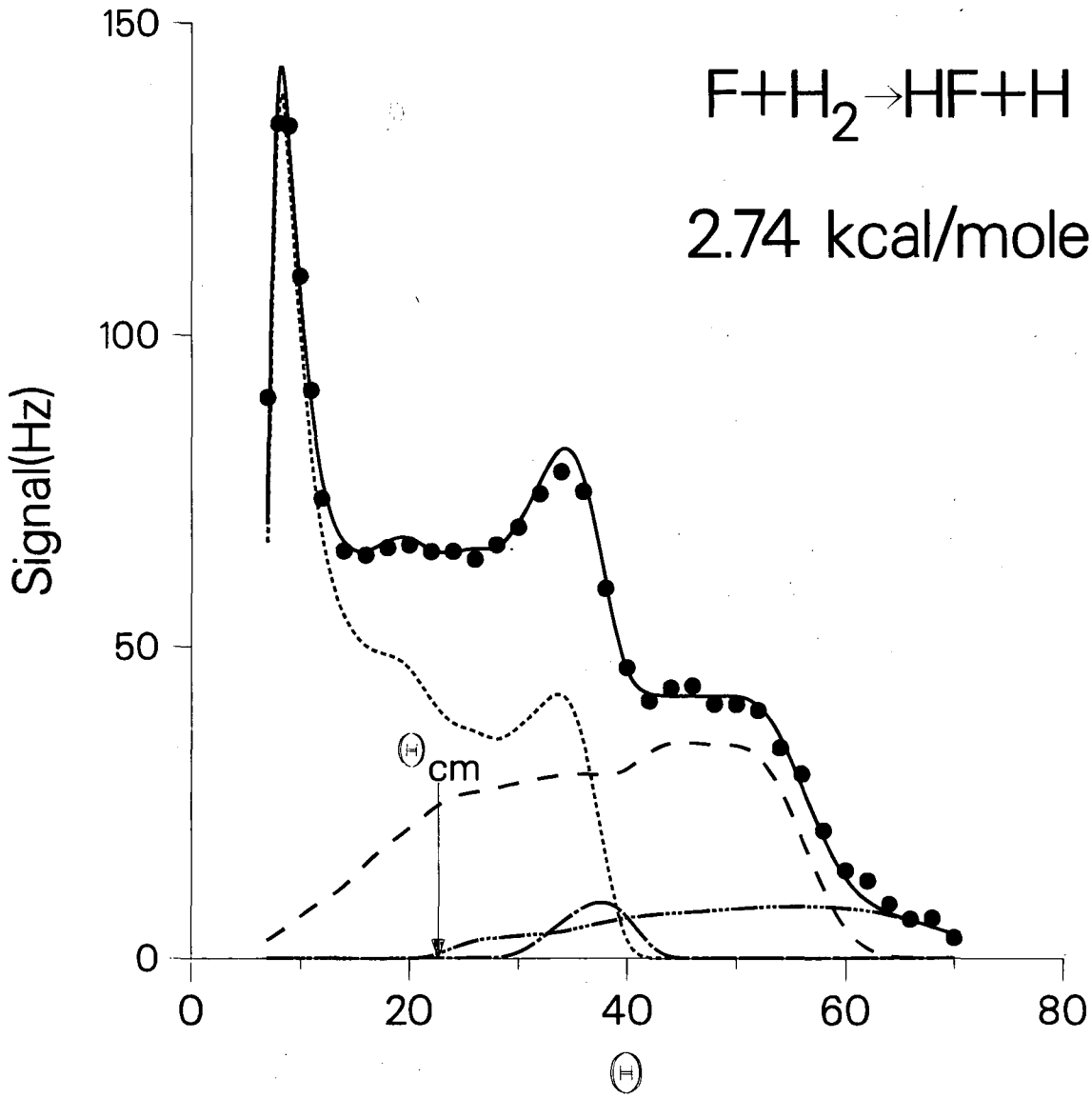
150
100
50
0
Signal(Hz)
F+H2→HF+H
2.74 kcal/mole
Θcm
0
20
40
60
80
Θ
XBL 841-90

Fig. 11

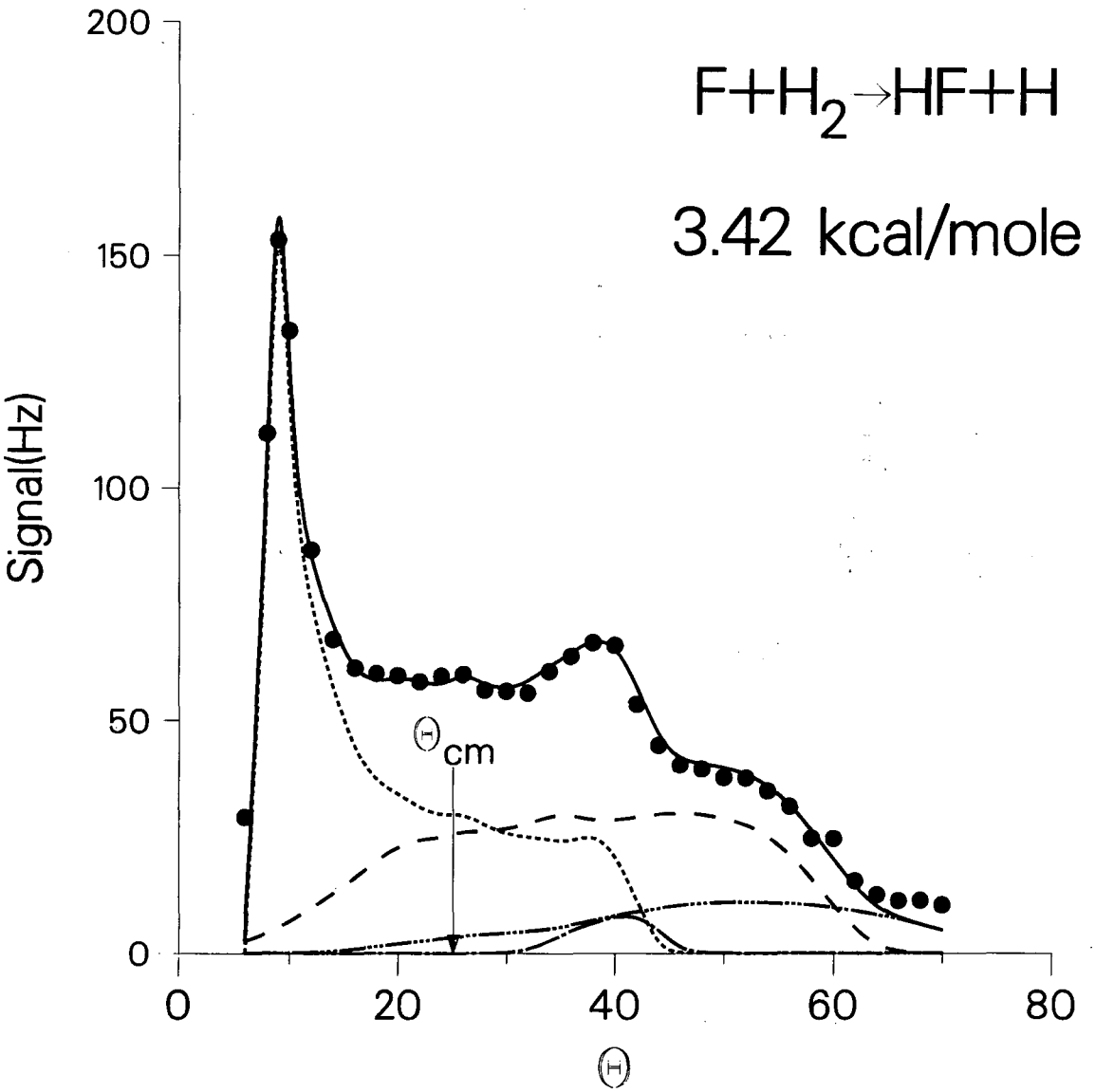

XBL 841-74

Fig. 12

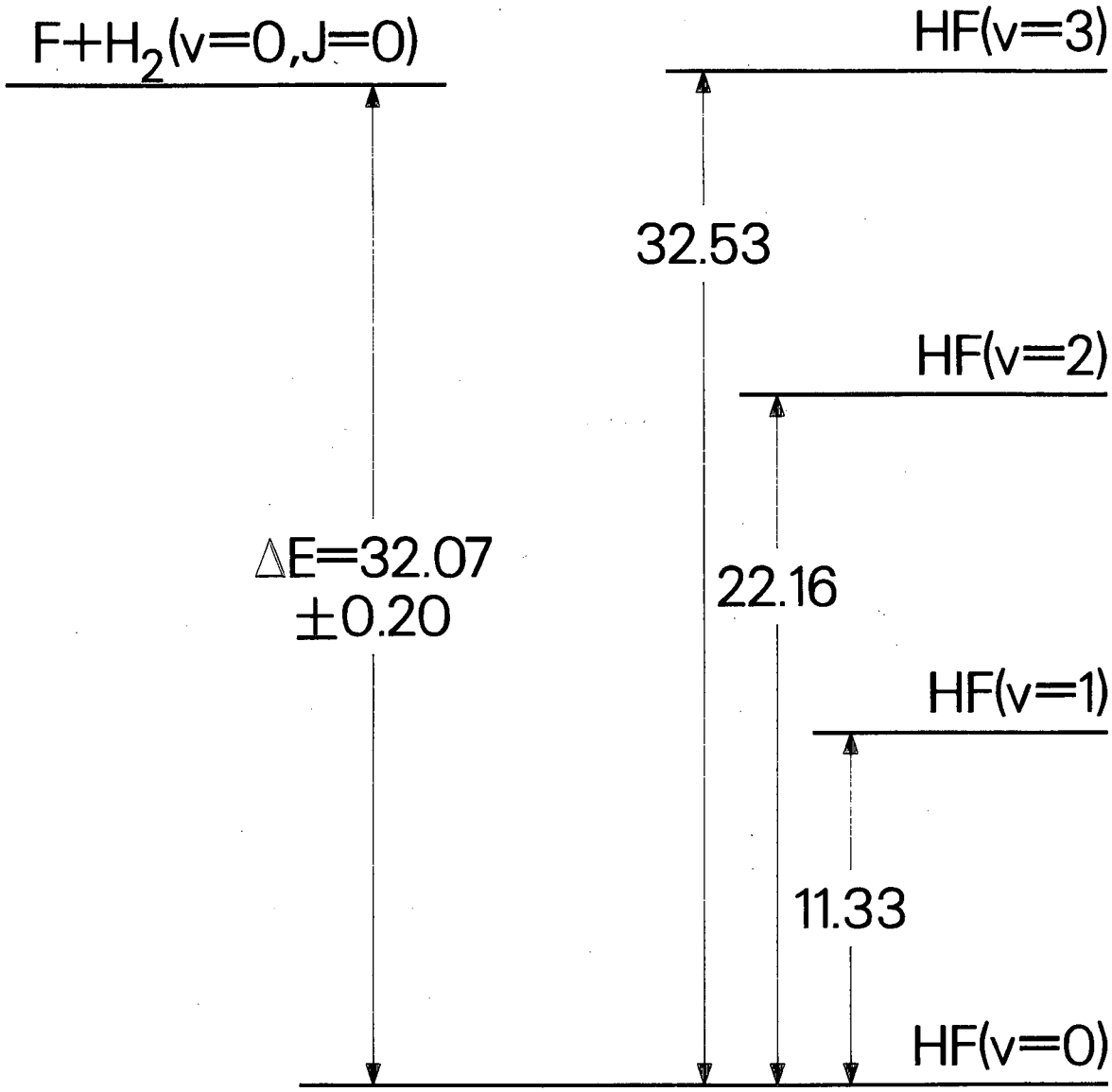

XBL 841-104

Fig. 13

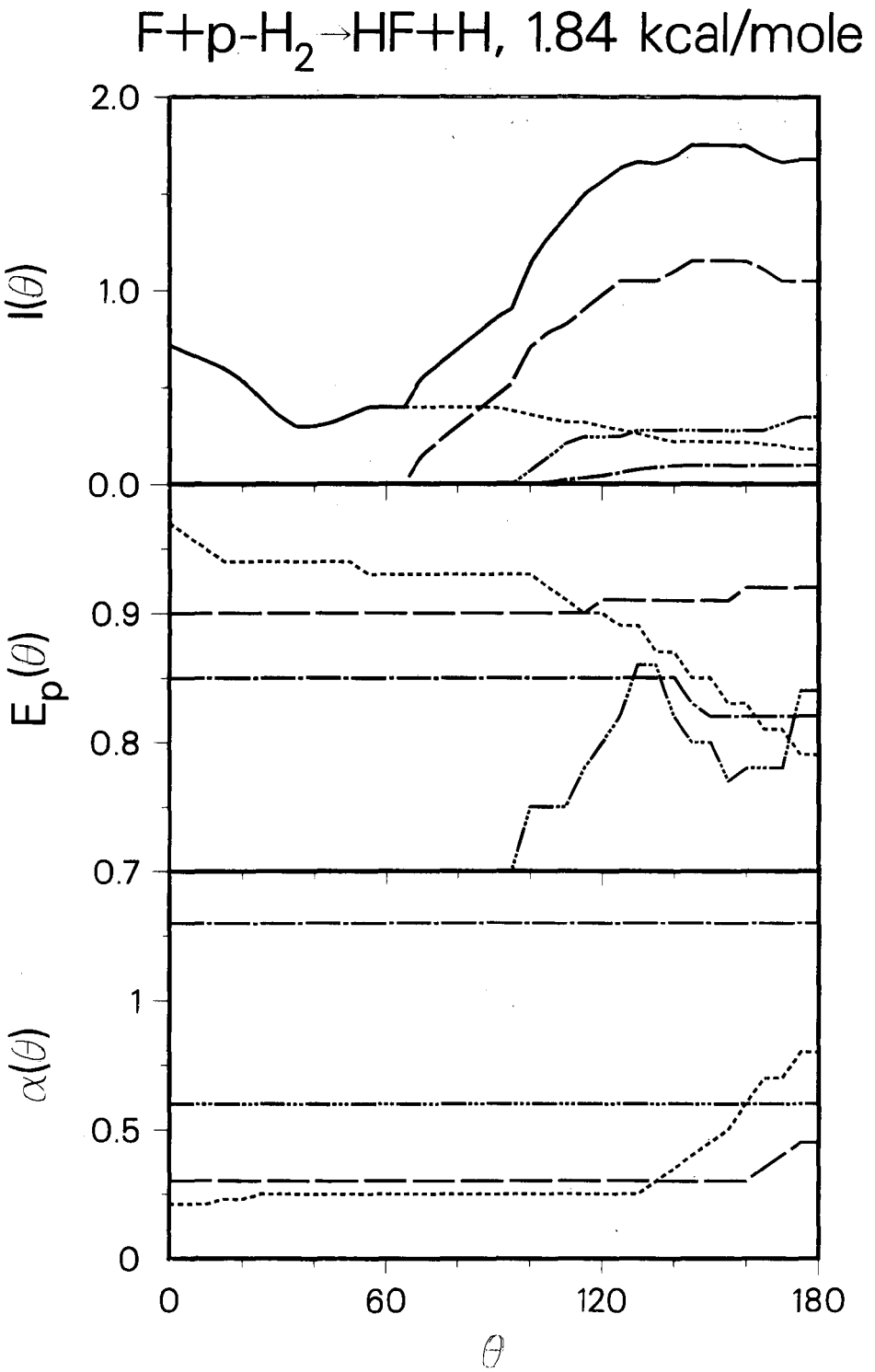

XBL 841-89

Fig. 14

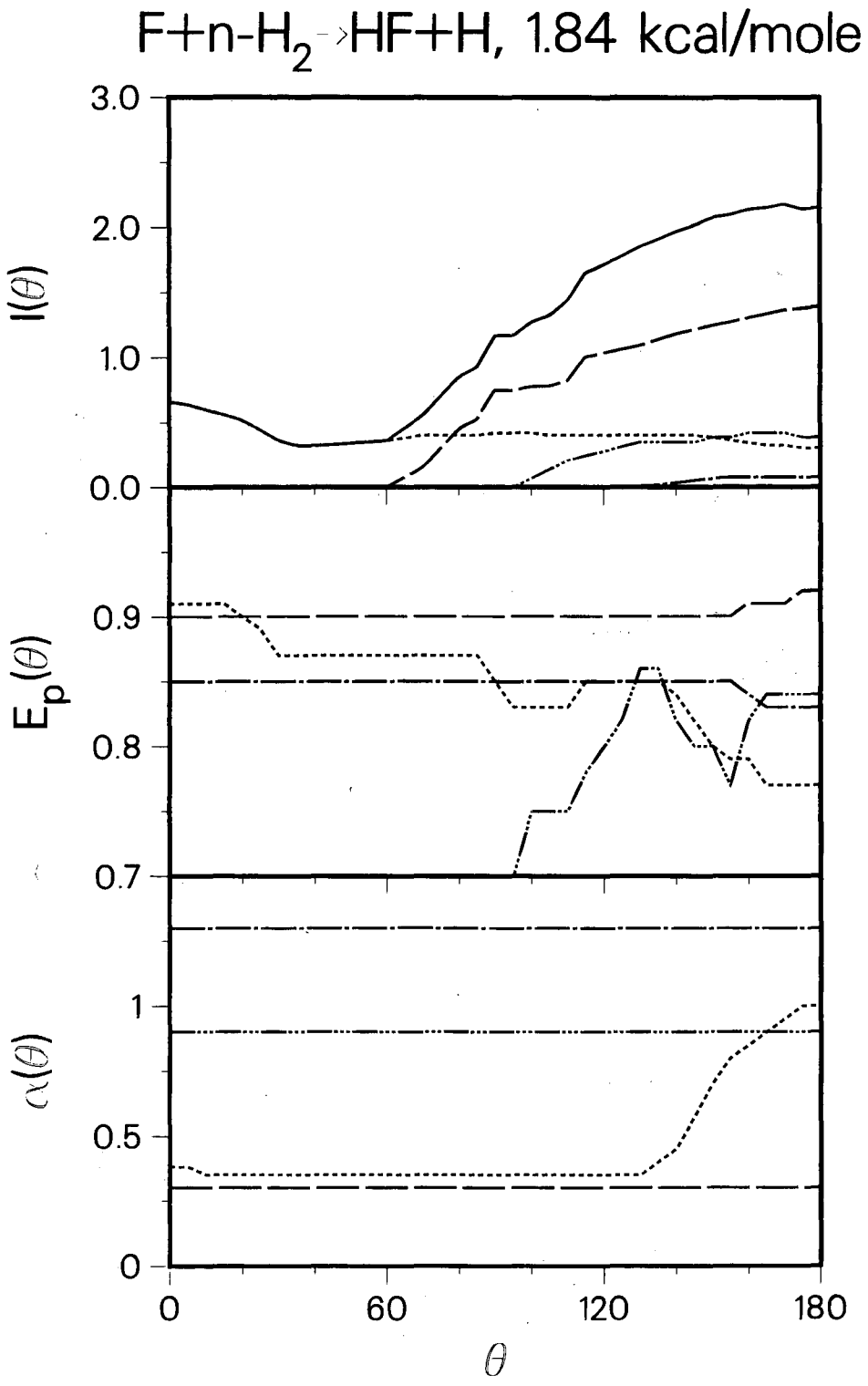

XBL 841-136

Fig. 15

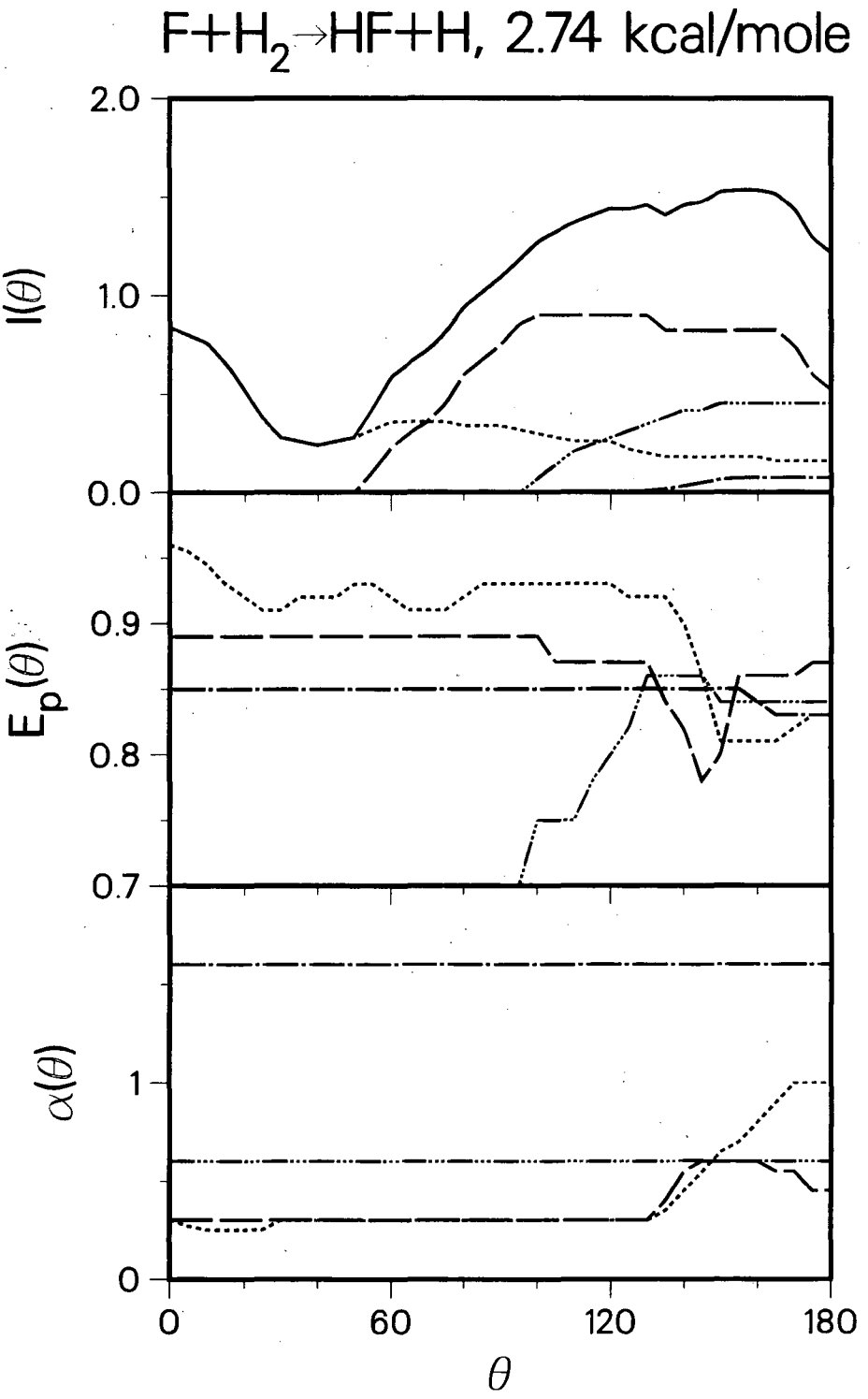

XBL 841-103

Fig. 16

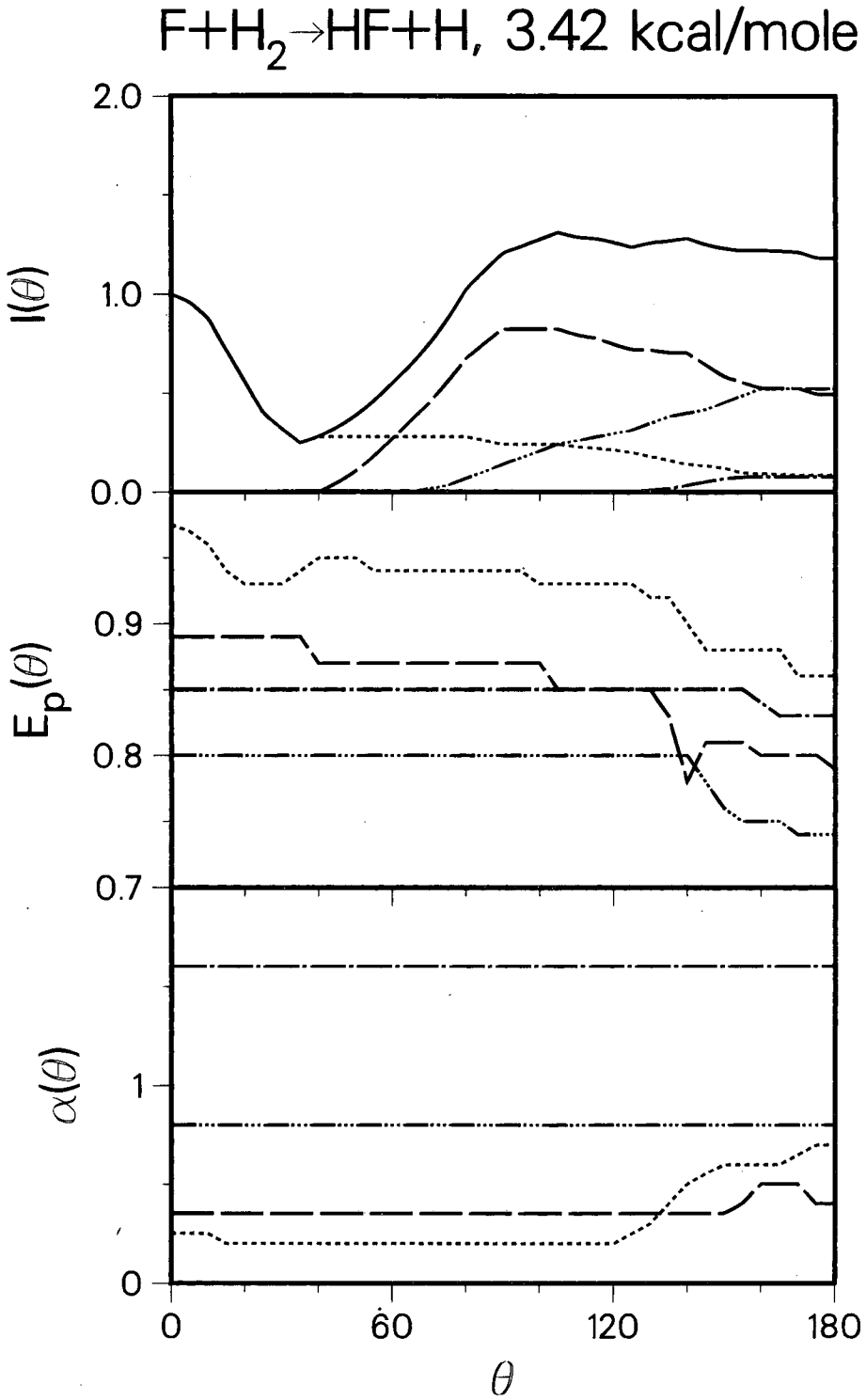

XBL 841-102

Fig. 17

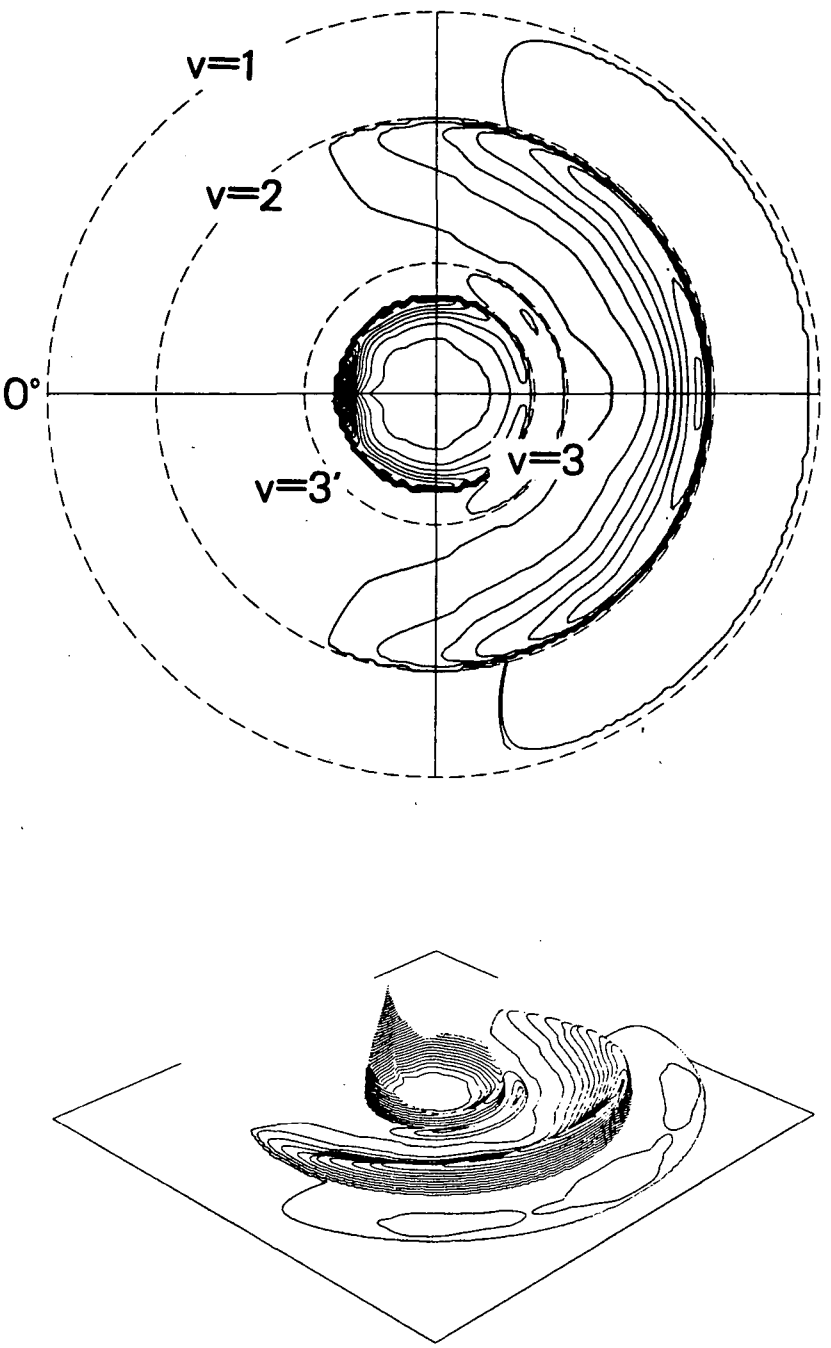

XBL 841-21A

Fig. 18

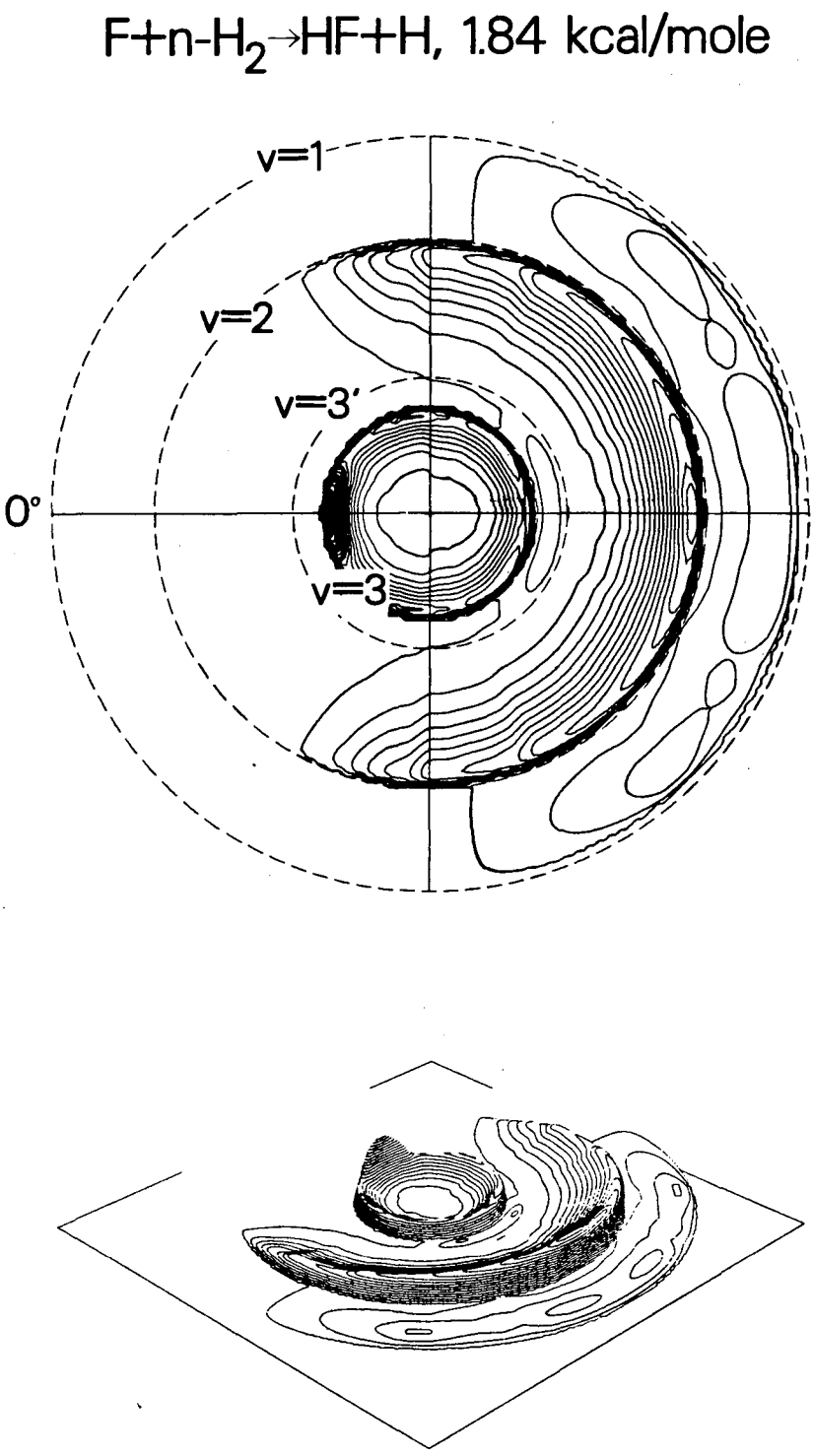

XBL 841-137

Fig. 19

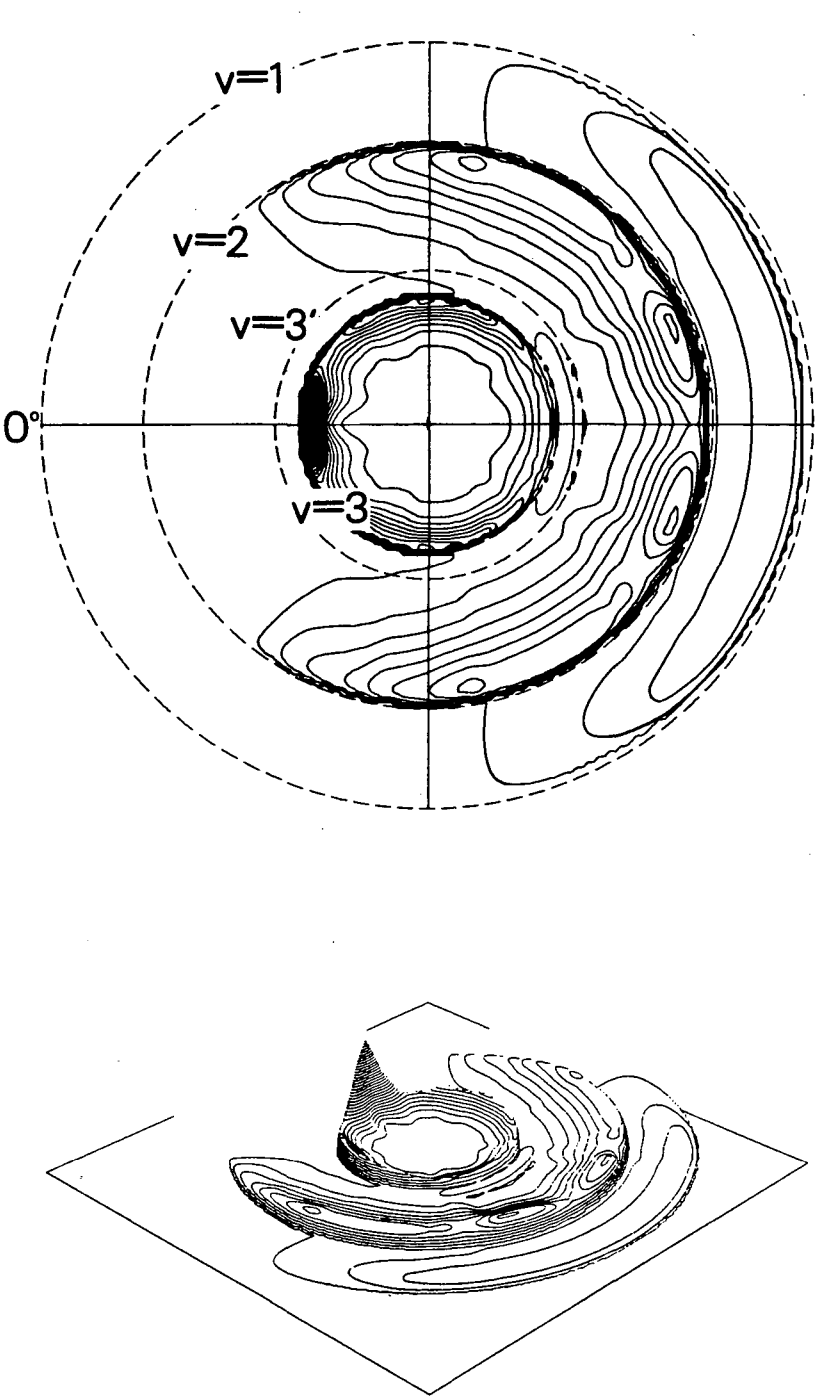

XBL 841-111

Fig. 20

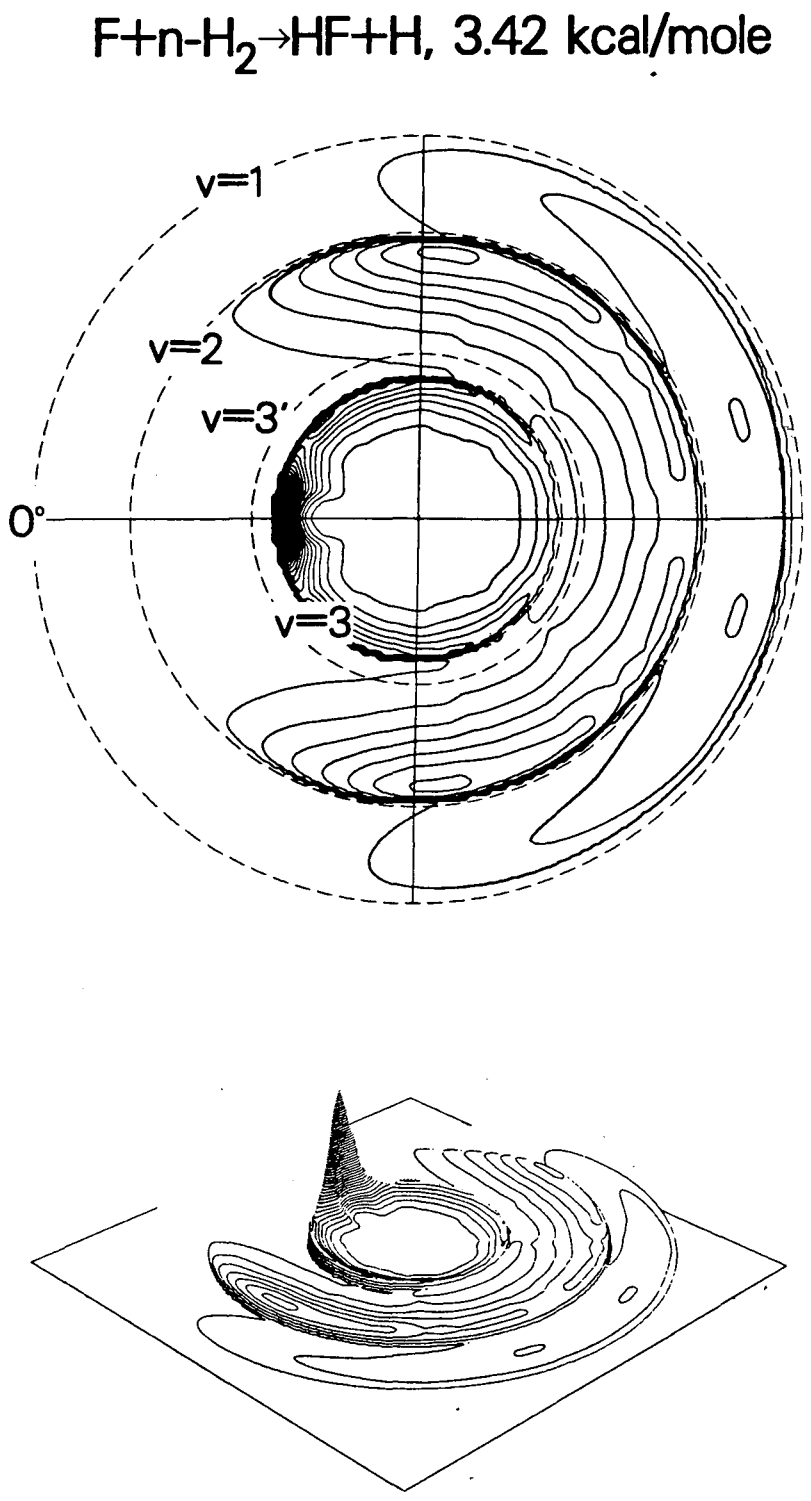

XBL 841-20A

Fig. 21

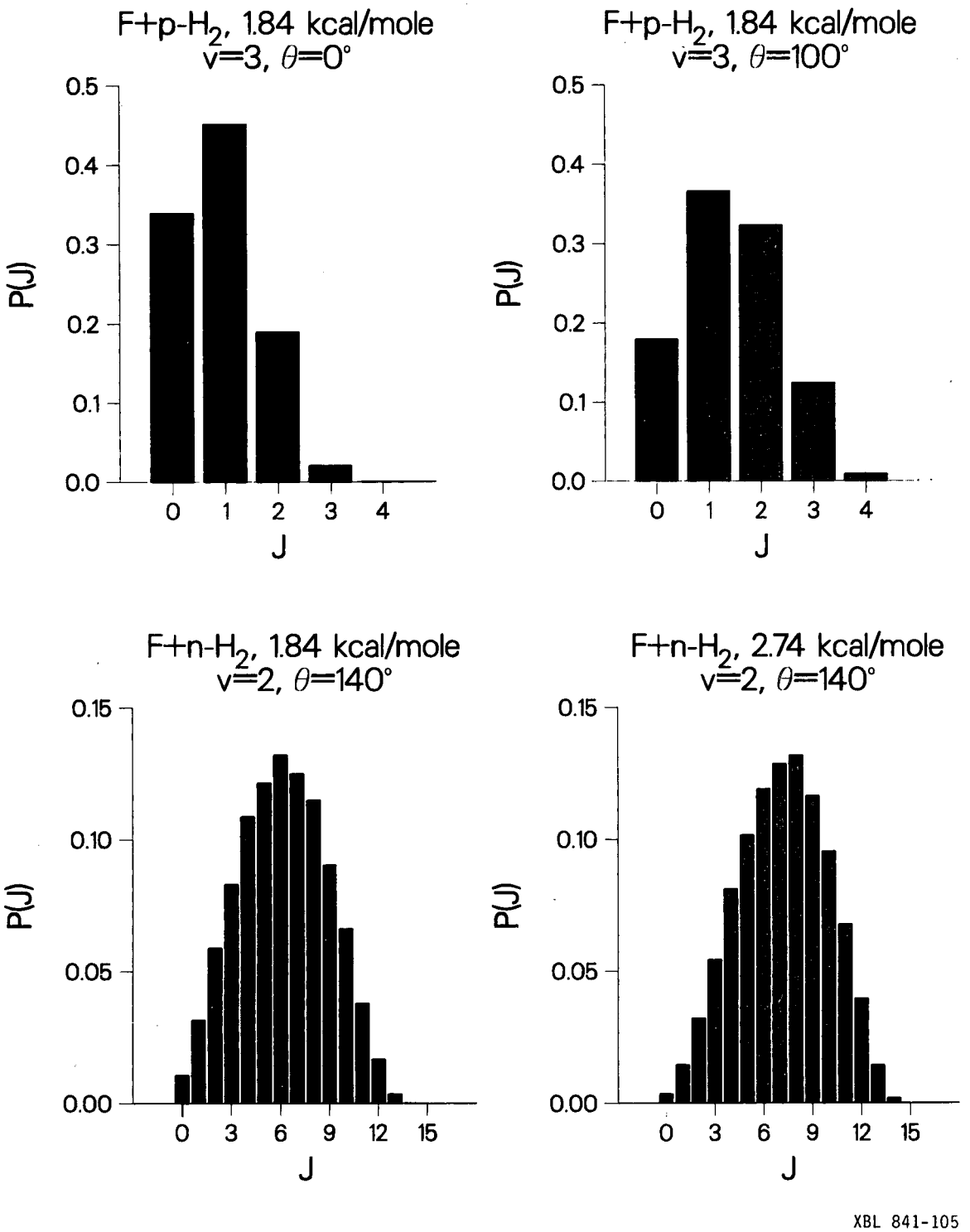
F+p-H2, 1.84 kcal/mole
v=3, θ=0°
F+p-H2, 1.84 kcal/mole
v=3, θ=100°
F+n-H2, 1.84 kcal/mole
v=2, θ=140°
F+n-H2, 2.74 kcal/mole
v=2, θ=140°
P(J)
J
XBL 841-105

Fig. 22

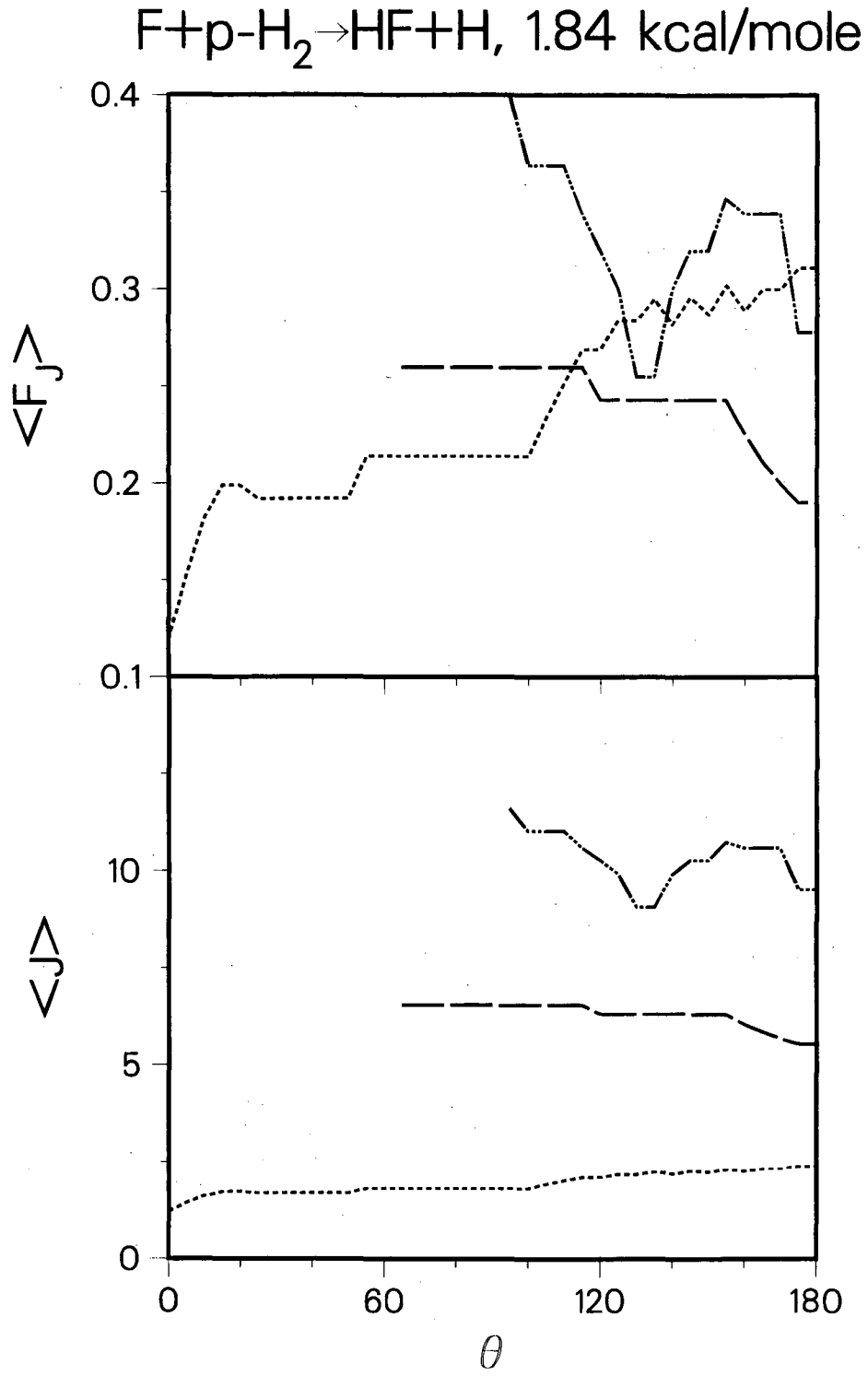

XBL 841-78

Fig. 23

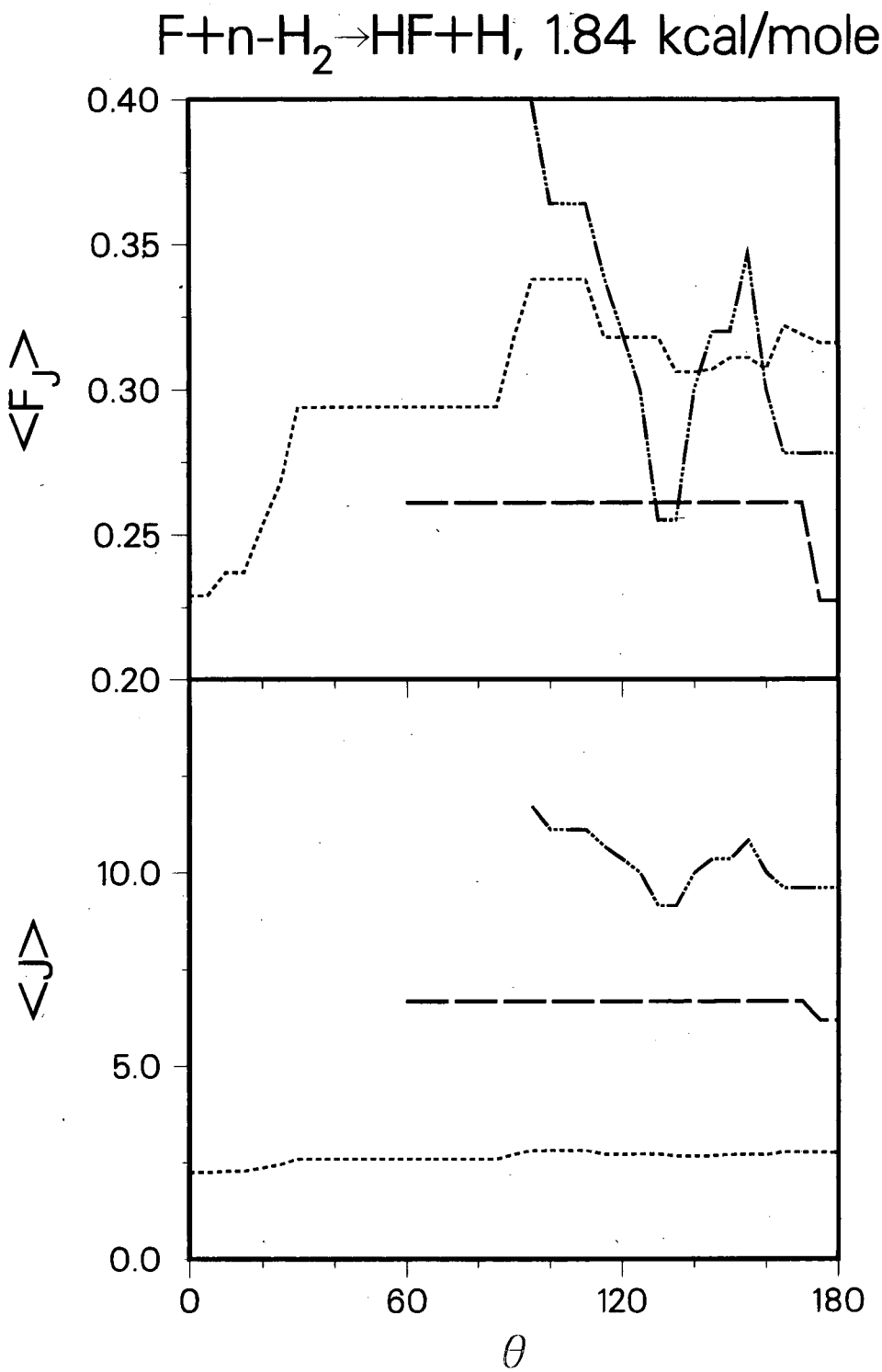

XBL 841-76

Fig. 24

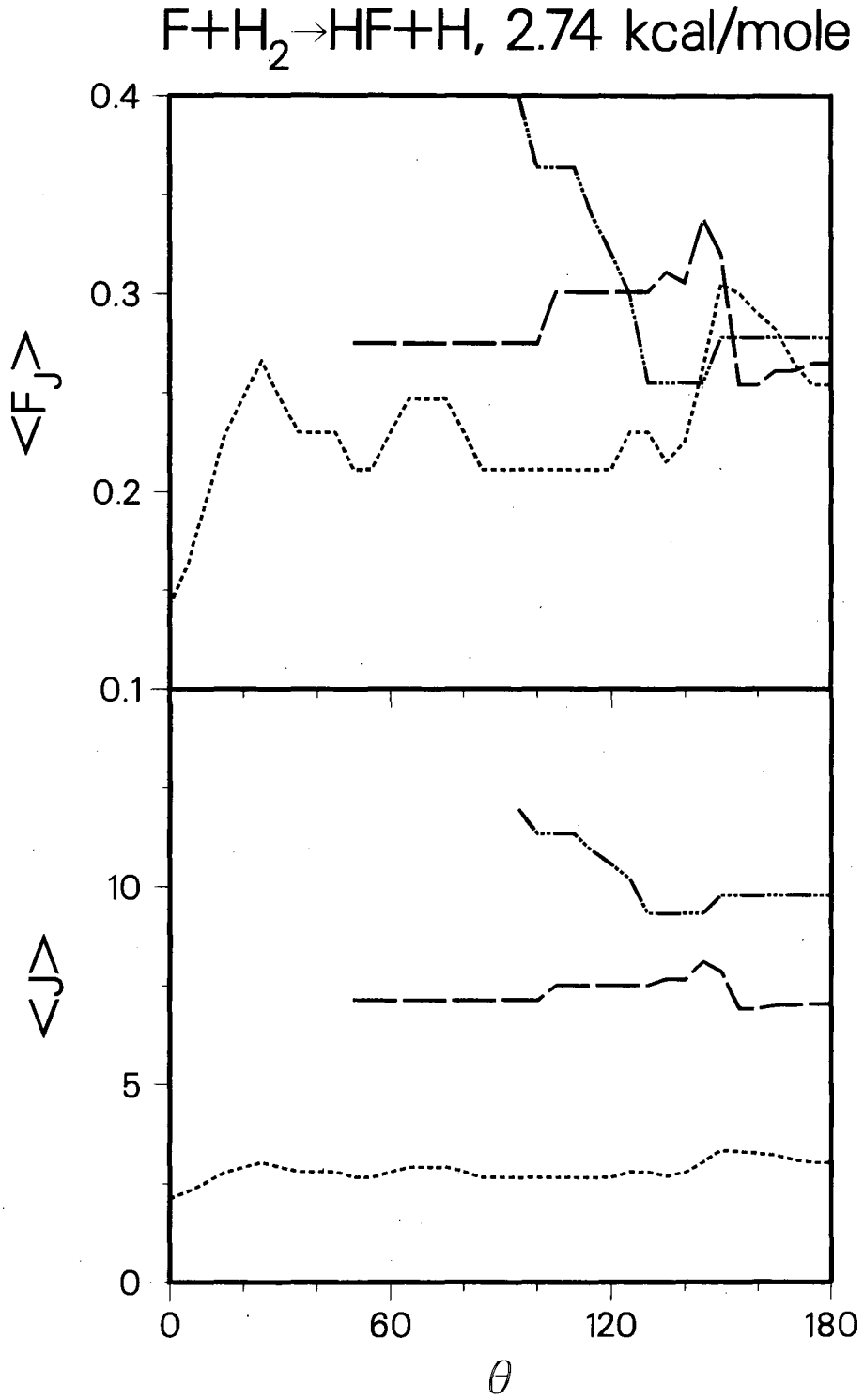

XBL 841-77

Fig. 25

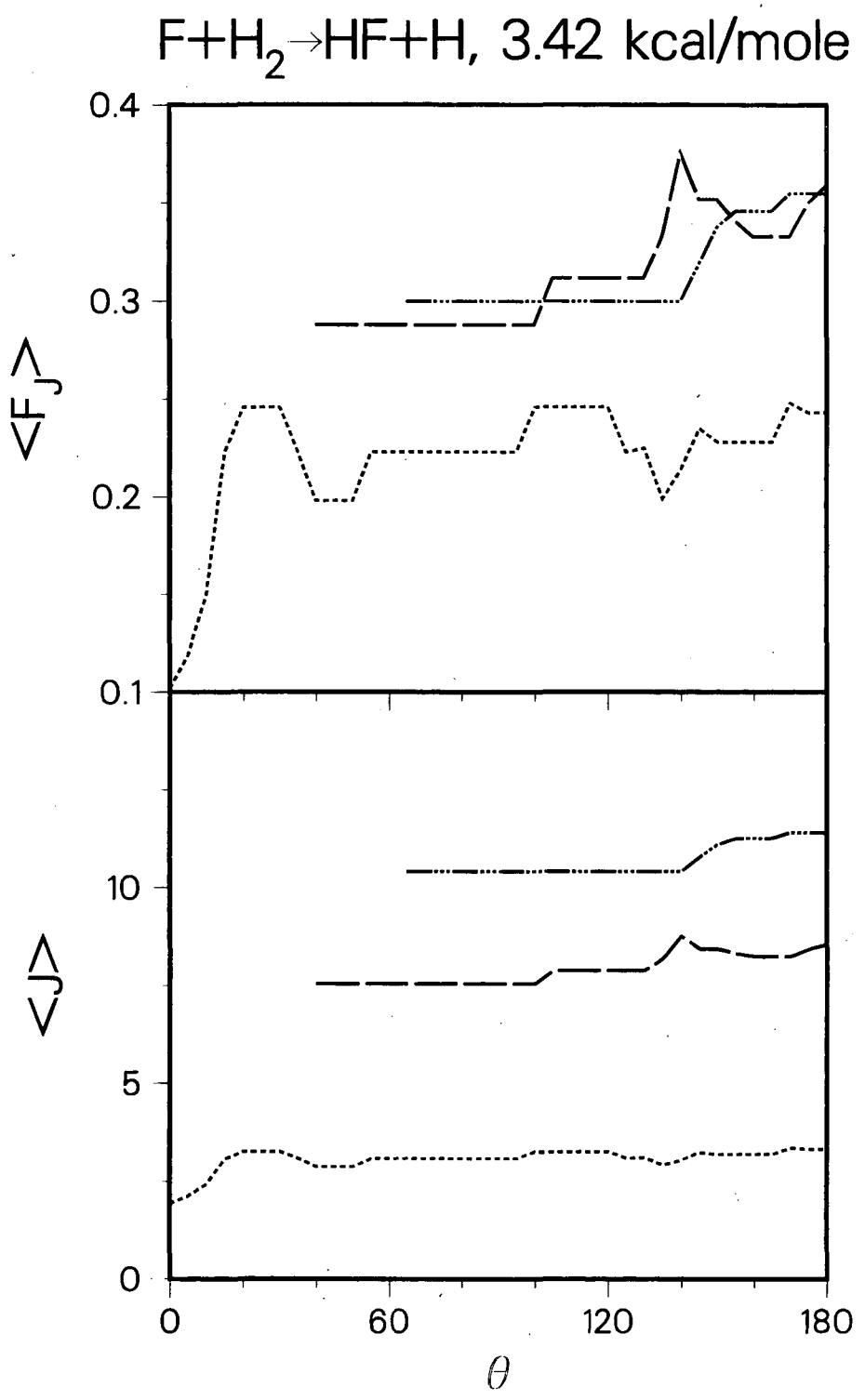

XBL 841-75

Fig. 26

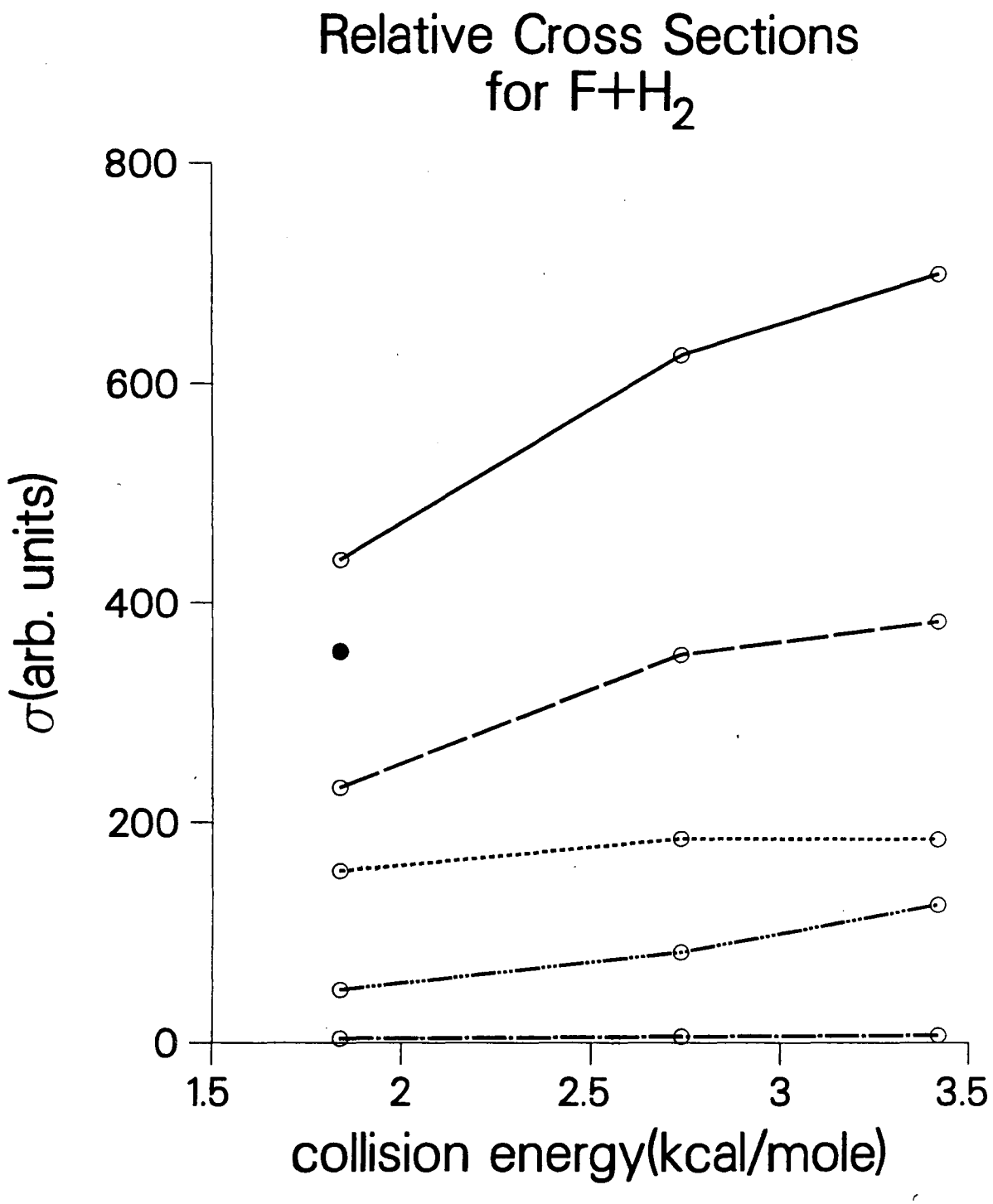
Relative Cross Sections
for F+H2
800
600
400
200
0
σ(arb. units)
1.5
2
2.5
3
3.5
collision energy(kcal/mole)
XBL 841-107

Fig. 27

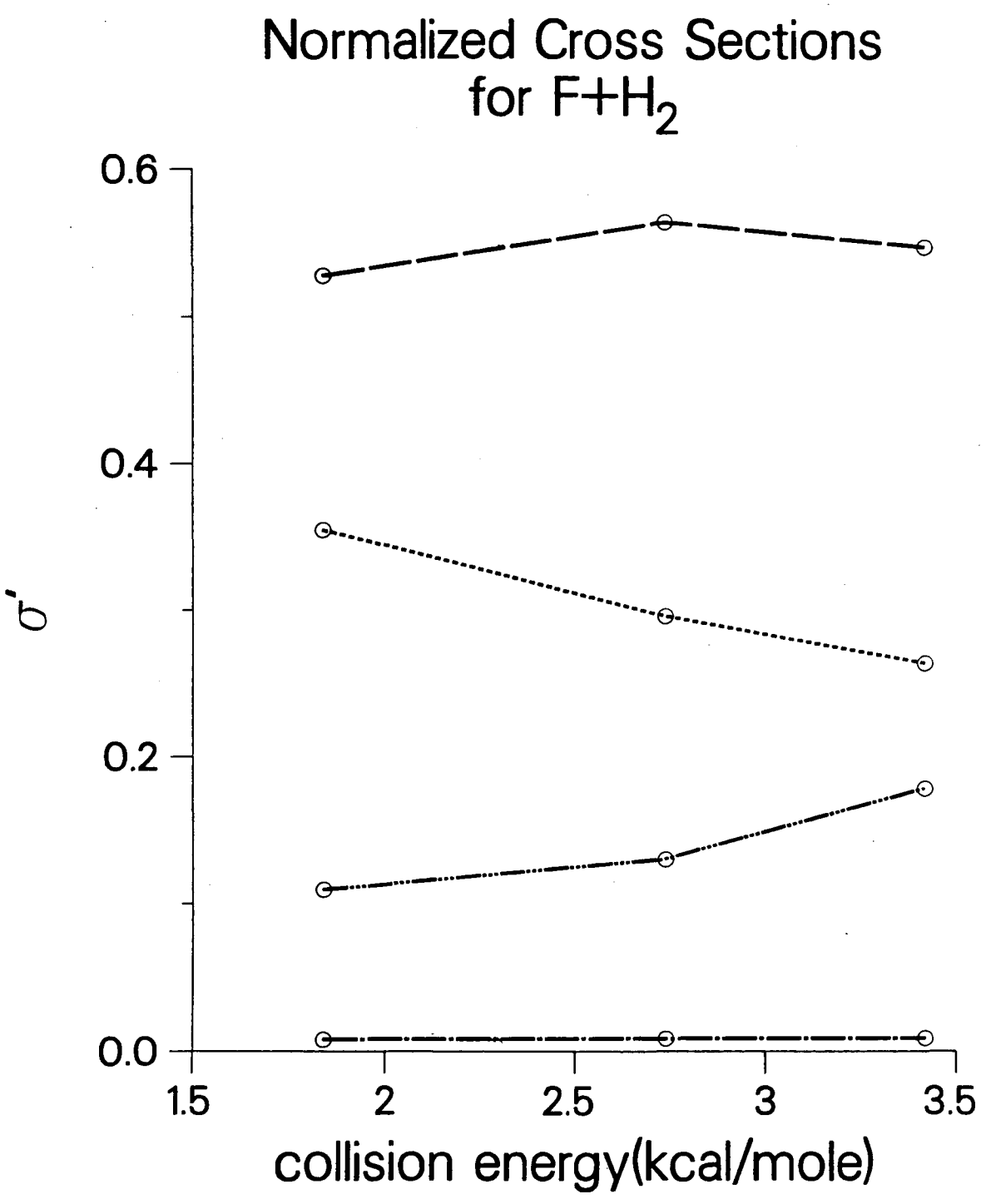
Normalized Cross Sections
for F+H2
0.6
0.4
0.2
0.0
q
1.5
2
2.5
3
3.5
collision energy(kcal/mole)
XBL 841-106

Fig. 28

This report was done with support from the Department of Energy. Any conclusions or opinions expressed in this report represent solely those of the author(s) and not necessarily those of The Regents of the University of California, the Lawrence Berkeley Laboratory or the Department of Energy.

Reference to a company or product name does not imply approval or recommendation of the product by the University of California or the U.S. Department of Energy to the exclusion of others that may be suitable.

TECHNICAL INFORMATION DEPARTMENT
LAWRENCE BERKELEY LABORATORY
UNIVERSITY OF CALIFORNIA
BERKELEY, CALIFORNIA 94720